Comparative Analysis of ACE-FTS, OSIRIS & PEARL FTIR Ozone Measurements

Sallam Saka

University of Toronto, Department of Physics

Supervisor: Professor Kaley Walker

Mentor: Dr Paul Jeffery

August 6, 2025

Abstract

This study presents a comparative analysis of stratospheric ozone measurements from the Atmospheric Chemistry Experiment Fourier Transform Spectrometer (ACE-FTS), the Optical Spectrograph and InfraRed Imager System (OSIRIS), and the ground-based Polar Environment Atmospheric Research Laboratory Fourier Transform InfraRed spectrometer (PEARL FTIR). Pairs of coincident ozone profile and column measurements (≤500 km, ≤8 hours apart) were compared using absolute and relative differences and Pearson correlation coefficients to assess measurement agreement and correlation, and time-series regression to quantify measurement divergence over time. Key findings reveal high correlation ($r > 0.8$) between all instruments for ozone column comparisons and strong agreement with most relative and absolute differences concentrated near 0 % and 0 Dobson Units (DU), respectively. Profile comparisons also showed good agreement with mean relative and absolute differences confined between -20 and 20 % and -0.5 and 0.5 ppmv, respectively. Relative and absolute differences between coincident pairs of profiles were consistent across seasons. However, correlation between column measurements differed significantly between seasons having differences up to 0.38, possibly due to lower sample sizes. Time series analysis indicated no significant long-term measurement divergence between instruments, with the steepest slope translating to just ≈Δ1 DU per decade. These results validate the consistency of ACE-FTS, OSIRIS and PEARL FTIR measurements, reinforcing their reliability for atmospheric ozone monitoring, particularly in the high Arctic.

Table of Contents

1 INTRODUCTION **4**

1.1 Background 4

1.2 Instruments 4

1.2.1 ACE-FTS *4*

1.2.2 OSIRIS *5*

1.2.3 PEARL FTIR *7*

2 METHODOLOGY **7**

2.1 Coincidence Criteria and Comparison Metrics 7

3 RESULTS **8**

3.1 Preliminary Findings 8

3.2 Profile comparisons 14

3.2.1 OSIRIS vs ACE-FTS Profile Comparisons *14*

3.2.1.1 Global OSIRIS vs ACE-FTS Profile Comparisons 14

3.2.1.2 Above PEARL OSIRIS vs ACE-FTS Comparisons 19

3.2.2 Satellite-based vs PEARL FTIR Profile Comparisons *24*

3.2.2.1 ACE-FTS vs PEARL FTIR Profile Comparisons 24

3.2.2.2 OSIRIS vs PEARL FTIR Profile Comparisons 29

3.3 Column comparisons 33

3.3.1 Partial Column Altitude Range *33*

3.3.1.1 Partial Column Upper Bound Choice 33

3.3.1.2 Partial Column Lower Bound Choice 33

3.3.2 OSIRIS vs ACE-FTS Column Comparisons *34*

3.3.2.1 Global OSIRIS vs ACE-FTS Column Comparisons 34

3.3.2.2 Above PEARL OSIRIS vs ACE-FTS Column Comparisons 37

3.3.3 Satellite-based vs PEARL FTIR Column Comparisons *40*

3.3.3.1 ACE-FTS vs PEARL FTIR Column Comparisons 40

3.3.3.2 OSIRIS vs PEARL FTIR Column Comparisons 43

3.3.4 Time Series Column Comparisons *46*

4 CONCLUSION **47**

5 APPENDIX **48**

6 REFERENCES **55**

1 Introduction

1.1 Background

The atmosphere is a mixture of gases and aerosols that surround the earth and practically extends up to about 100 km away from earth, reducing in density with increasing altitude (NOAA, 2024a). One of the atmosphere's minor constituents is ozone (O_3), yet it is one of the most important atmospheric gases (Salawitch et al., 2023). About 10% of ozone resides in the troposphere, while the rest is in the stratosphere (Salawitch et al., 2023). The main reason for the importance of ozone is its ability to absorb ultraviolet light, specifically, UV-C and UV-B radiation which are dangerous to all life forms (Salawitch et al., 2023). Additionally, ozone is responsible for the thermal structure of the stratosphere (NOAA, 2024b). The crucial role of ozone in the atmosphere makes it an important gas to monitor, along with other atmospheric gases (Salawitch et al., 2023).

Atmospheric remote sensing and spectroscopy are routinely performed by satellite-based instruments and ground-based instruments around the world to monitor atmospheric composition. To ensure satellite-based instruments are working properly and providing reliable data, their data needs to be routinely validated using other data sets. This verification process requires an independent data source against which to compare the satellite data which is provided by other satellite-based and ground-based instruments. Every year, there is an intensive validation campaign done in the Canadian high Arctic, specifically, at the Polar Environment Atmospheric Research Laboratory (PEARL) in Eureka, Nunavut (80°N, 86°W) (Kerzenmacher et al., 2005; Batchelor et al., 2010; Adams et al., 2012). These campaigns involve measuring the atmosphere using various instruments (Department of Physics, University of Toronto, n.d.; Kerzenmacher et al., 2005). The collection of these measurements provides an extensive dataset to use for comparison with the measurements retrieved from satellite-based instruments. One of the Fourier Transform Spectrometers at PEARL, referred to as PEARL FTIR in this report, will act as an independent source of data for comparison with the satellite-based instruments, Atmospheric Chemistry Experiment Fourier Transform Spectrometer (ACE-FTS), and Optical Spectrograph and InfraRed Imager System (OSIRIS). Additionally, the satellite-based instruments' data will be compared against each other. Comparisons will involve computing and visualizing relative and absolute differences and Pearson correlation coefficients between individual pairs of coincident measurements to measure similarity between the measurements.

1.2 Instruments

1.2.1 ACE-FTS

Atmospheric Chemistry Experiment (ACE) is a Canadian satellite mission intended for remote sensing of Earth's atmosphere (Bernath, 2005). The satellite, SCISAT, was launched into a circular orbit at an altitude of 650 km with an inclination of 74° on 12 August 2003 (Bernath, 2005). The purpose of ACE is to understand the chemical and dynamical processes that control the distribution

of ozone in the stratosphere and upper troposphere, explore the relationship between atmospheric chemistry and climate change, study the effects of biomass burning on free-tropospheric composition and measure aerosols and clouds to reduce the uncertainties in their effects on the global energy balance (Bernath, 2005). To achieve its goals, the satellite contains two instruments, ACE-FTS (ACE Fourier Transform Spectrometer) and ACE-MAESTRO (ACE Measurement of Aerosol Extinction in the Stratosphere and Troposphere Retrieved by Occultation) (Bernath, 2005). ACE-FTS is a high resolution (0.02 cm^{-1}) Fourier transform spectrometer, operating in the wavenumber range of 750-4400 cm^{-1} (Bernath, 2005). During the satellite's sunrise and sunset, ACE-FTS measures solar absorption spectra in the limb viewing geometry, looking towards the sun, with a vertical resolution of 4 km. ACE-FTS is also augmented by two imagers which provide measurements of atmospheric extinction, all three instruments share one sun tracker (Bernath, 2005). Due to SCISAT's orbital path, ACE-FTS collects data over the same latitudes annually seen in Figure 1.

1.2.2 OSIRIS

The Optical Spectrograph and Infrared Imager System (OSIRIS), along with the Sub-Millimeter Radiometer (SMR), is on-board the Odin satellite which was launched on 20 February 2001 into a circular Sun-synchronous orbit at 620 km elevation (Llewellyn, 2004; Murtagh, 2002). The satellite is intended for investigations in aeronomy and astronomy. The objective of the aeronomy mission is to study stratospheric ozone, mesospheric ozone and summer mesosphere sciences and mechanisms involved in coupling of atmospheric regions (Murtagh, 2002). OSIRIS is composed of two different parts, the Optical Spectrograph (OS) and the InfraRed Imager (IRI) (Llewellyn, 2004). The OS measures Rayleigh-scattered sunlight spectra within the wavelength range of 280-800 nm and atmospheric emission features such as airglow and auroral emissions (Llewellyn, 2004). The IRI data also includes Rayleigh-scattered sunlight and airglow near 1270 nm and 1530 nm wavelengths (Murtagh, 2002). The satellite is pointed at the limb of the earth, oriented along the direction of orbit, allowing it to collect scattered sunlight (Llewellyn, 2004). The OSIRIS data used in this paper is from the OS. Similar to ACE-FTS, OSIRIS collects data over the same latitudes annually seen in Figure 2.

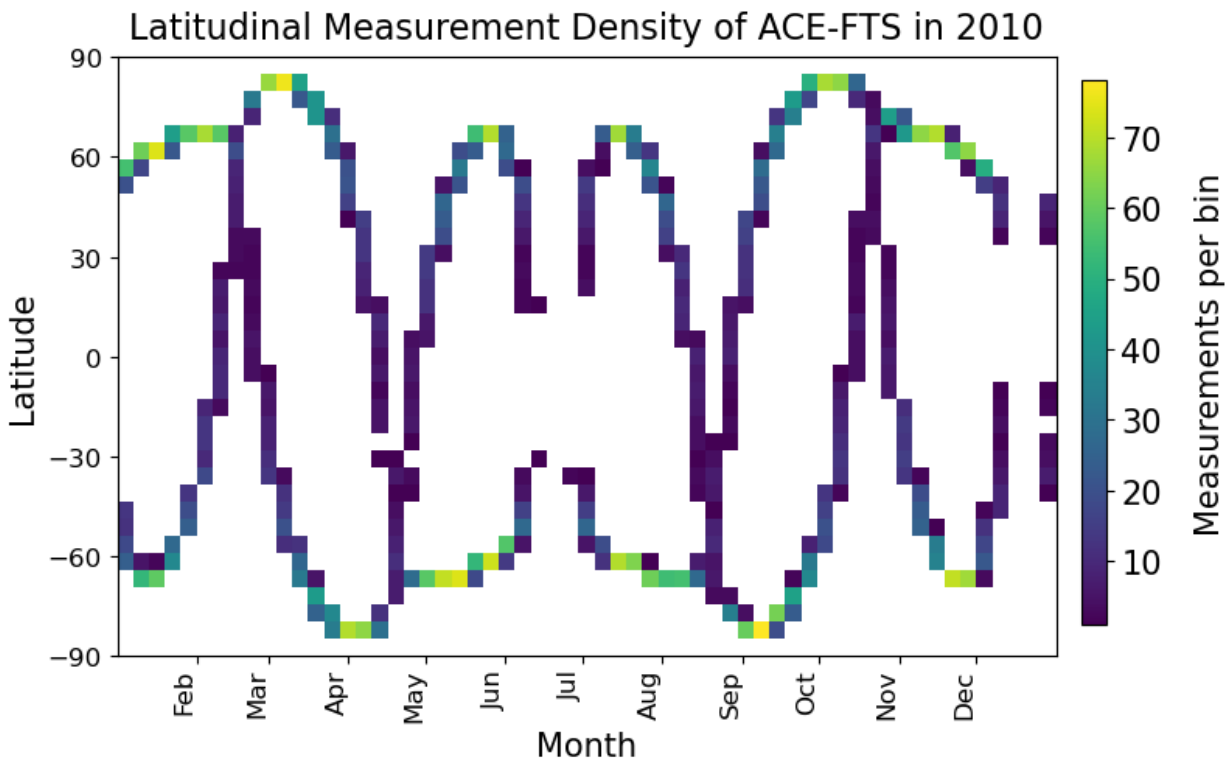

Figure 1. Representative annual latitudinal measurement density of ACE-FTS.

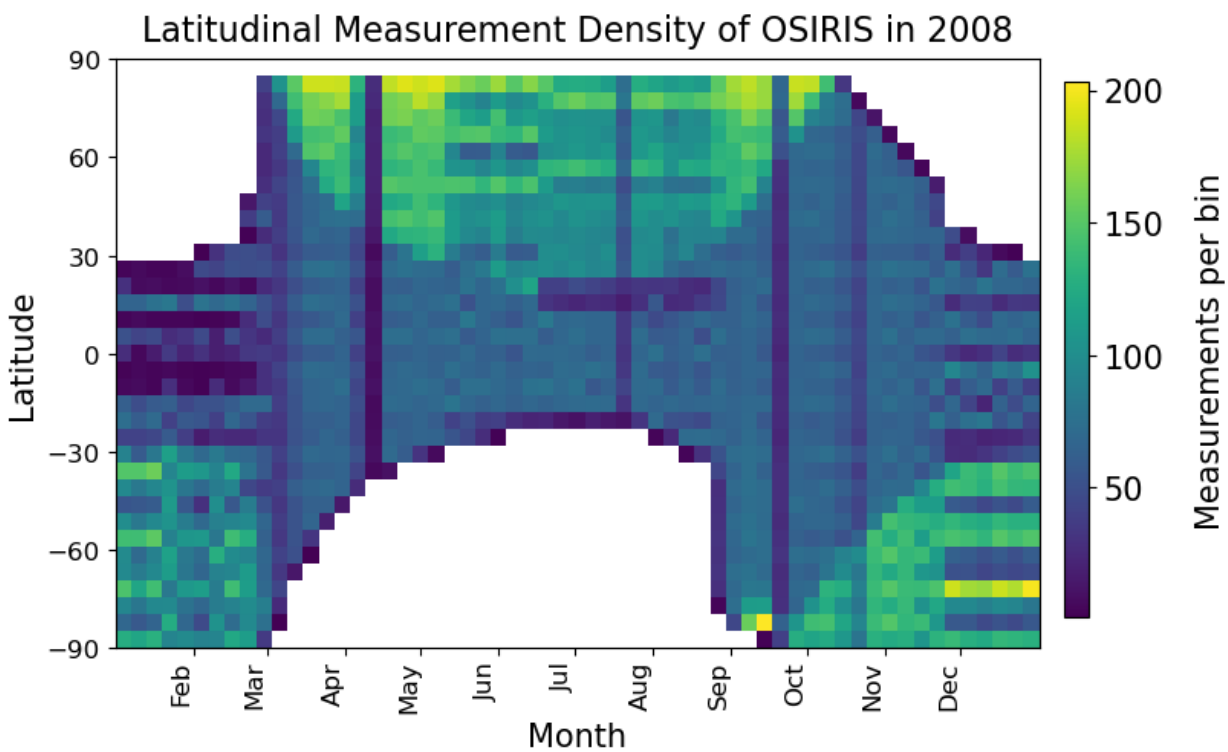

Figure 2. Representative annual latitudinal measurement density of OSIRIS.

1.2.3 PEARL FTIR

PEARL Fourier Transform InfraRed spectrometer (PEARL FTIR), also referred to as a Bruker FTIR, is a ground-based Michelson interferometer (Batchelor, 2009). PEARL FTIR was permanently installed at PEARL in 2006 (Adams, 2012). It operates between the wavenumber ranges of 1850-10000 cm^{-1} and 600-6000 cm^{-1} using two different detectors at a high resolution of up to 0.0024 cm^{-1} (Batchelor, 2009). PEARL FTIR makes solar-absorption measurements when the sun is above the horizon in the Arctic (approximately 21st February – 20th October) using a sun tracker installed on the roof of its lab enclosure to direct sunlight to itself (Batchelor, 2009; Griffin, 2017). PEARL FTIR has also been used in several studies for comparison against various instruments (Griffin, 2017; Batchelor, 2010; Adams, 2012).

2 Methodology

2.1 Coincidence Criteria and Comparison Metrics

Comparisons were made between individual pairs of coincident measurements for each pair of instruments (i.e. OSIRIS vs ACE-FTS, OSIRIS vs PEARL FTIR, ACE-FTS vs PEARL FTIR). Two sets of OSIRIS vs ACE-FTS comparisons were done. The first set of comparisons had no spatial restrictions apart from the coincidence criteria while the other set was restricted to a maximum of 500 km great-circle distance away from PEARL in addition to the coincidence criteria. The coincidence criteria used in this report to assess whether two measurements could be similar enough to be appropriate for comparison was that each pair of measurement must be made within a maximum of 500 km and 8 hours apart. The distance criterion represents the great-circle distance between the measurement locations.

The great-circle distance was computed using the haversine distance formula below where λ_2 and λ_1 represents longitudes of each measurement, Φ_1 and Φ_2: represents latitudes of each measurement, d represents the great-circle distance between the measurements, and 6371 km is earth's radius.

$$\text{Longitudinal difference: } \Delta\lambda = \lambda_2 - \lambda_1$$

$$\text{Latitudinal difference: } \Delta\phi = \phi_2 - \phi_1$$

$$a = \sin^2\left(\frac{\Delta\phi}{2}\right) + \cos(\phi_1) \cdot \cos(\phi_2) \cdot \sin^2\left(\frac{\Delta\lambda}{2}\right)$$

$$Great - circle\ distance: d = 2 \cdot \arcsin\left(\sqrt{a}\right) \cdot 6371\ km$$

Experimentation with different criteria showed that the chosen criteria seem to yield results that best represent the actual measurement differences because it is narrow enough to minimize outliers but wide enough to get a representative sample of measurement pairs. To compare

measurement pairs, various statistics were computed which are shown in Table 1. By convention, in this report, the instrument on the left of "and/vs", in "OSIRIS and/vs PEARL FTIR", "ACE-FTS and/vs PEARL FTIR" and "OSIRIS and/vs ACE-FTS" will be the "S_1" instrument, while the other instrument would be "S_2" when performing computations. To ensure accurate profile comparisons, satellite profiles were linearly interpolated to the same altitude grid as the PEARL FTIR data which has a more sporadic altitude grid.

Statistic	Formula
Absolute Difference	$S_1 - S_2$
Relative Difference	$200\% \times \frac{S_1 - S_2}{S_2 + S_2}$
Pearson Correlation Coefficient	$r = \frac{\sum_{i=1}^{n}(S_{1i} - \bar{S_1})(S_{2i} - \bar{S_2})}{\sqrt{\sum_{i=1}^{n}(S_{1i} - \bar{S_1})^2}\sqrt{\sum_{i=1}^{n}(S_{2i} - \bar{S_2})^2}}$
Mean Absolute Difference	$\frac{(\sum_{i=1}^{n} Absolute\ Difference_i)}{n}$
Mean Relative Difference	$\frac{(\sum_{i=1}^{n} Relative\ Difference_i)}{n}$

Table 1. Formulas of Comparison Statistics. S_1 and S_2 represents the measurement value of the S_1 instrument and the S_2 instrument, respectively, as defined previously.

3 Results

3.1 Preliminary Findings

Prior to finding coincident measurements, computing comparison metrics and visualizing the computed values, the data of each satellite were plotted and explored individually. This exploratory data analysis allows for familiarization with the data and ensures data quality because unexpected data can be spotted. The ACE-FTS data were initially filtered using the data quality flags outlined in Sheese et al. (2015) by only using data with a flag value of 0 which is deemed by Sheese et al. to have no known issues. Figures 3 and 4 below made from the ACE-FTS and OSIRIS data, respectively, showcase the latitudinal (x-axis) and altitudinal (y-axis) distribution of ozone in units

of parts per million by volume (ppmv) during various seasons. The time range of 2006 to 2020 was chosen because this is the time range where all three instruments have recorded measurements.

In Figure 3, it is evident that ozone mostly resides in the stratosphere, specifically, between 20 and 45 km altitudes which is an expected result (Salawitch et al., 2023). This pattern is also demonstrated in the OSIRIS plot in Figure 4. Additionally, the latitudes where ozone is most concentrated shifts seasonally in both plots. For example, at higher latitudes in the northern hemisphere, during the boreal spring season, ozone Volume Mixing Ratio (VMR) are noticeably higher compared to boreal winter which is also expected due to increased ozone transport from the tropics (Salawitch et al., 2023). These plots serve as good verification that the measurements taken by the instruments align with expectations and capture similar ozone distribution patterns.

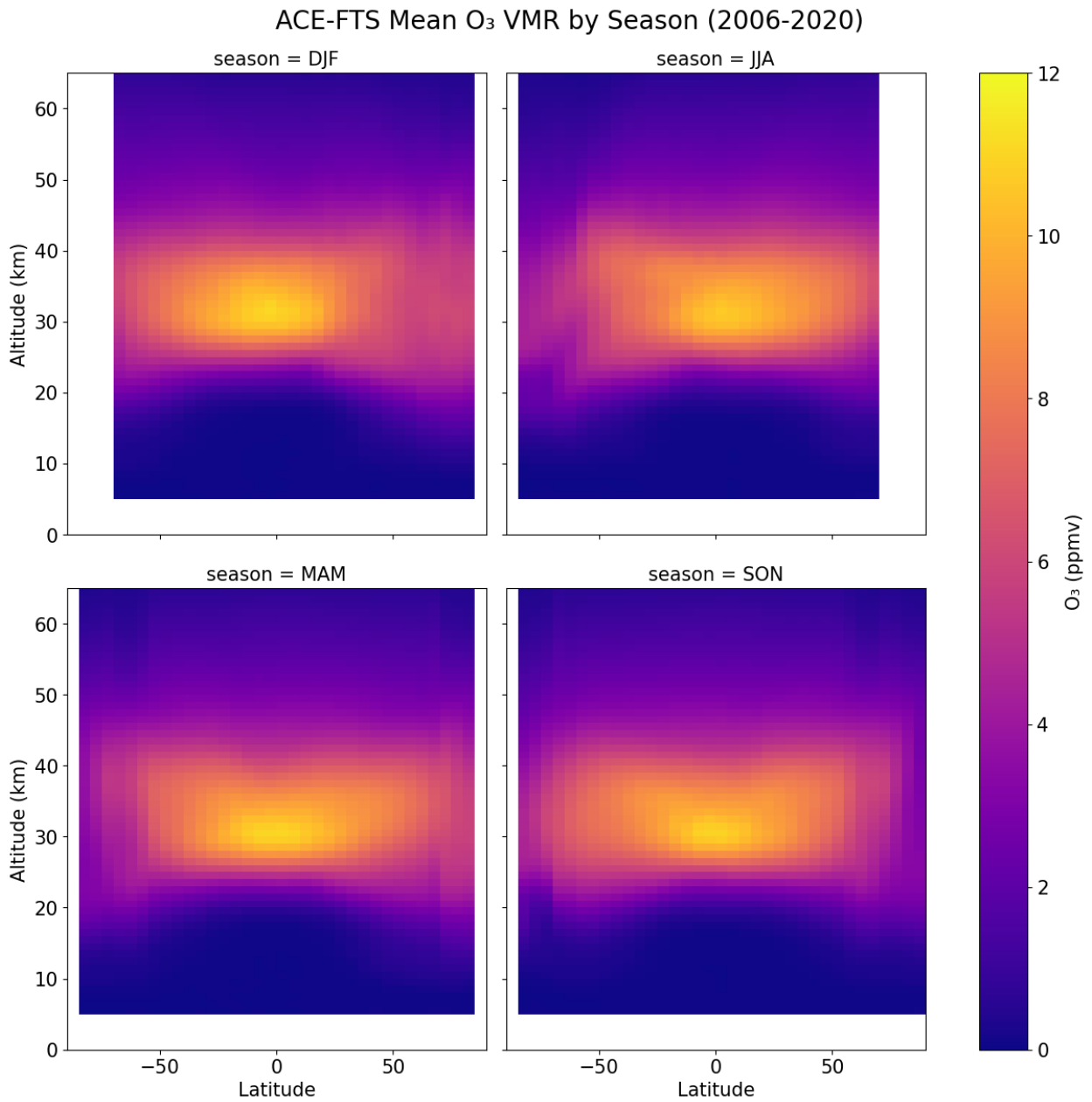

Figure 3. Climatology plot depicting zonal mean distribution of ozone VMR by ACE-FTS between 2006 and 2020.

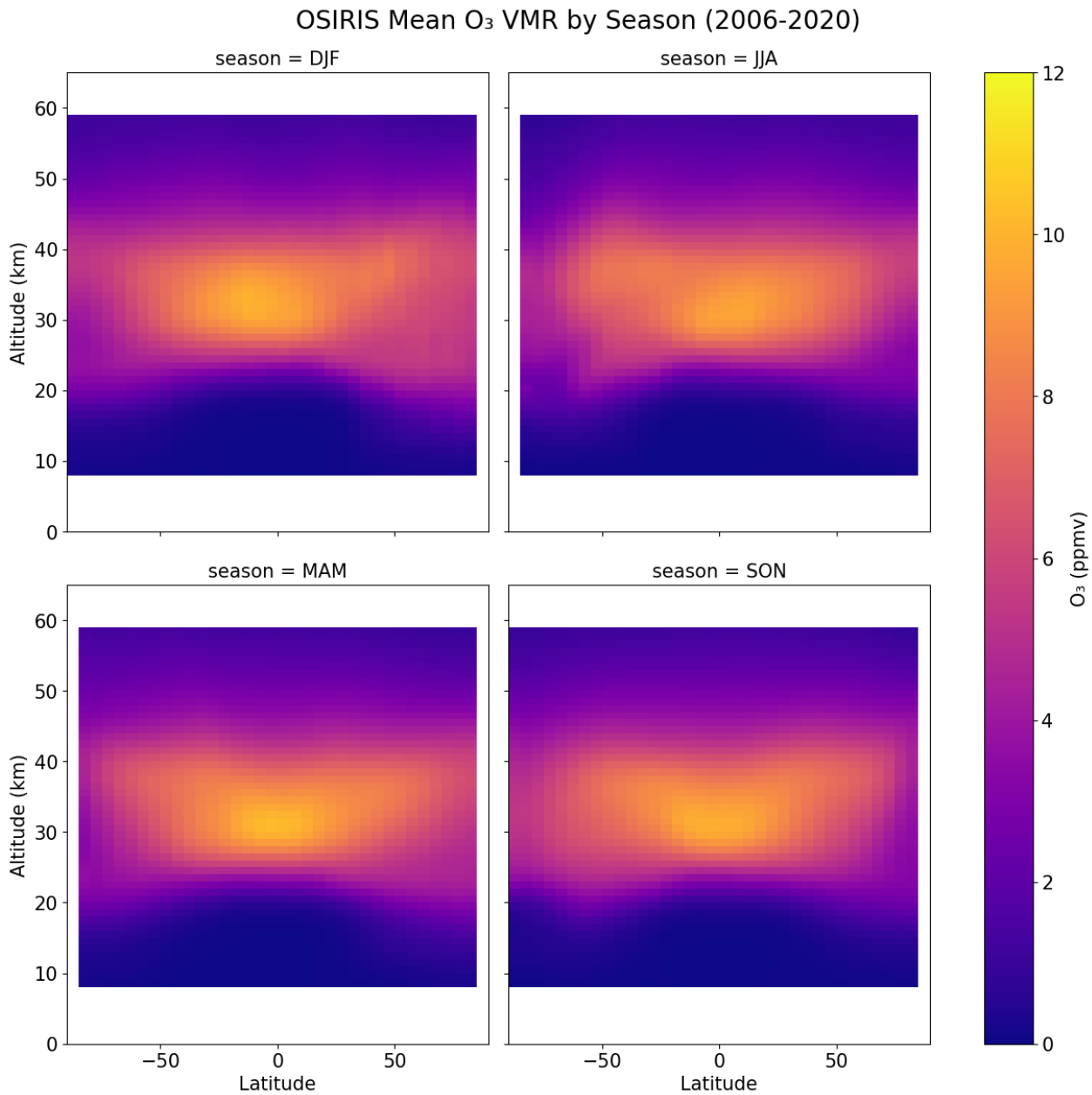

Figure 4. Climatology plot depicting zonal mean distribution of ozone VMR by OSIRIS between 2006 and 2020.

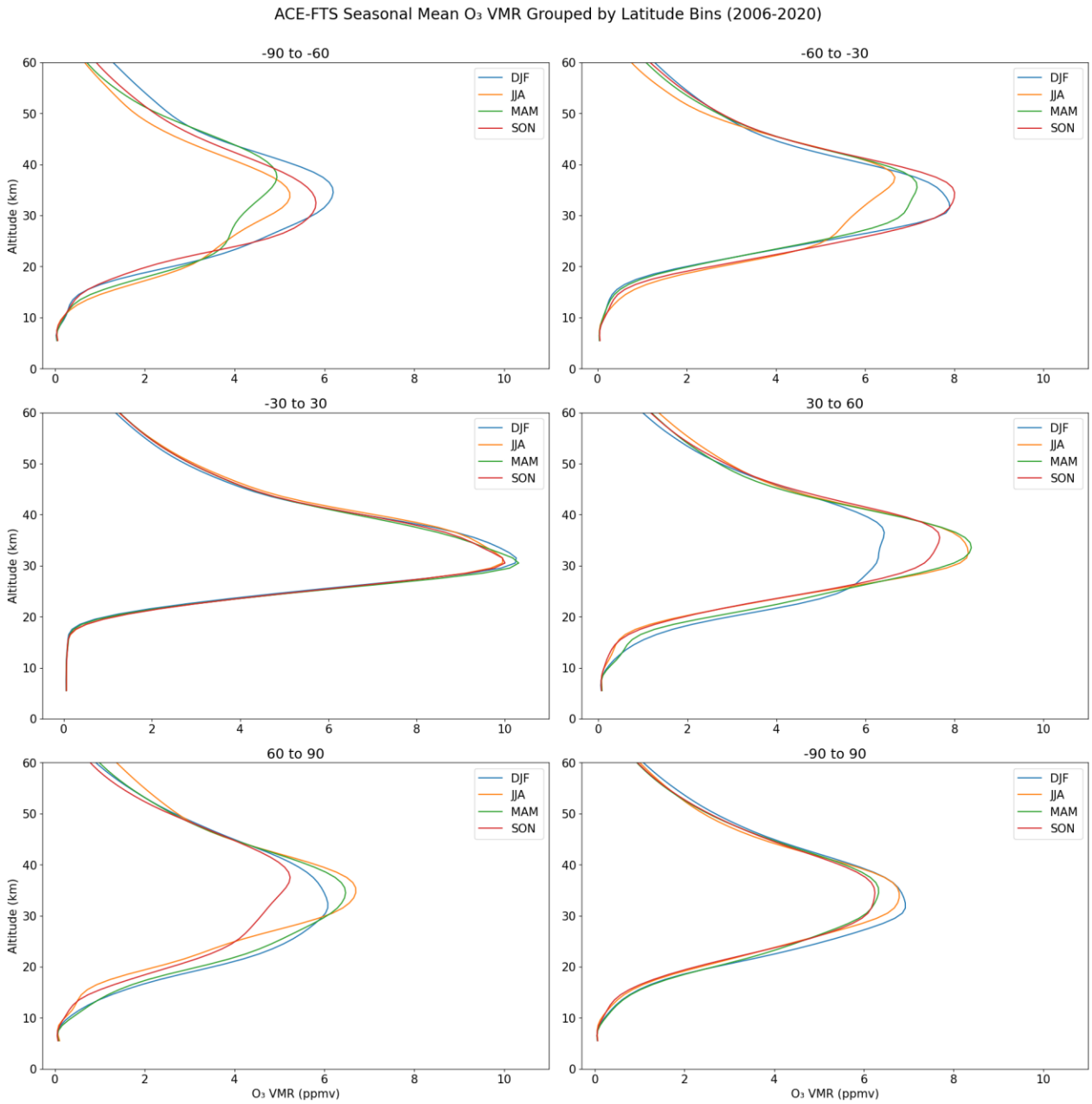

Figure 5. Plots depicting seasonally averaged ozone VMR measurements by ACE-FTS in six different latitude bins between 2006 and 2020.

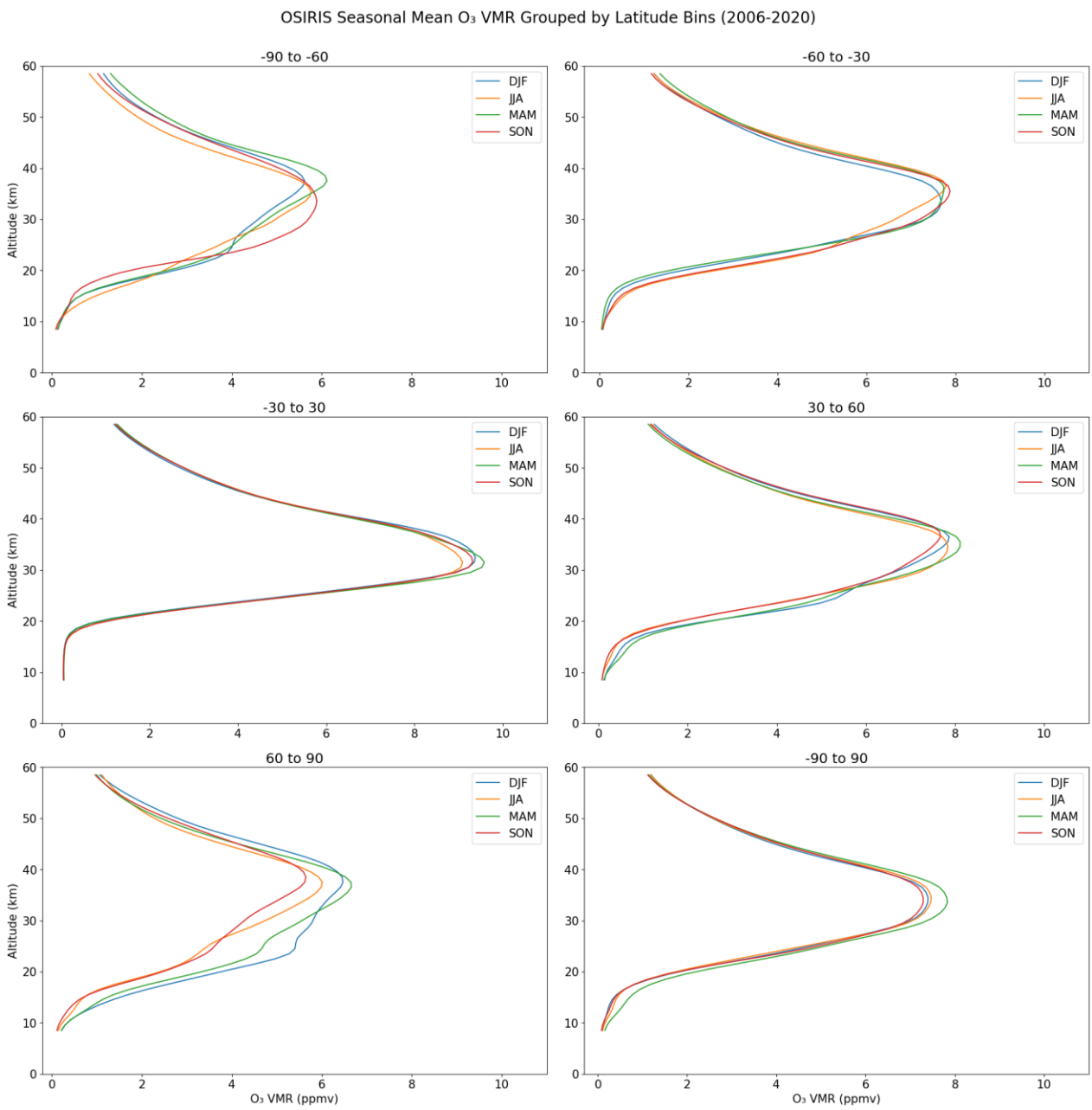

Figure 6. Plots depicting seasonally averaged ozone VMR measurements by OSIRIS in six different latitude bins between 2006 and 2020.

Figures 5 and 6, computed from ACE-FTS and OSIRIS data, respectively, compare seasonally averaged ozone profiles, within six different latitude bins. General ozone patterns such as higher ozone VMR in the tropics and lower ozone VMR at the poles are captured by both plots. However, these series of plots reveal some differences that are not clearly discernable from the climatology plot. For example, the mean ozone VMR in the tropics (-30° to 30°) is higher in ACE-FTS measurements compared to OSIRIS measurements for all seasons. Furthermore, the global ozone mean tends to be higher in the OSIRIS plot. There are many other noticeable differences in the plots in other latitude bands. These differences may arise from different temporal and spatial

measurement densities of the instruments as well as different measurement techniques. To account for the differences that arise due to different temporal and spatial measurement densities, comparing individual pairs of coincident measurements is crucial which will be the methodology adopted in ensuing sections.

3.2 Profile comparisons

For each set of profile comparisons, a series of plots will be shown. These include plots of the individual coincident profiles, absolute and relative differences, and Pearson correlation coefficients. All the plots mentioned above will be followed by a version showing a seasonal perspective. For pairs of coincident measurements, data from all available time periods were included in the analysis. All these plots will be discussed simultaneously as they are shown.

3.2.1 OSIRIS vs ACE-FTS Profile Comparisons

3.2.1.1 Global OSIRIS vs ACE-FTS Profile Comparisons

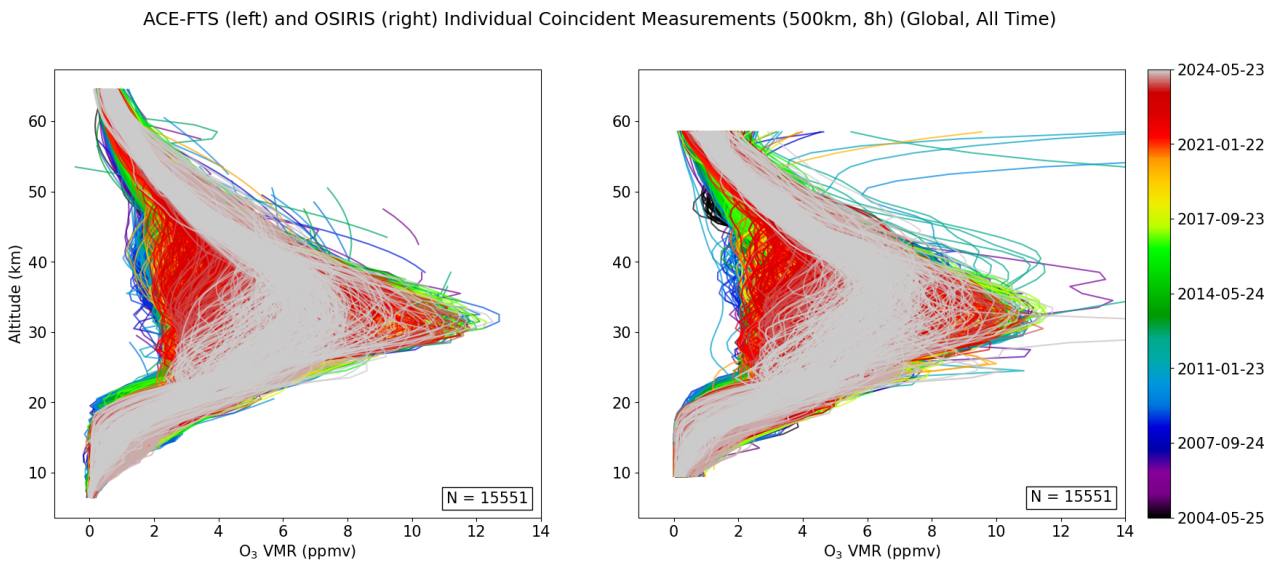

Figure 7. Plots of individual global coincident ozone profiles from ACE-FTS (left) and OSIRIS (right). N is the number of coincidences.

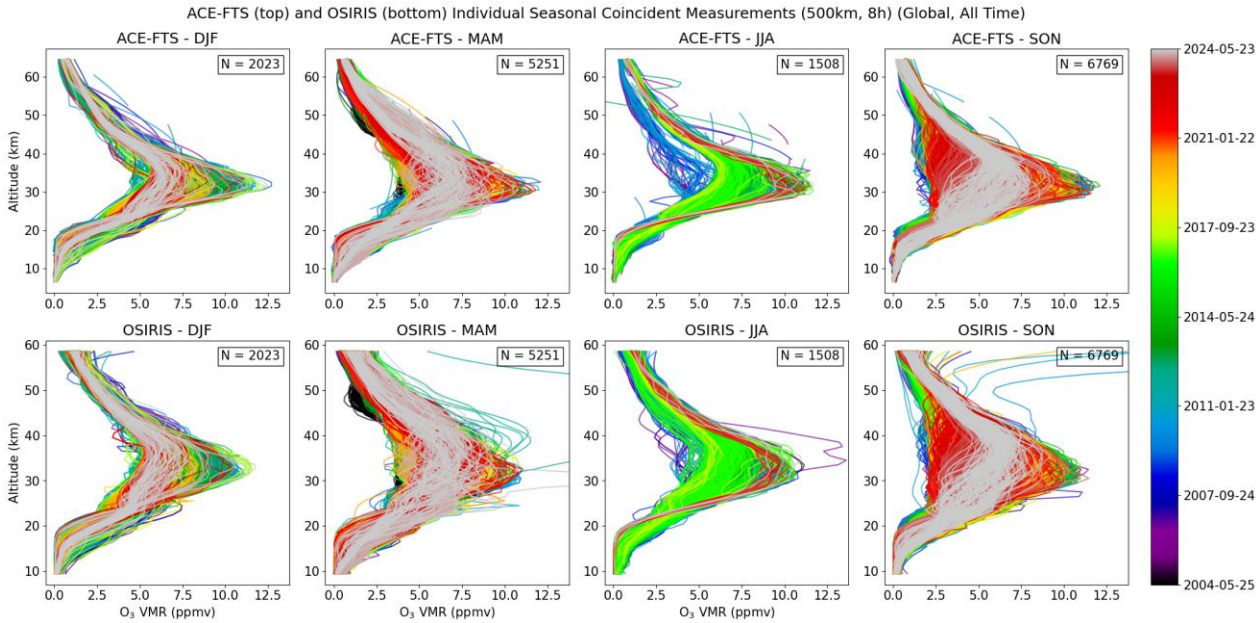

Figure 8. Seasonal plots of individual global coincident ozone profiles from ACE-FTS (top) and OSIRIS (bottom). N is the number of coincidences.

Figure 7 highlights several prominent features, including a narrower peak in the ACE-FTS plot and the presence of more extreme values in the OSIRIS plot which both indicate more variability in the OSIRIS measurements. Figure 8 shows that these features are present in all seasons but most prevalent during boreal fall and spring seasons.

Figure 9 suggests that the measurements are similar, with average absolute differences being confined between -0.40 and 0.25 ppmv at all altitudes shown. Figure 10 shows that the pattern of agreement between the instruments at the various altitudes is similar across all seasons, so, no season skews the average absolute differences.

Figures 11 and 12 support the insights derived from Figures 9 and 10. Firstly, they show that the mean relative differences are mostly confined between -10 and 5 % for most altitudes shown. The increase in relative differences at the edges of the stratosphere result from small absolute differences between low ozone VMR producing large relative differences. Like the absolute difference seasonal plots, the pattern of agreement across various altitudes is similar between the seasons.

Figures 13 and 14 confirm the pattern of consistent agreement in all seasons seen in the relative and absolute difference plots. They also show that the measurements are highly correlated ($r > 0.8$) in the stratosphere, and more specifically, the ozone layer (~15 to 35 km) before the correlation drops off at the edges of the stratosphere. The seasonal correlation plots indicate that in boreal winter and summer, the correlation decreases faster with altitude.

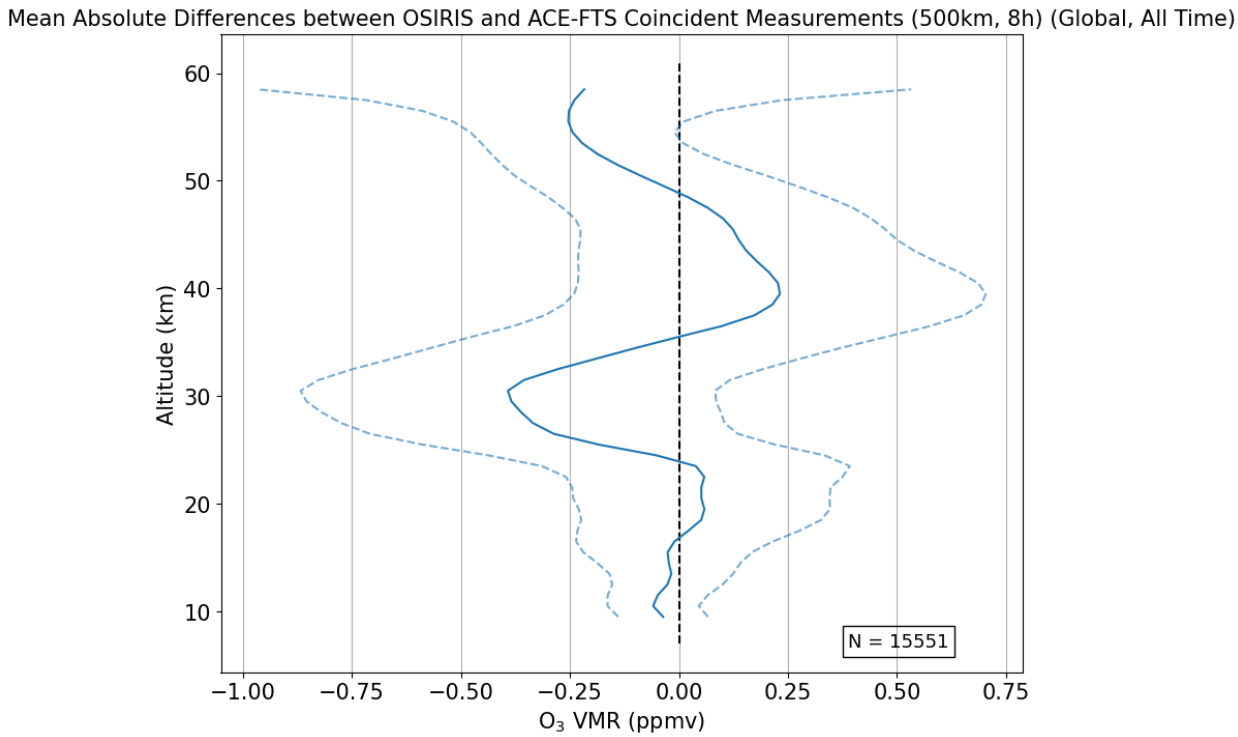

Figure 9. Plot of the mean absolute difference of all OSIRIS and ACE-FTS global coincident ozone measurements at each altitude. N is the number of coincidences. Dashed boundaries represent one standard deviation from the mean.

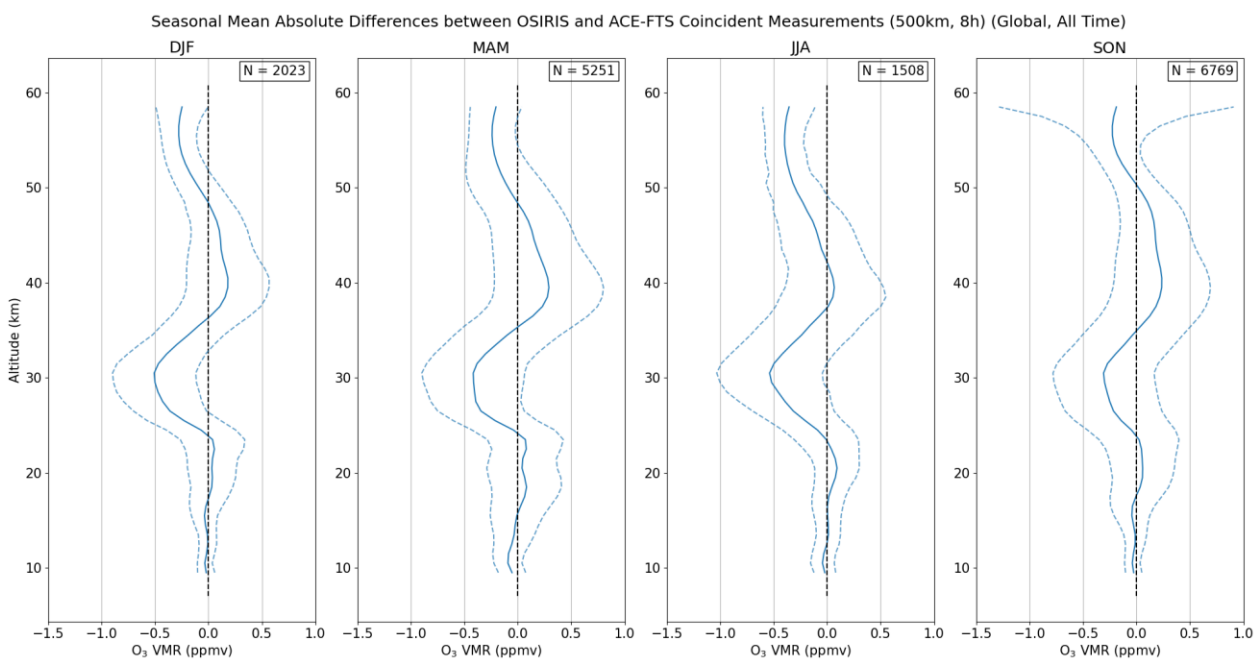

Figure 10. Seasonal plots of the mean absolute difference of all OSIRIS and ACE-FTS global coincident ozone measurements at each altitude. N is the number of coincidences. Dashed boundaries represent one standard deviation from the mean.

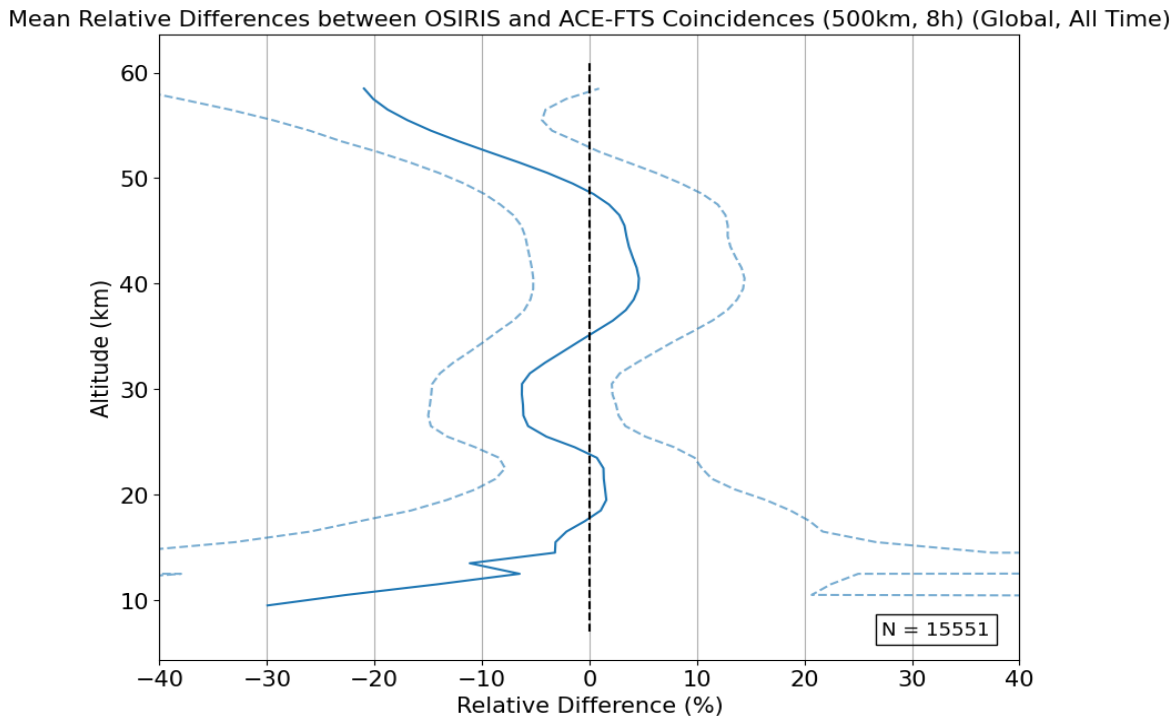

Figure 11. Plot of the mean relative difference of all OSIRIS and ACE-FTS global coincident ozone measurements at each altitude. N is the number of coincidences. Dashed boundaries represent one standard deviation from the mean.

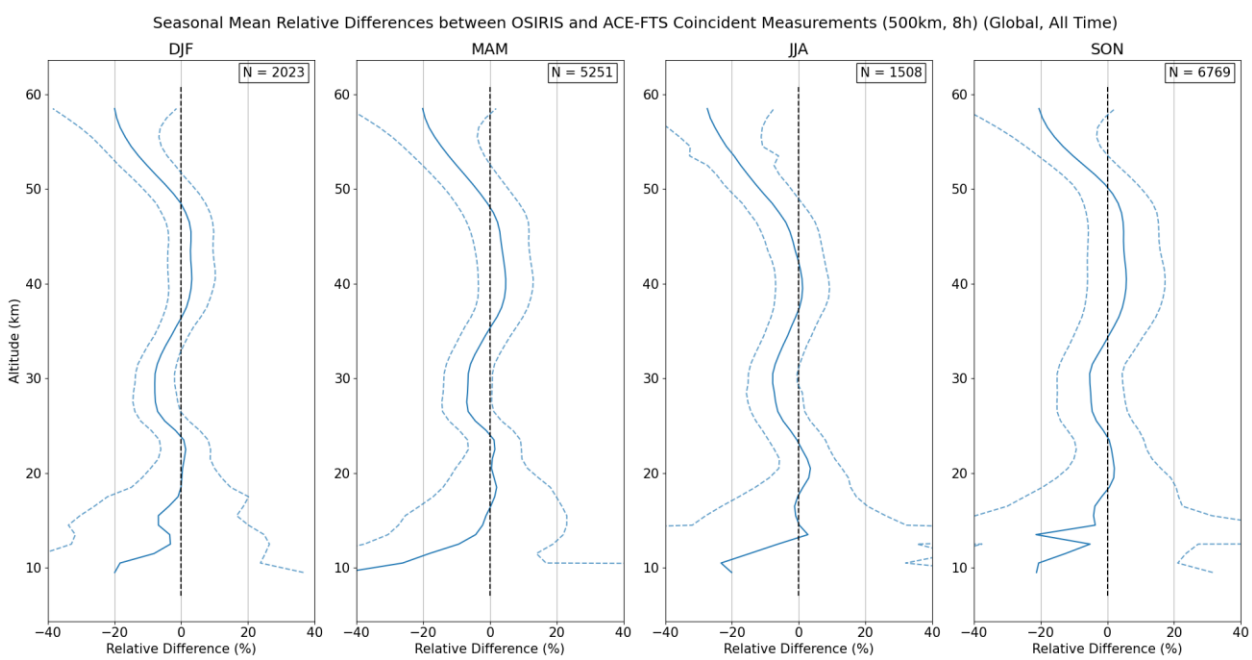

Figure 12. Seasonal plots of the mean relative difference of all OSIRIS and ACE-FTS global coincident ozone measurements at each altitude. N is the number of coincidences. Dashed boundaries represent one standard deviation from the mean.

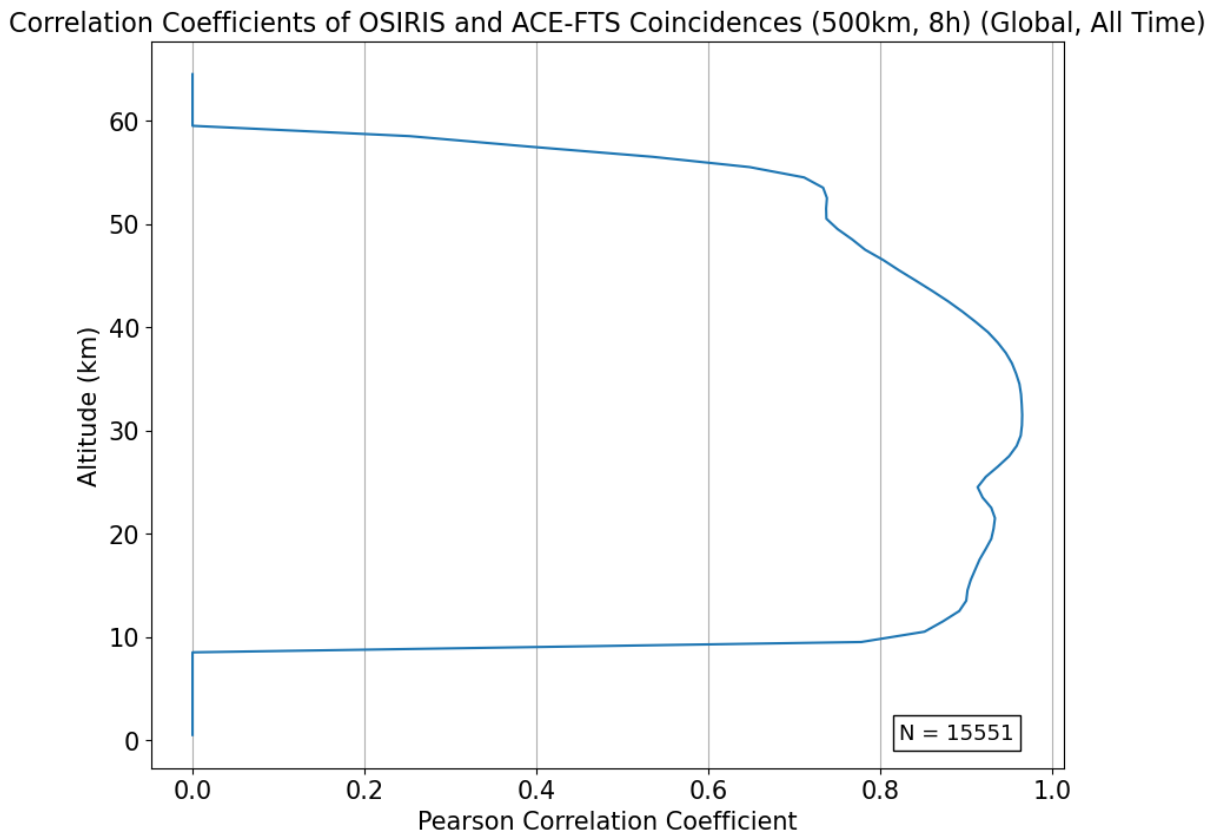

Figure 13. Plot of the Pearson correlation coefficient of all OSIRIS and ACE-FTS global coincident ozone measurements at each altitude. N is the number of coincidences.

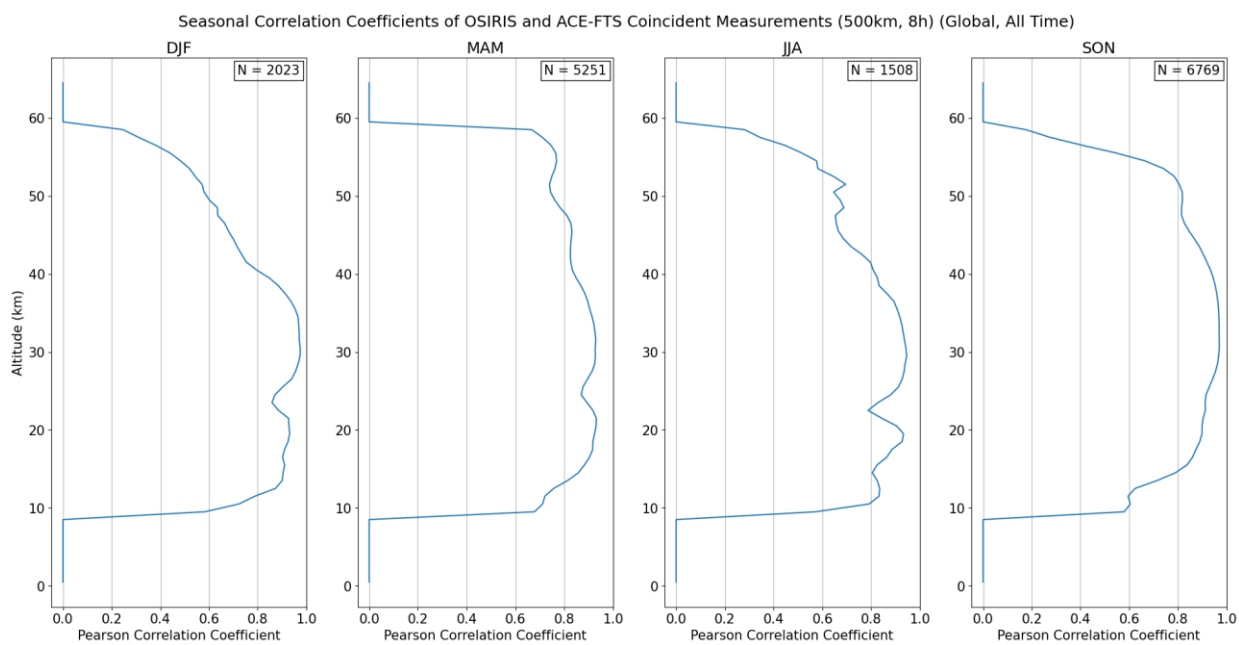

Figure 14. Seasonal plots of the Pearson correlation coefficient all OSIRIS and ACE-FTS global coincident ozone measurements at each altitude. N is the number of coincidences.

3.2.1.2 Above PEARL OSIRIS vs ACE-FTS Comparisons

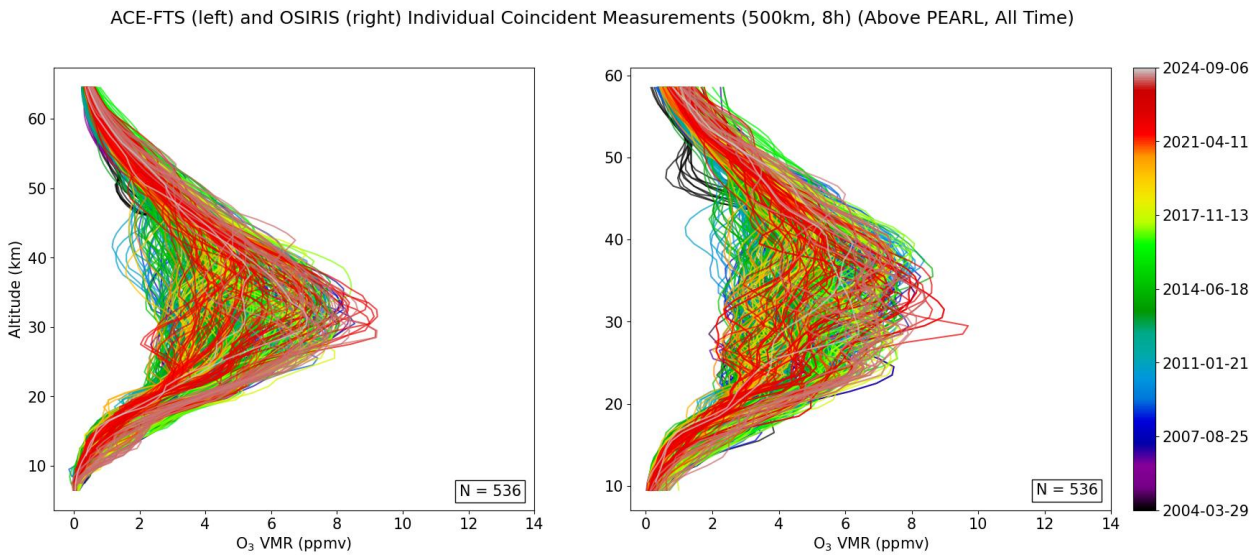

Figure 15. Plots of individual coincident ozone profiles above PEARL from ACE-FTS (left) and OSIRIS (right). N is the number of coincidences.

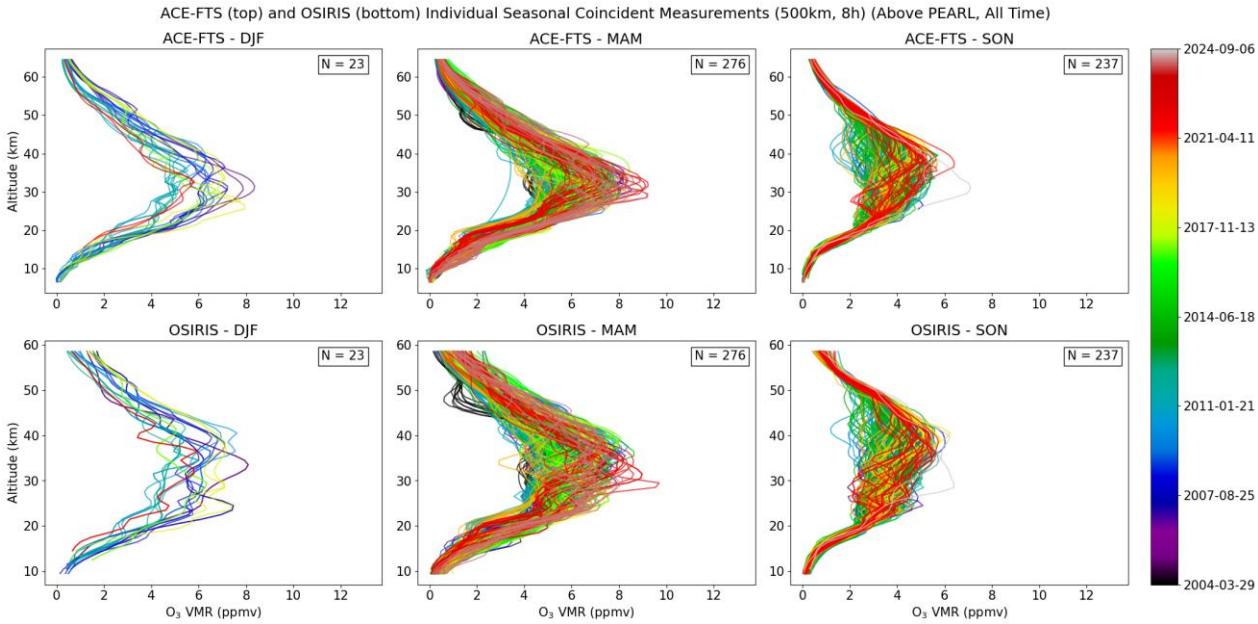

Figure 16. Seasonal plots of individual coincident ozone profiles above PEARL from ACE-FTS (top) and OSIRIS (bottom). Plot of JJA season is missing due to lack of coincident measurements. N is the number of coincidences.

In comparison to Figures 7 and 8, the individual measurements in Figures 15 and 16 show less outliers, however, OSIRIS plots still show higher variability compared to ACE-FTS plots. Compared to Figure 8, the seasonal plots in Figure 16 show a closer match between the satellites.

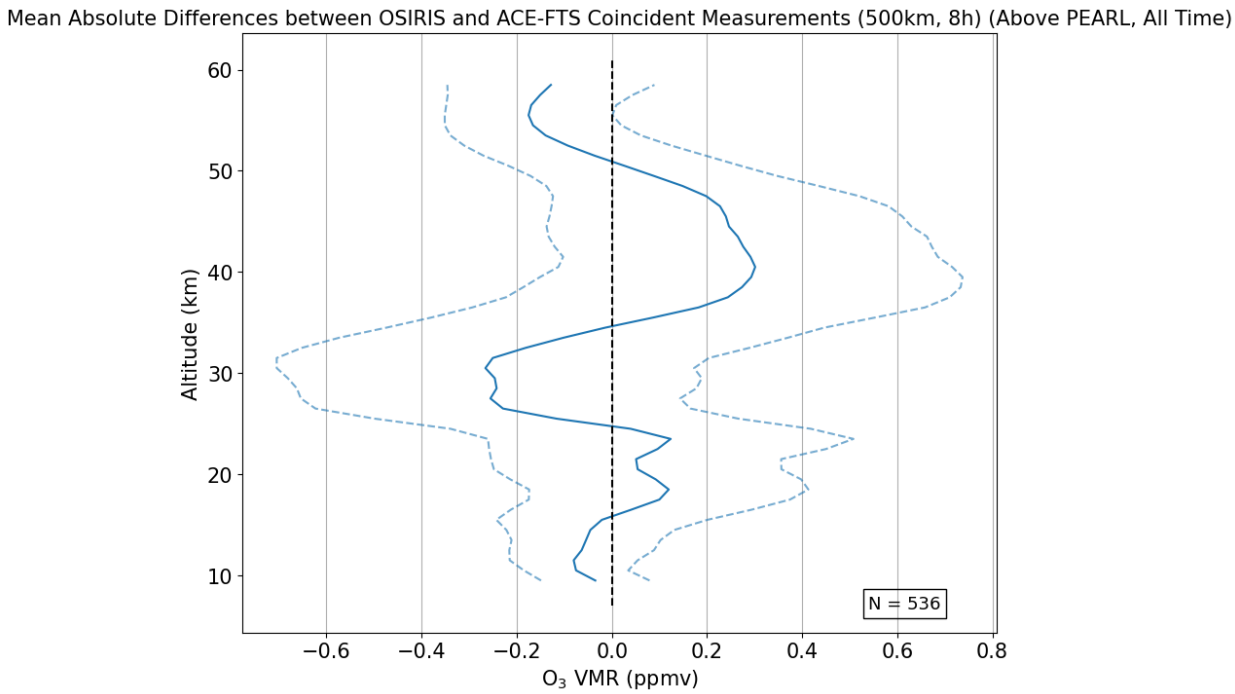

Figure 17. Plot of the mean absolute difference of all OSIRIS and ACE-FTS coincident ozone measurements above PEARL at each altitude. N is the number of coincidences. Dashed boundaries represent one standard deviation from the mean.

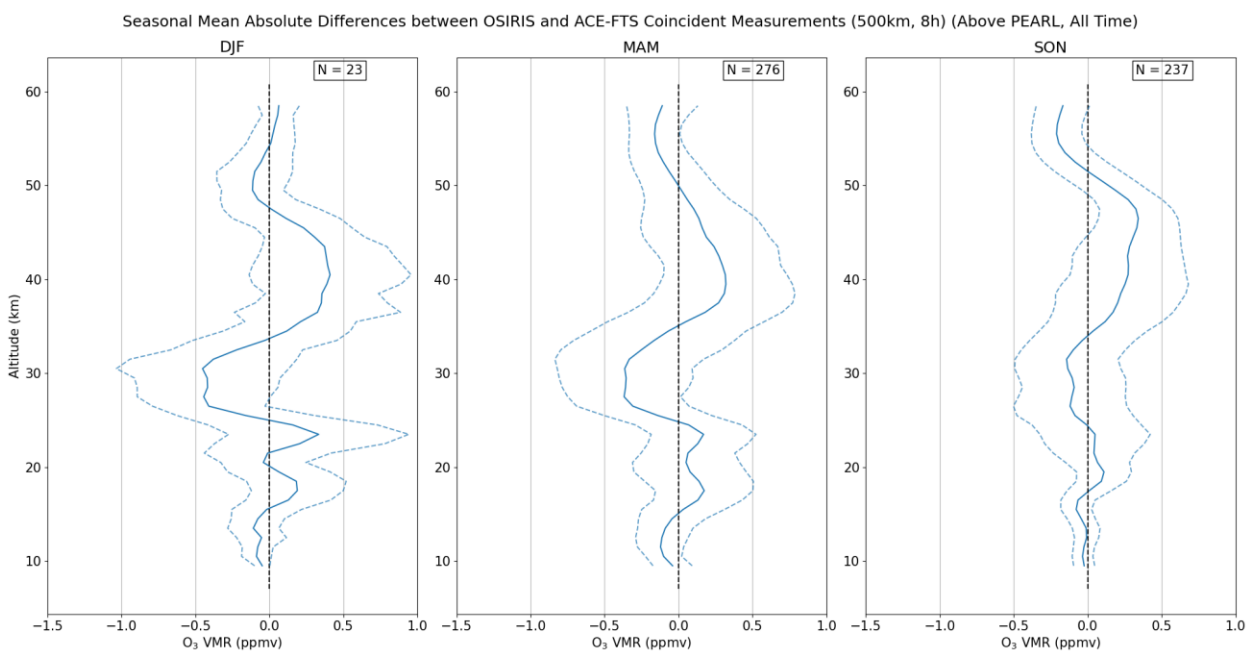

Figure 18. Seasonal plots of the mean absolute difference of all OSIRIS and ACE-FTS coincident ozone measurements above PEARL at each altitude. Plot of JJA season is missing due to lack of coincident measurements. N is the number of coincidences. Dashed boundaries represent one standard deviation from the mean.

Like global coincidences, coincidences above PEARL have the same pattern of agreement between seasons which can be seen in Figure 18. The absolute differences are all confined to between -0.5 and 0.5 ppmv in all seasons. Figure 17 shows that in aggregate, absolute differences are mostly between -0.2 and 0.2 ppmv.

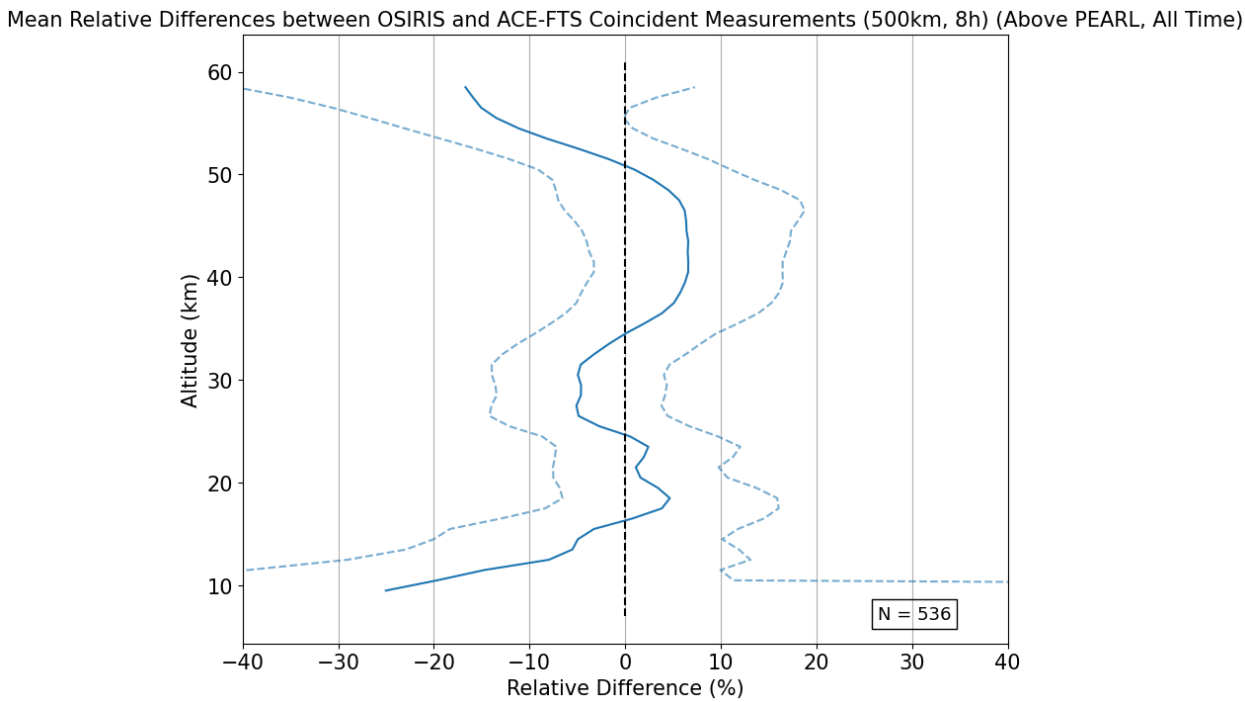

Figure 19. Plot of the mean relative difference of all OSIRIS and ACE-FTS coincident ozone measurements above PEARL at each altitude. N is the number of coincidences. Dashed boundaries represent one standard deviation from the mean.

Figure 19 shows that the mean relative differences tend to be within -10 and 7.5 % which can also be seen in Figure 11. Like Figure 12, Figure 20 shows that the relative difference between the measurements is similar across all seasons. Together, these demonstrate that global measurement difference patterns persist above PEARL.

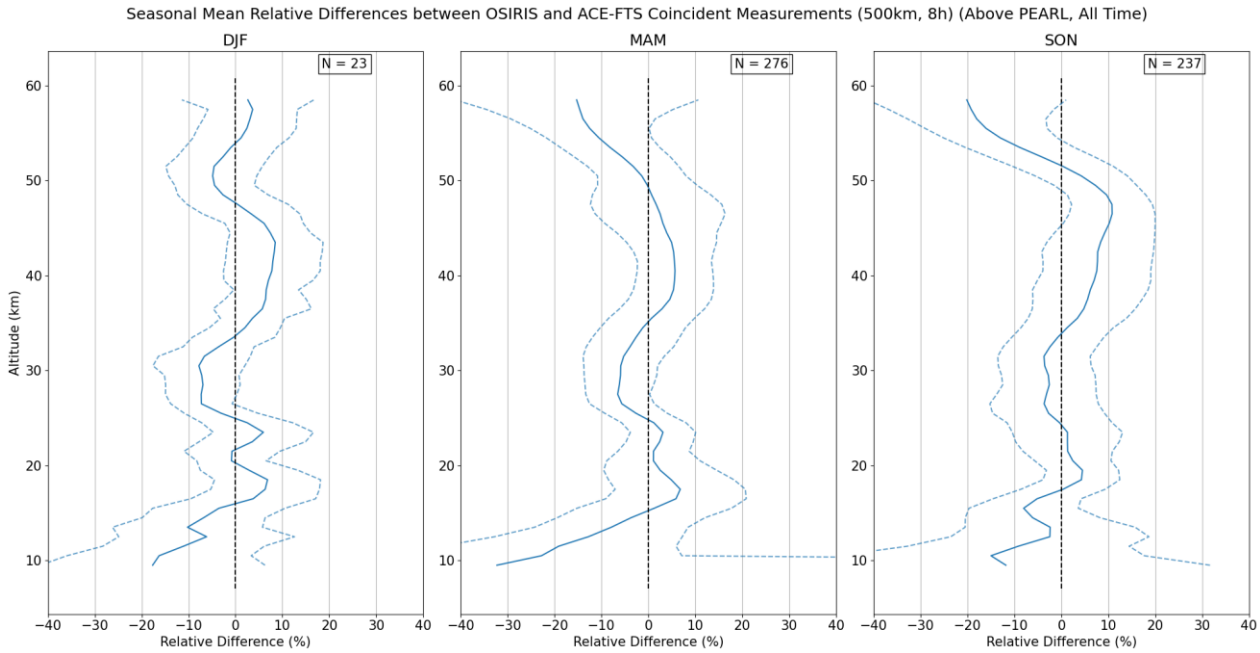

Figure 20. Seasonal plots of the mean relative difference of all OSIRIS and ACE-FTS coincident ozone measurements above PEARL at each altitude. Plot of JJA season is missing due to lack of coincident measurements. N is the number of coincidences. Dashed boundaries represent one standard deviation from the mean.

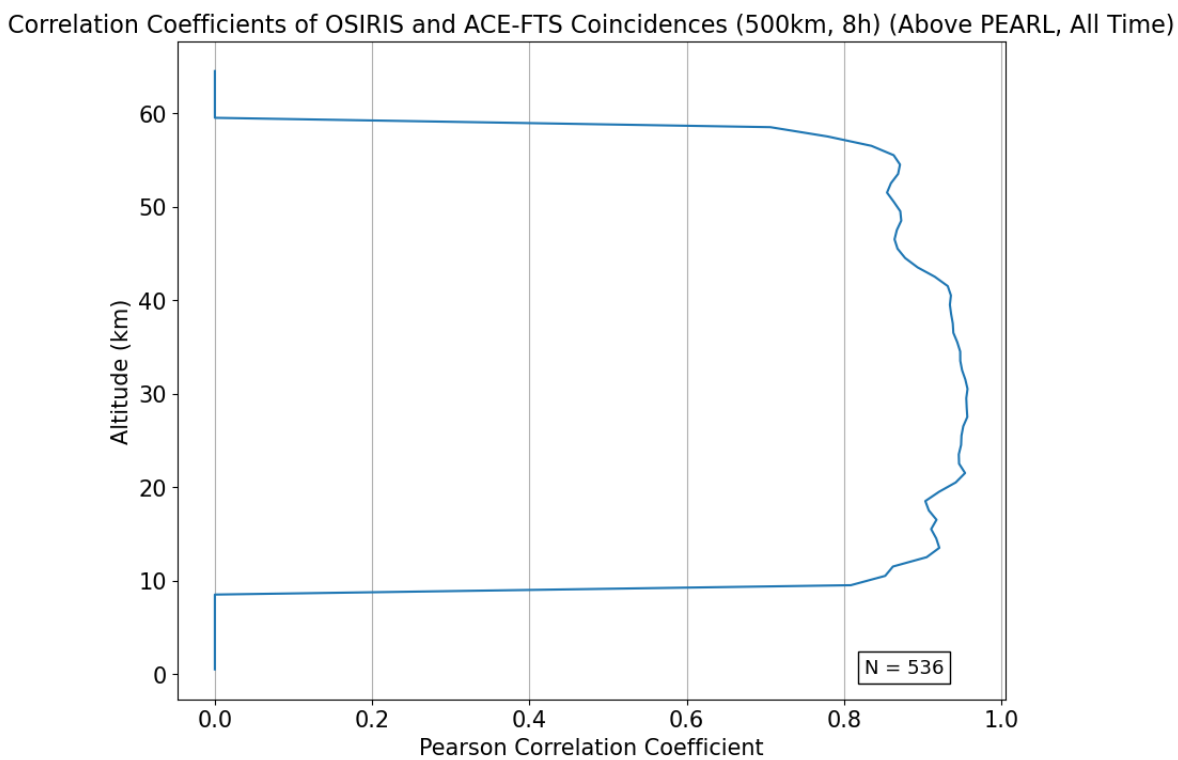

Figure 21. Plot of the Pearson correlation coefficient of all OSIRIS and ACE-FTS coincident ozone measurements above PEARL at each altitude. N is the number of coincidences.

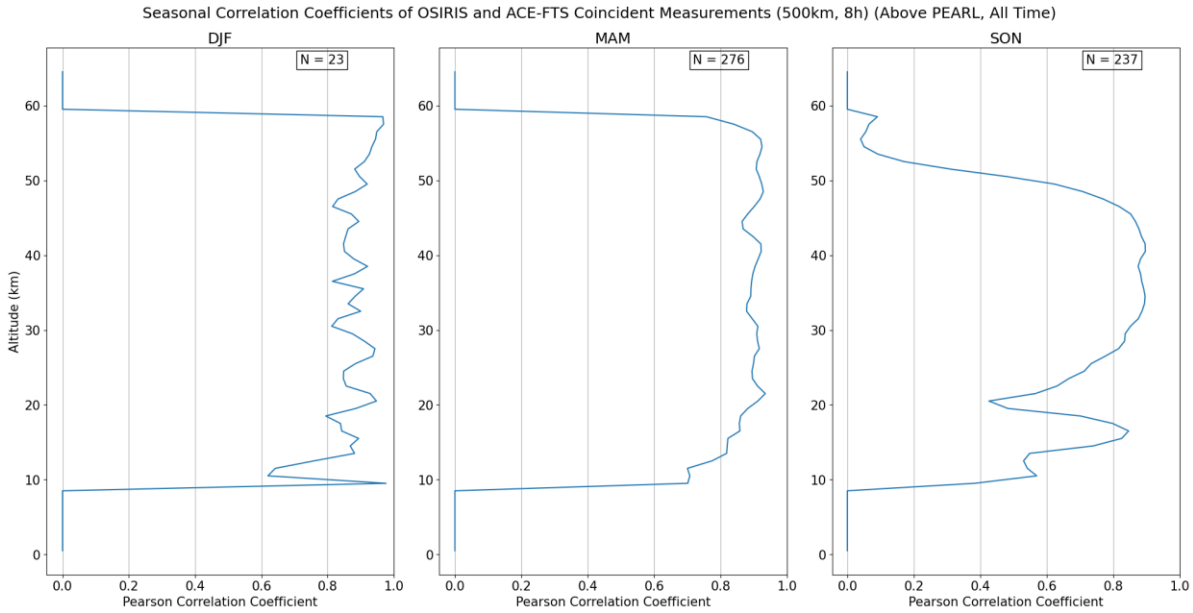

Figure 22. Seasonal plots of the Pearson correlation coefficient of all OSIRIS and ACE-FTS coincident ozone measurements above PEARL at each altitude. Plot of JJA season is missing due to lack of coincident measurements. N is the number of coincidences.

Excluding boreal fall season, the Pearson correlation coefficient plots in Figures 21 and 22 show that the measurements above PEARL have high correlation ($r > 0.8$) throughout the stratosphere and into the mesosphere unlike global coincident measurements. These plots suggest that the measurements above PEARL are more strongly correlated compared to global measurements. However, during boreal fall, the measurements above PEARL are generally less correlated compared to global measurements.

3.2.2 Satellite-based vs PEARL FTIR Profile Comparisons

3.2.2.1 ACE-FTS vs PEARL FTIR Profile Comparisons

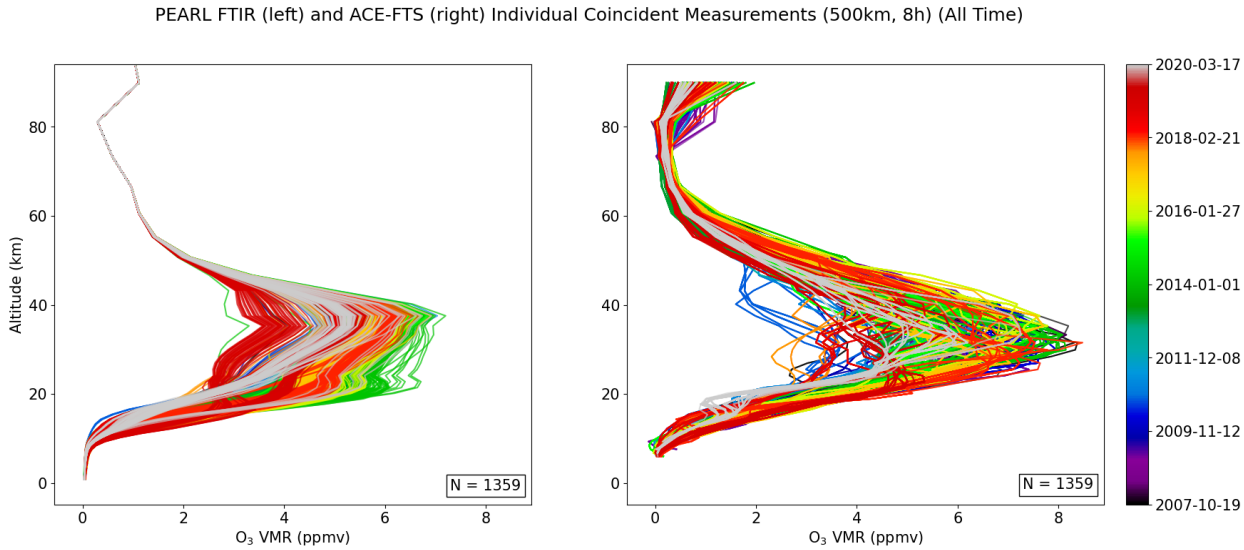

Figure 23. Plots of individual coincident ozone profiles from PEARL FTIR (left) and ACE-FTS (right). N is the number of coincidences.

Figure 24 shows that there are no ACE-FTS measurements above PEARL during boreal summer. In the other seasons, ACE-FTS has a narrower and slightly misaligned peak relative to PEARL FTIR, indicating less variability around the peak. However, ACE-FTS has more variability at higher altitudes (altitudes > 45 km) due to PEARL FTIR's retrievals being less sensitive to the atmospheric composition at higher altitudes. The decreased sensitivity causes PEARL FTIR's measurements to converge on the a priori estimate of atmospheric composition.

Figure 25 shows good agreement between the coincident measurements since most of the differences are confined between -0.5 - 0.5 ppmv. The seasonal plot in Figure 26 shows that during boreal fall, the absolute difference plot has a negative peak beginning from about 22 km to 43 km, meaning that ACE-FTS measurements are lower on average than the PEARL FTIR measurements within this altitude range. During other seasons, mean differences oscillate near zero without outliers.

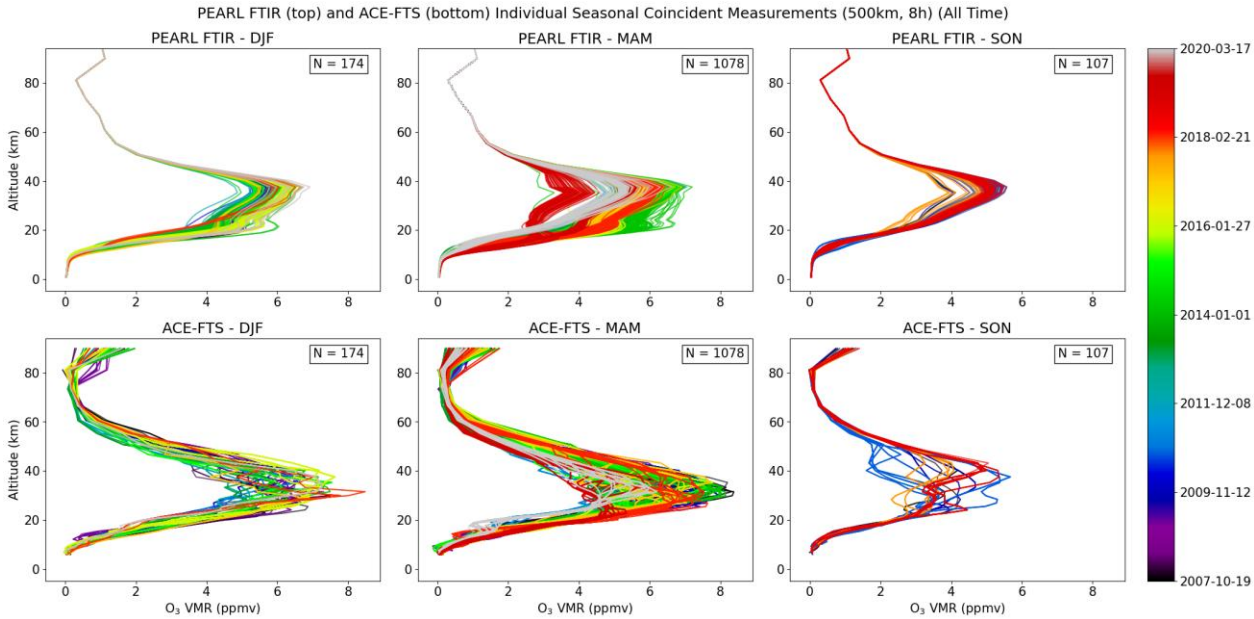

Figure 24. Seasonal plots of individual coincident ozone profiles from PEARL FTIR (top) and ACE-FTS (bottom). Plot of JJA season is missing due to lack of coincident measurements. N is the number of coincidences.

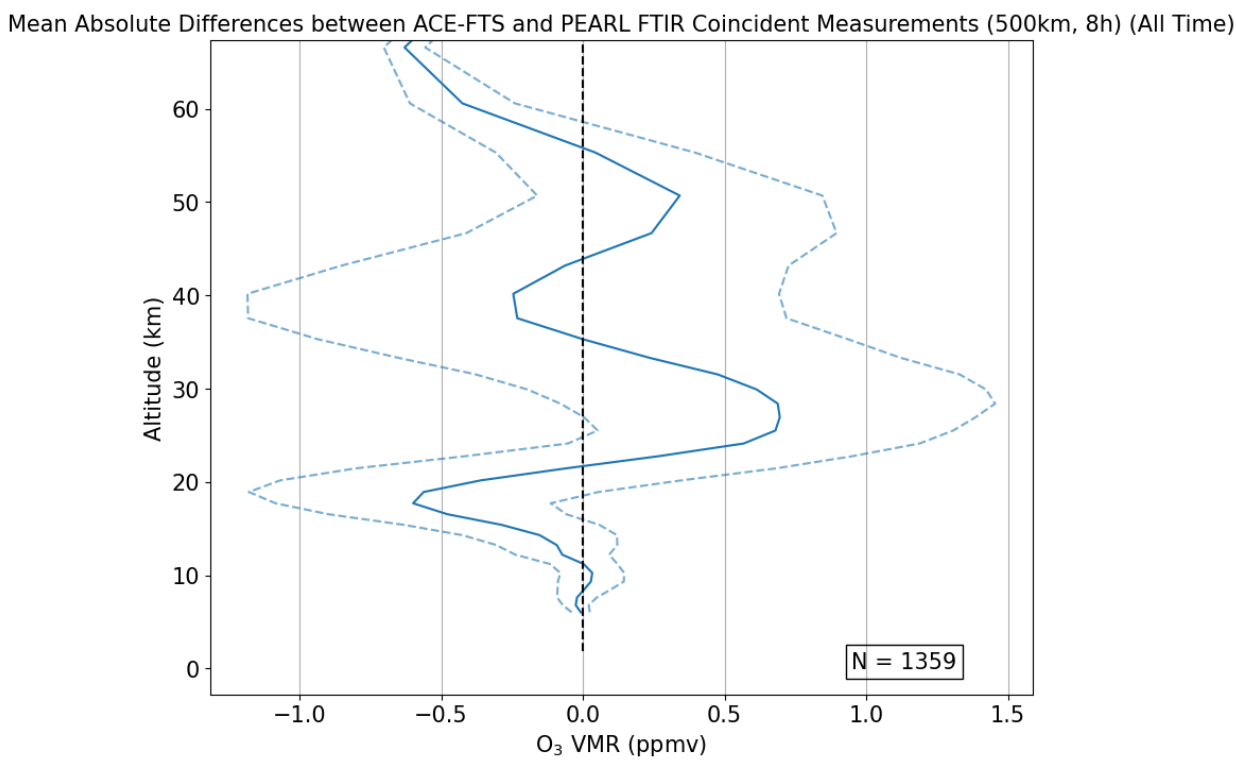

Figure 25. Plot of the mean absolute difference of all ACE-FTS and PEARL FTIR coincident ozone measurements at each altitude. N is the number of coincidences. Dashed boundaries represent one standard deviation from the mean.

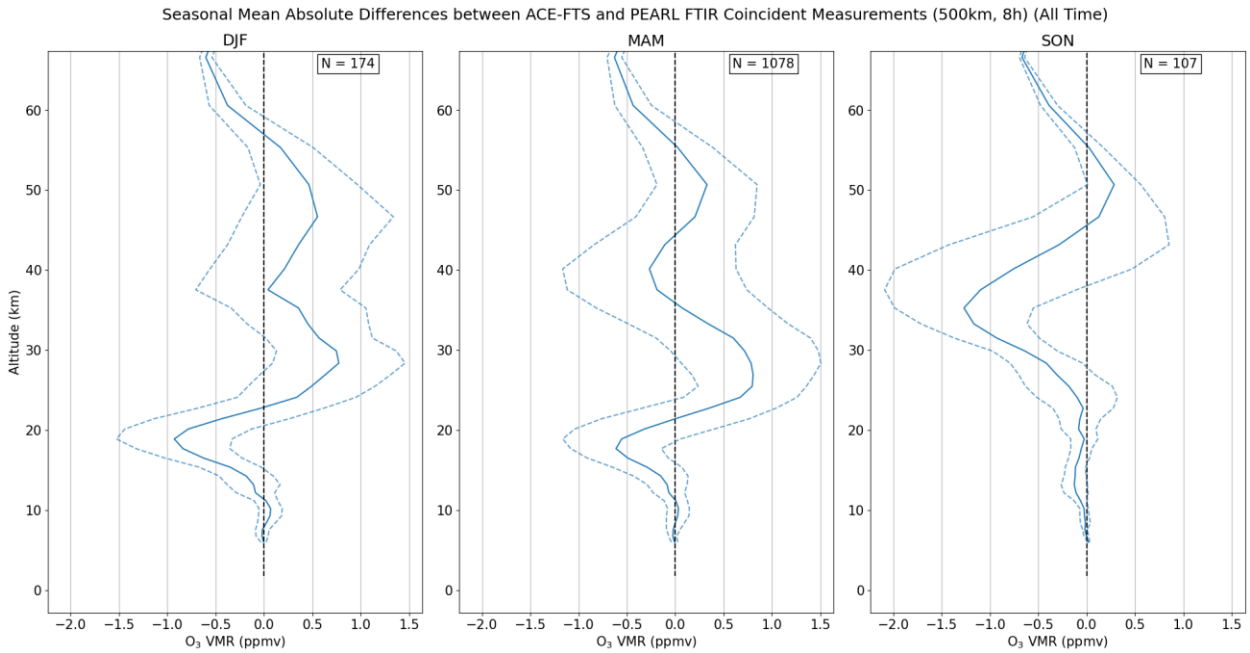

Figure 26. Seasonal plots of the mean absolute difference of all ACE-FTS and PEARL FTIR coincident ozone measurements at each altitude. Plot of JJA season is missing due to lack of coincident measurements. N is the number of coincidences. Dashed boundaries represent one standard deviation from the mean.

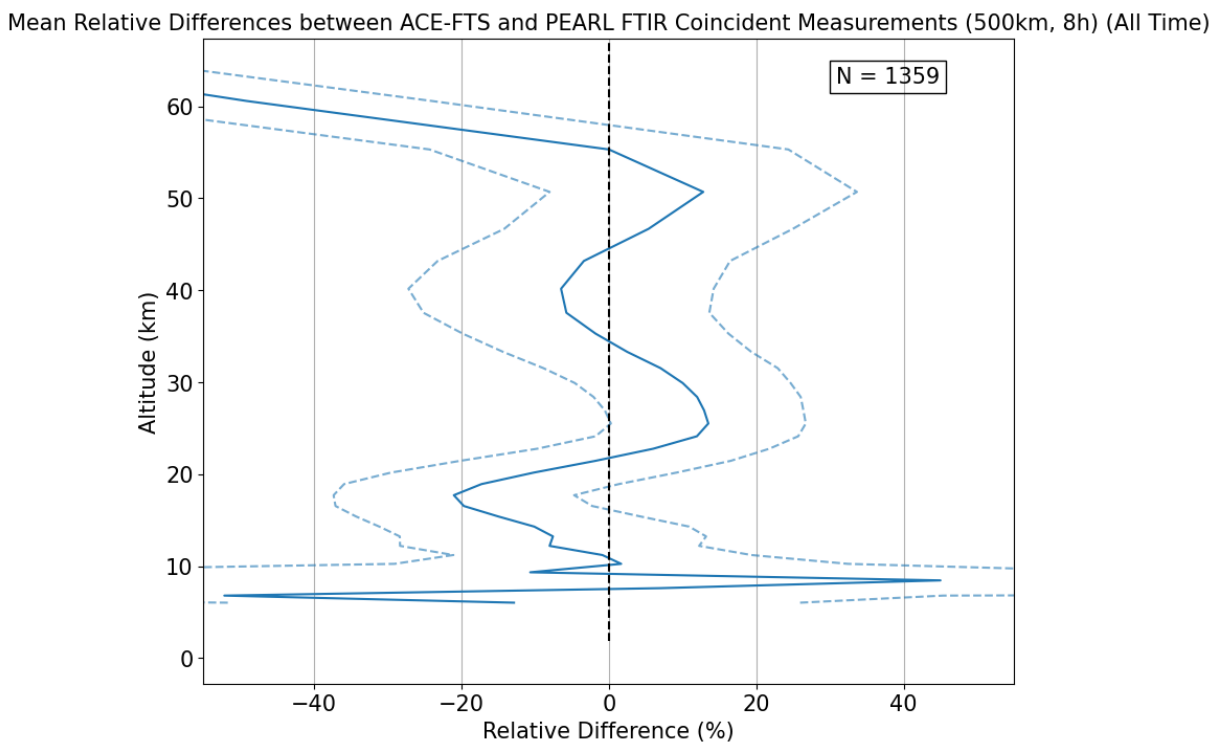

Figure 27. Plot of the mean relative difference of all ACE-FTS and PEARL FTIR coincident ozone measurements at each altitude. N is the number of coincidences. Dashed boundaries represent one standard deviation from the mean.

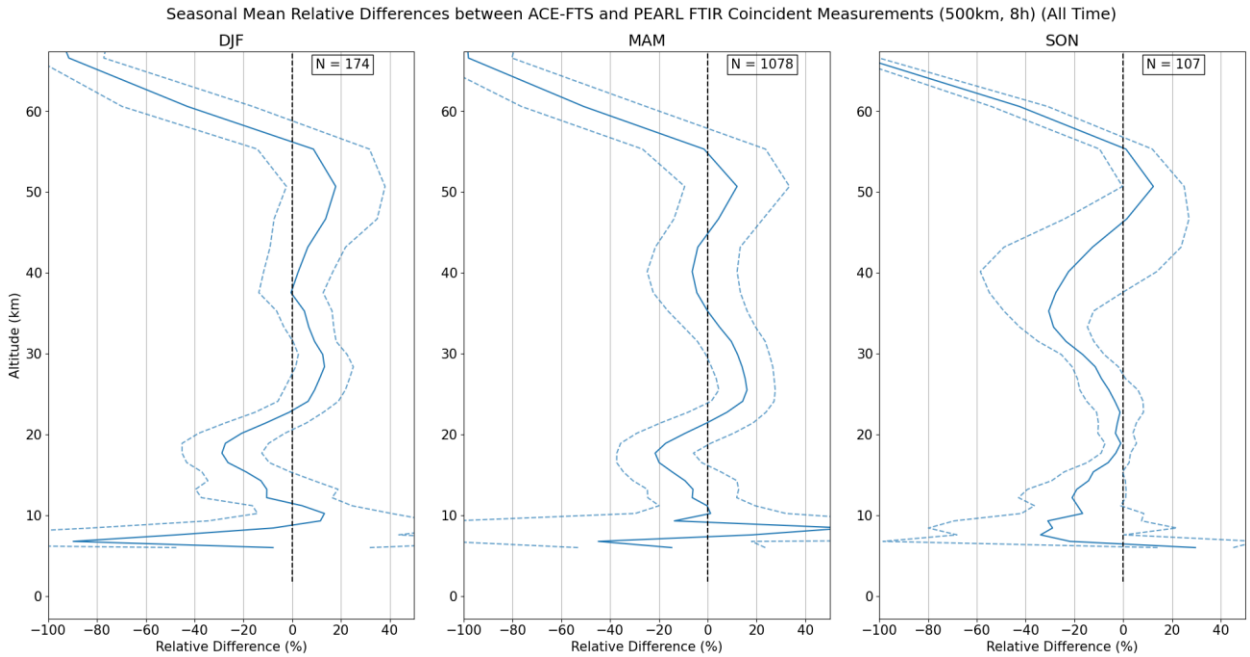

Figure 28. Seasonal plots of the mean relative difference of all ACE-FTS and PEARL FTIR coincident ozone measurements at each altitude. Plot of JJA season is missing due to lack of coincident measurements. N is the number of coincidences. Dashed boundaries represent one standard deviation from the mean.

The relative difference plots in Figures 27 and 28 mirror the same pattern observed in the absolute difference plots including the peak in boreal fall. Most of the seasonal relative differences are confined between -20 and 20 % which indicates that the measurements tend to agree.

Figures 29 and 30 indicate that the measurements are not highly correlated ($r < 0.8$). However, considering the mean difference plots, it seems like on average, the measurements tend to be similar. The higher variability of measurements is a probable cause of the Pearson correlation coefficient plots suggesting low correlation at higher stratospheric altitudes.

In comparison to the ACE-FTS and PEARL FTIR individual coincident profiles plot, the peaks and variability of OSIRIS and PEARL FTIR coincident profiles in Figures 31 and 32 seem to align more closely. Most of the coincident measurements occur during boreal spring and summer due to the orbital path of Odin.

As Figures 31 and 32 suggest, the instruments do indeed have very good agreement, with mean absolute difference being mostly confined between -0.25 and 0.25 ppmv shown in Figure 33. Figure 34 also has a peak like the one seen in Figure 26 in the same season. The mean absolute difference in the rest of the seasons oscillate close to 0 and are mostly confined between -0.5 and 0.5 ppmv. Overall, these plots show that the measurements agree on average.

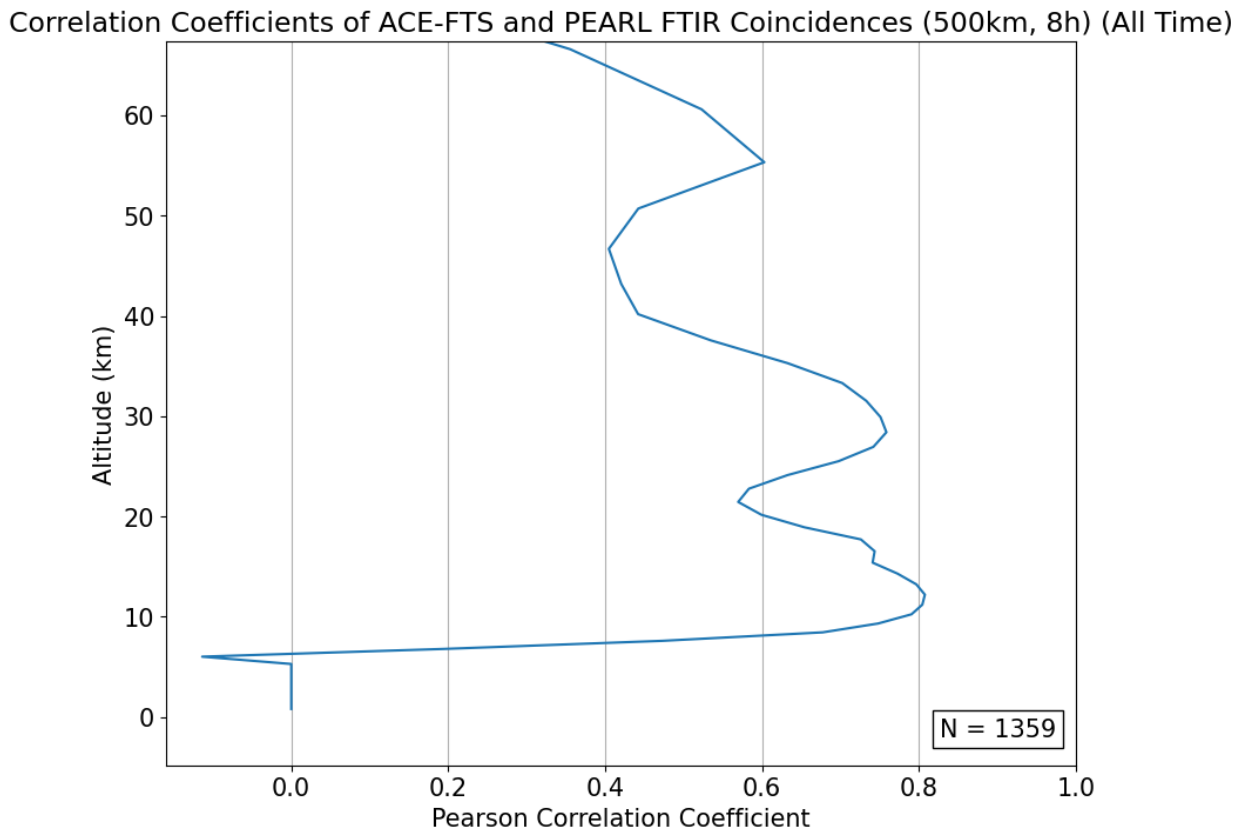

Figure 29. Plot of the Pearson correlation coefficient of all ACE-FTS and PEARL FTIR coincident ozone measurements at each altitude. N is the number of coincidences.

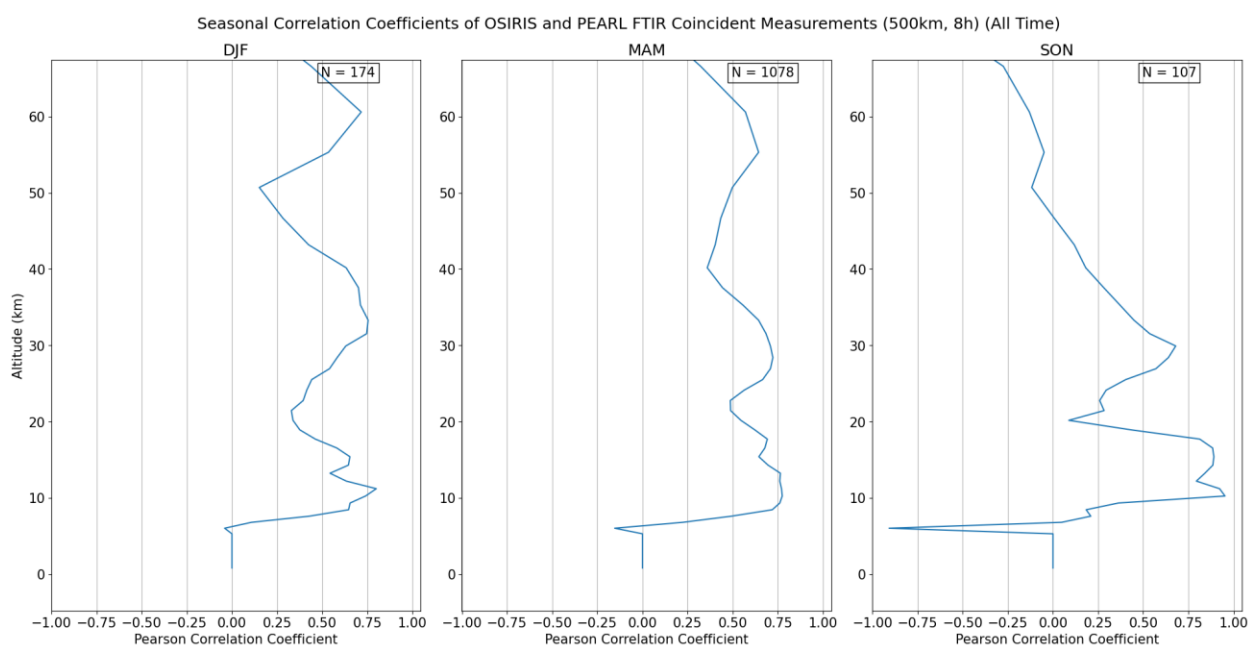

Figure 30. Seasonal plots of the Pearson correlation coefficient of all ACE-FTS and PEARL FTIR coincident ozone measurements at each altitude. Plot of JJA season is missing due to lack of coincident measurements. N is the number of coincidences.

3.2.2.2 OSIRIS vs PEARL FTIR Profile Comparisons

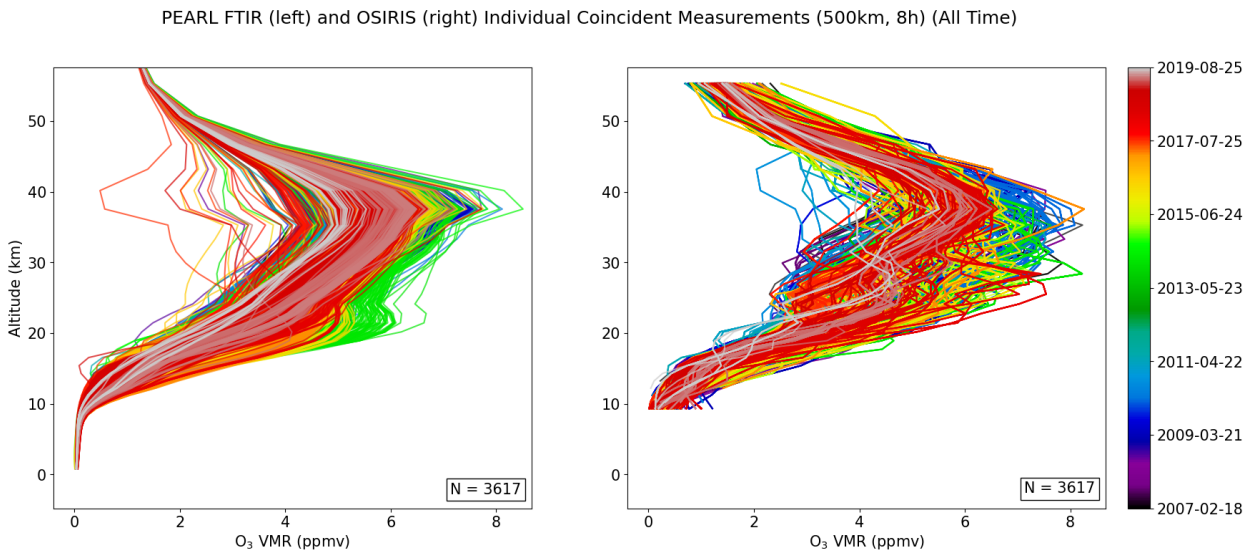

Figure 31. Plots of individual coincident ozone profiles from PEARL FTIR (left) and OSIRIS (right). N is the number of coincidences.

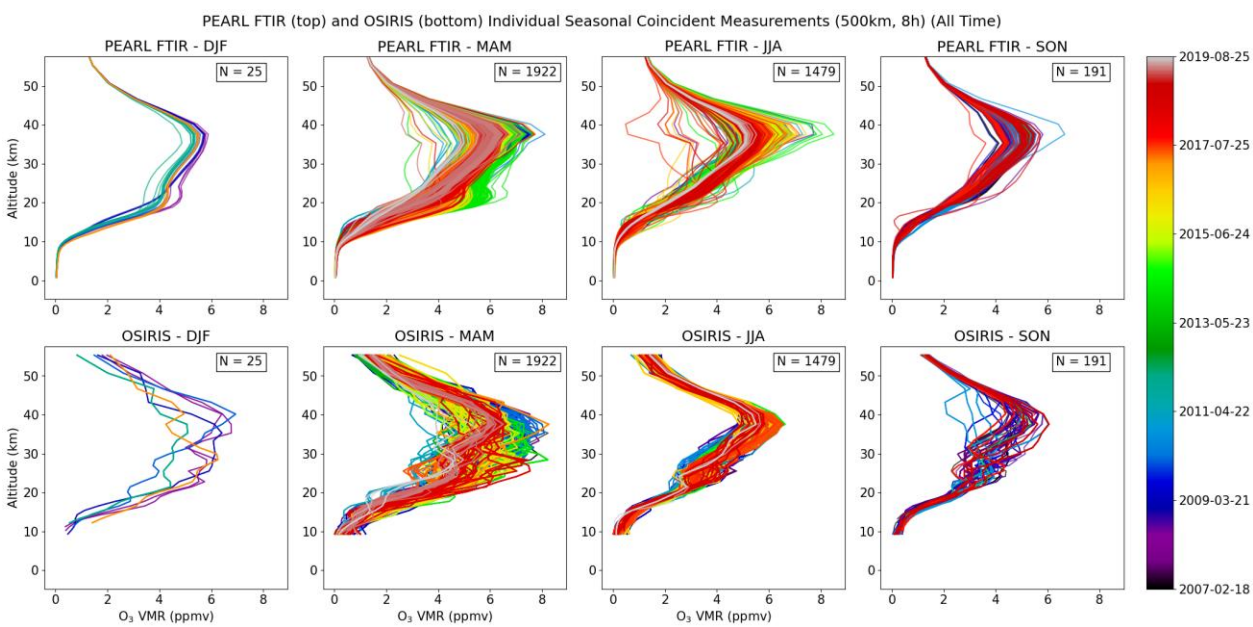

Figure 32. Seasonal plots of individual coincident ozone profiles from PEARL FTIR (top) and OSIRIS (bottom). N is the number of coincidences.

The relative difference plots in Figures 35 and 36 further affirms that on average, the measurements converge towards each other just as the previous figures suggest. Across seasons, mean relative differences typically span -12.5 to 12.5 %. In contrast, Figure 35's differences lie within -5 to 7.5 %, reflecting stronger aggregate agreement.

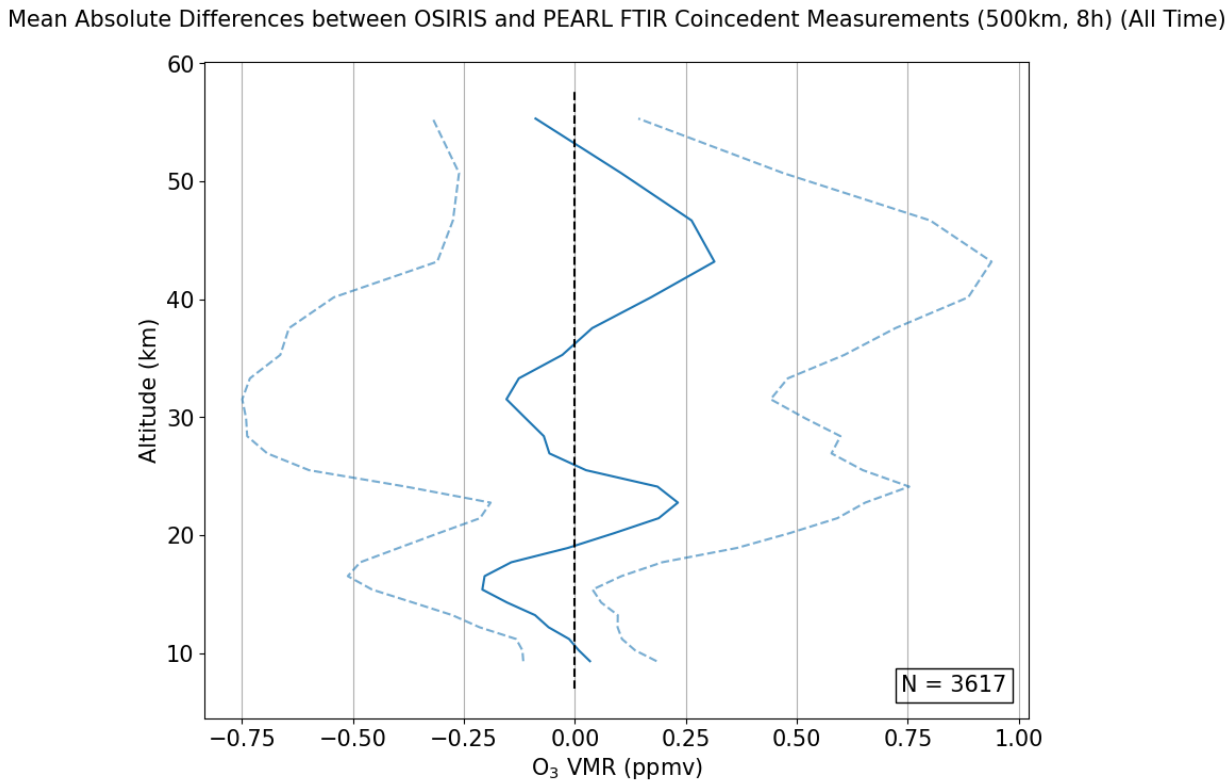

Figure 33. Plot of the mean absolute difference of all OSIRIS and PEARL FTIR coincident ozone measurements at each altitude. N is the number of coincidences. Dashed boundaries represent one standard deviation from the mean.

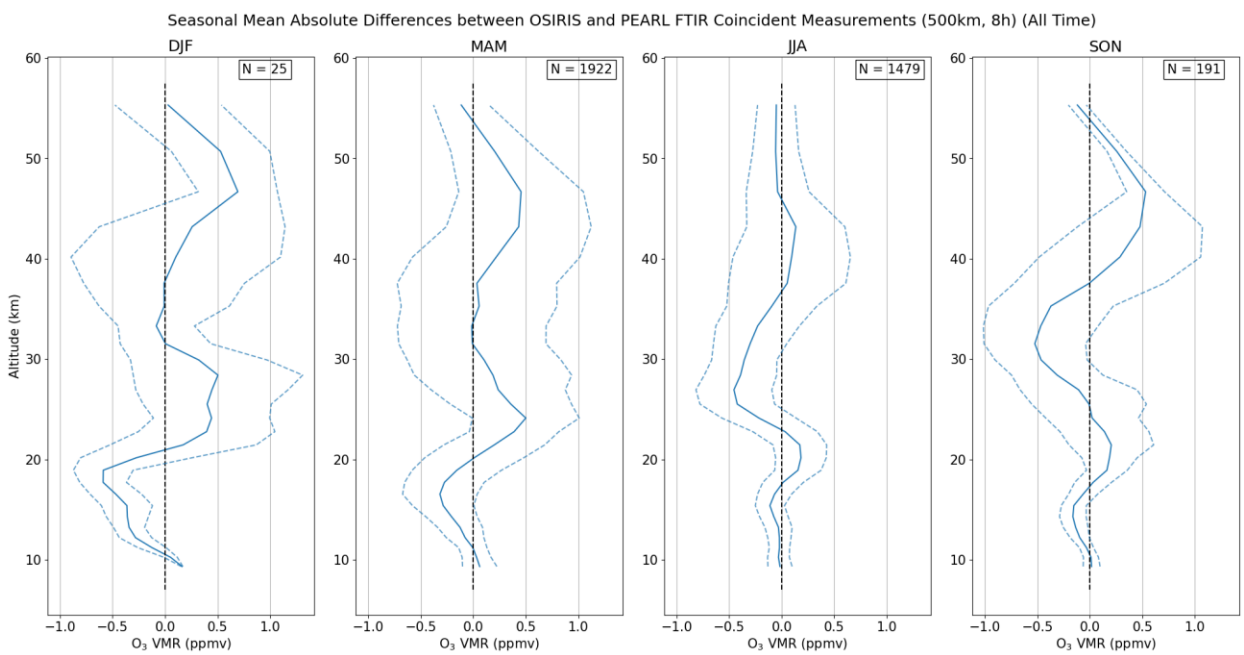

Figure 34. Seasonal plots of the mean absolute difference of all OSIRIS and PEARL FTIR coincident ozone measurements at each altitude. N is the number of coincidences. Dashed boundaries represent one standard deviation from the mean.

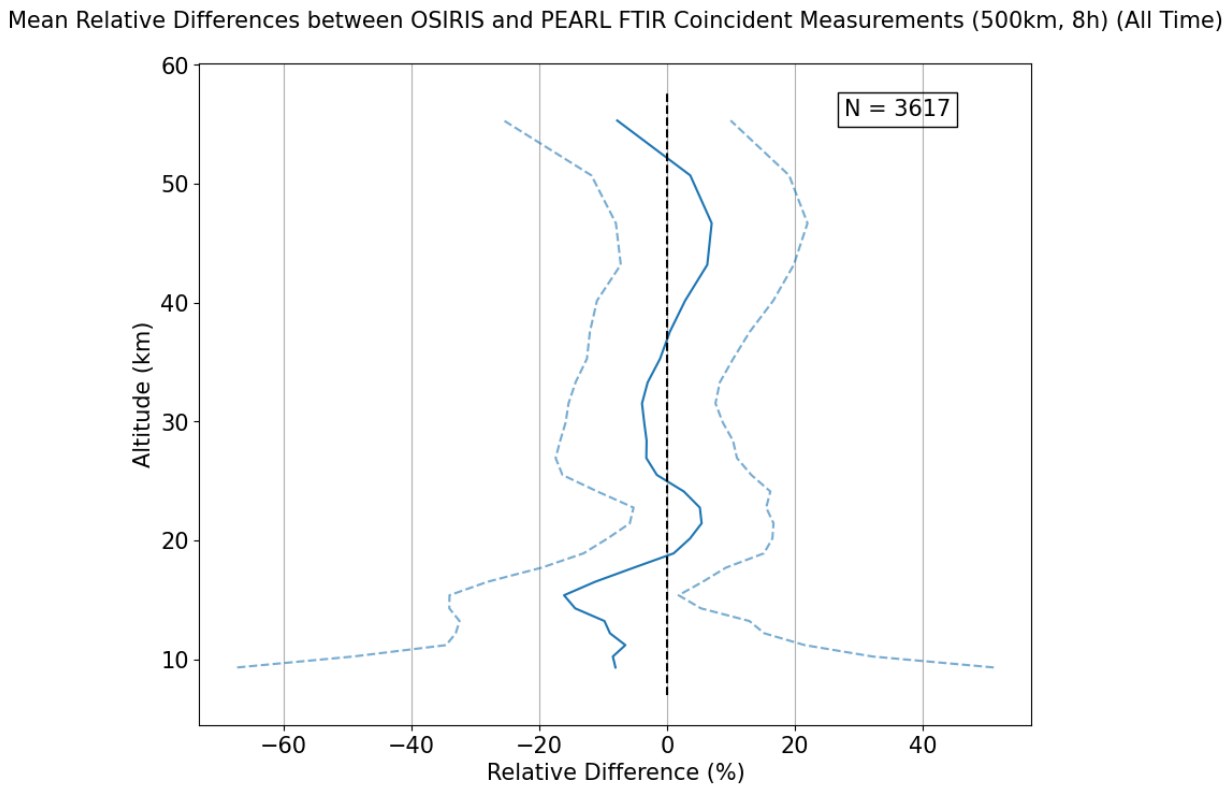

Figure 35. Plot of the mean relative difference of all OSIRIS and PEARL FTIR coincident ozone measurements at each altitude. N is the number of coincidences. Dashed boundaries represent one standard deviation from the mean.

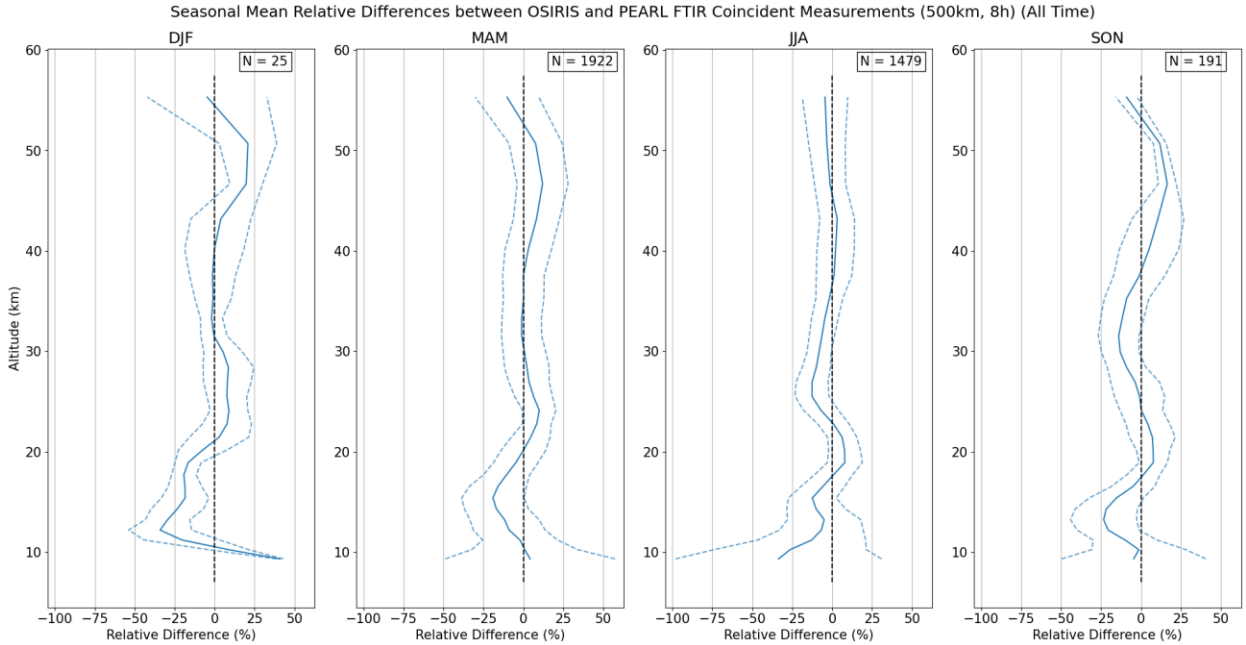

Figure 36. Seasonal plots of the mean absolute difference of all OSIRIS and PEARL FTIR coincident ozone measurements at each altitude. N is the number of coincidences. Dashed boundaries represent one standard deviation from the mean.

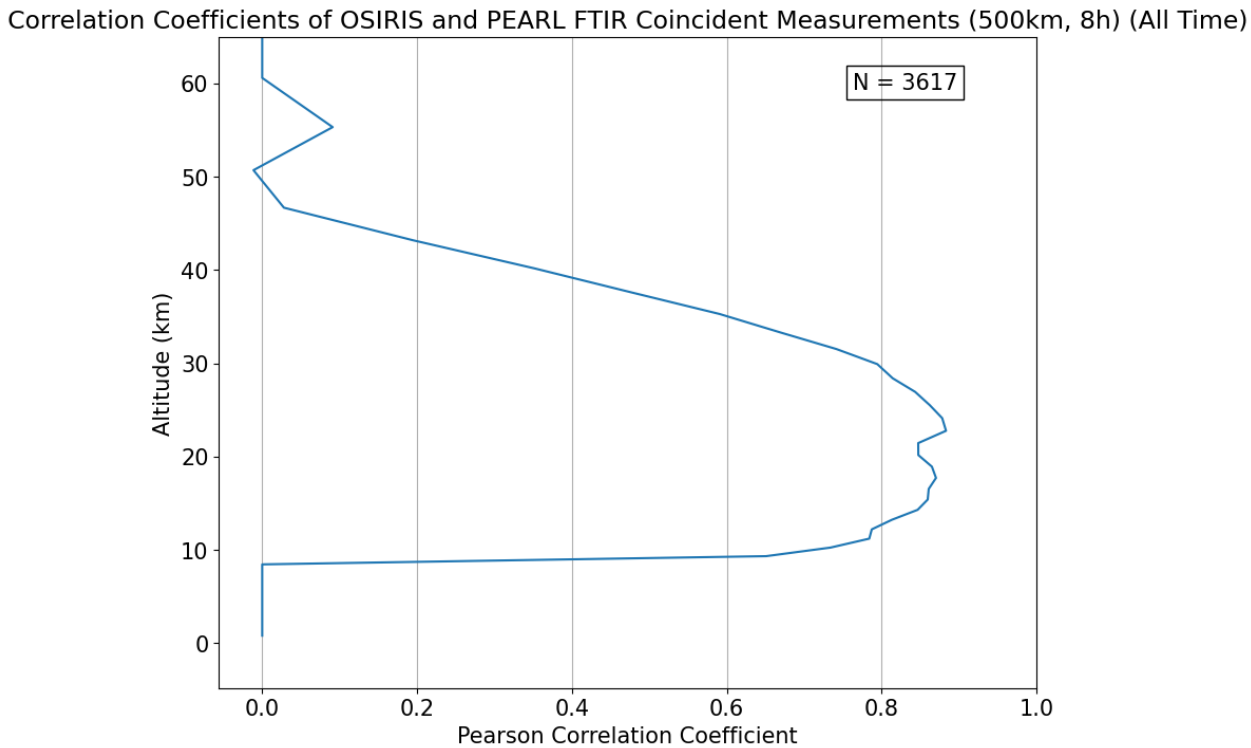

Figure 37. Plot of the Pearson correlation coefficient of all OSIRIS and PEARL FTIR coincident ozone measurements at each altitude. N is the number of coincidences.

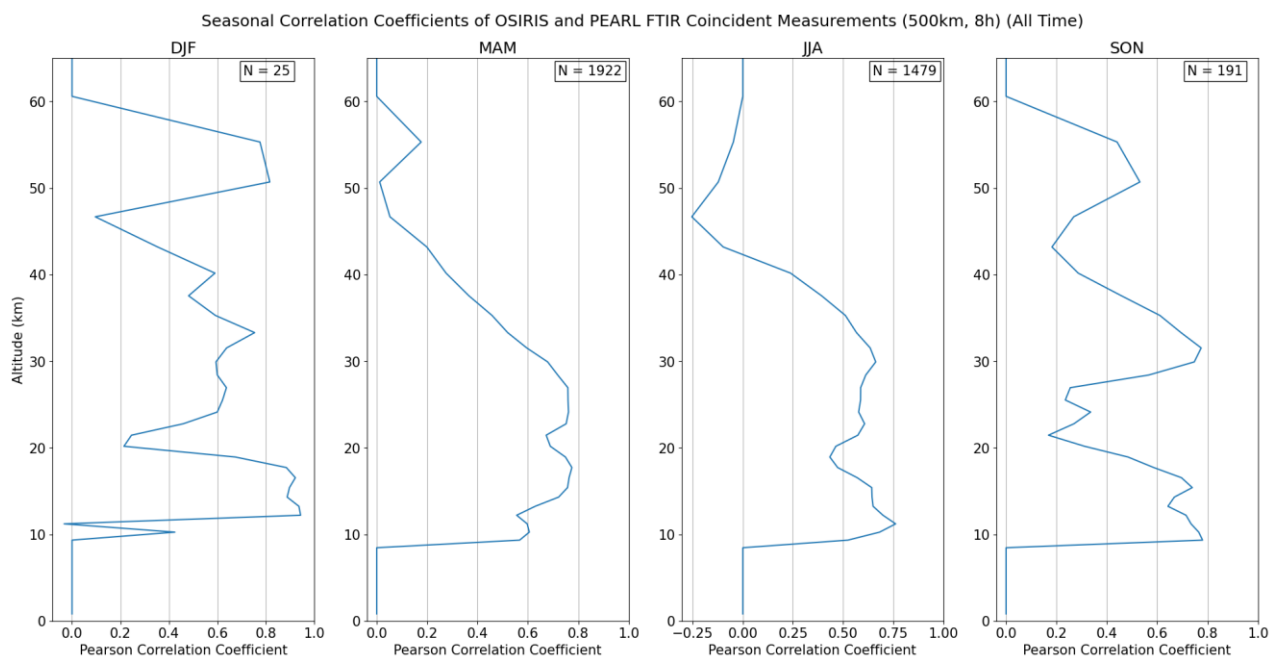

Figure 38. Seasonal plots of the Pearson correlation coefficient of all OSIRIS and PEARL FTIR coincident ozone measurements at each altitude. N is the number of coincidences.

Similar to the Pearson correlation coefficient plots in Figures 29 and 30, Figures 37 and 38 do not yield the same conclusions derived from the differences' plots. The correlation coefficient plots

show low correlation ($r < 0.8$) which does not reflect the agreement seen in the differences' plots. As before, despite good agreement on average, measurement variability may be the cause of this discrepancy. The correlation coefficient plots report higher correlations at lower altitudes compared to higher altitudes.

3.3 Column comparisons

Columns were calculated by first converting ozone VMR profiles to number density profiles and multiplying each altitude layer's number density by its thickness then summing up these layers' column amounts across all altitudes. Unlike ozone profile comparisons, column comparisons were not done with interpolation. To ensure column comparisons were accurate, all columns calculated from a profile with missing data at any altitude were discarded. This filtering led to a lower number of coincidences for column comparisons compared to profile comparisons. The units used to represent ozone columns in this report is Dobson Units (DU).

Each instrument pair will be presented with scatter plots of individual pairs of measurements along with a seasonal perspective and a fitted line in all scatter plots. Subsequently, individual absolute and relative column differences plotted against their measurement month will be presented. The end of this section will be assessing the extent to which the instruments' column measurements diverge over time.

3.3.1 Partial Column Altitude Range

The choice of partial column range of 10 to 51 km was consistent for all instrument pairs and can be divided into two different choices: upper bound choice and lower bound choice.

3.3.1.1 Partial Column Upper Bound Choice

The partial column upper bound of 51 km was chosen based on analysis of the averaging kernel matrix (AVK) of the PEARL FTIR retrievals. The averaging kernel of retrievals provides additional information about the retrievals such as the sensitivity of the retrieval to various altitudes which is the sum of the rows of the averaging kernel at each altitude layer (Jeffery, 2022, p. 49). Figures 55 to 57 in the appendix showcase averaging kernel data. The maximum altitude whereby the mean sensitivity of all PEARL FTIR retrievals is greater than or equal to 0.1 was the metric used for the upper bound choice. This metric ensures that the altitudes used in the columns had some impact on PEARL FTIR's retrieval and does not significantly limit the altitude range of the columns.

3.3.1.2 Partial Column Lower Bound Choice

The lower bound of 10 km was chosen to ensure a decently large, representative sample size for each instrument. Because a lower-bound below 10 km removed too many profiles, and a lower-bound above 10 km added little extra clean data, 10 km was chosen as the optimal cutoff.

3.3.2 OSIRIS vs ACE-FTS Column Comparisons

Similar to profile comparisons, OSIRIS vs ACE-FTS column comparisons will be divided into coincident comparisons globally and coincident comparisons above PEARL.

3.3.2.1 Global OSIRIS vs ACE-FTS Column Comparisons

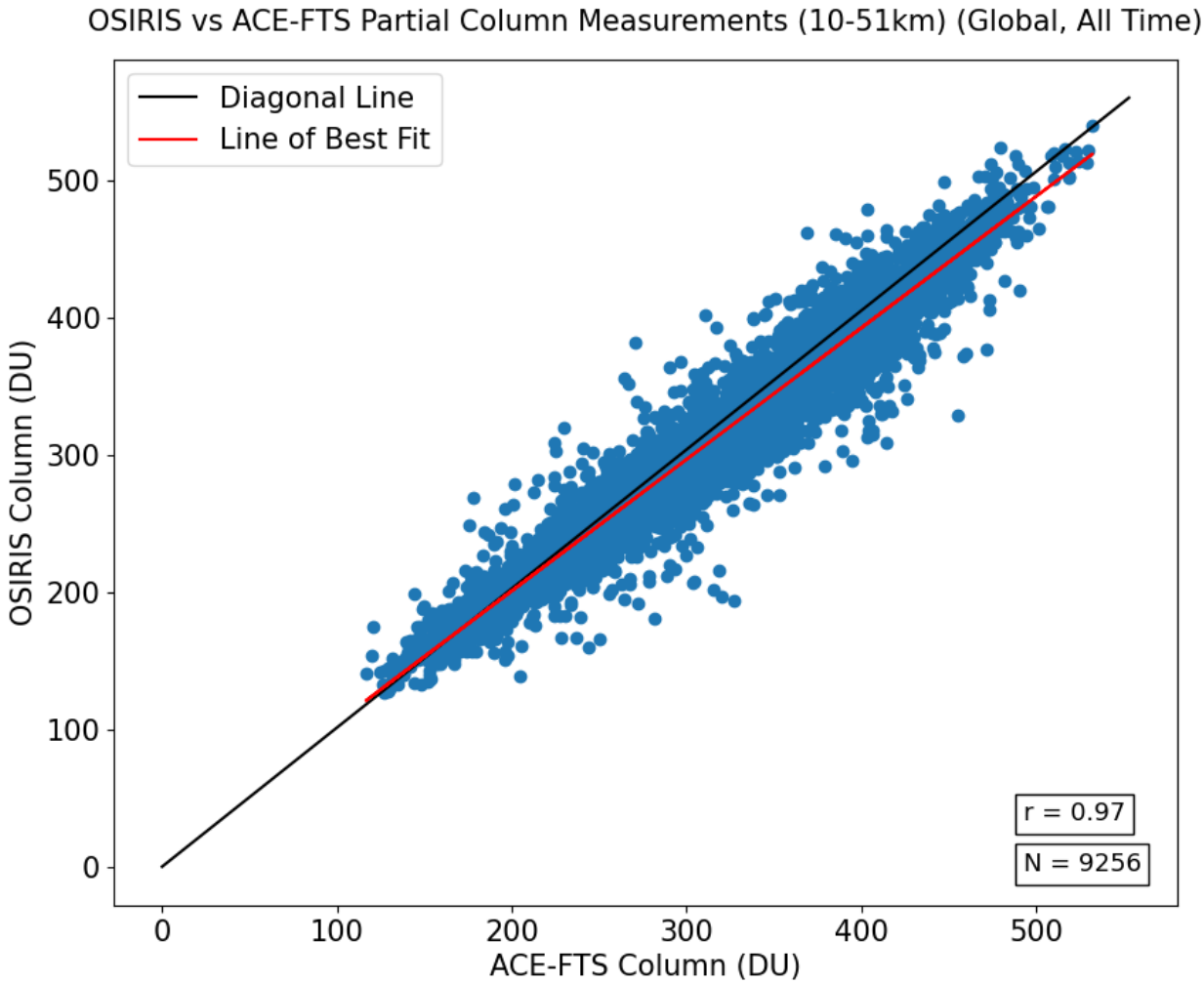

Figure 39. Plot of OSIRIS and ACE-FTS global coincident ozone column measurements. N and r represent number of coincidences and Pearson correlation coefficient, respectively.

Figures 39 and 40 show that the column measurements of OSIRIS and ACE-FTS globally are highly correlated (r = 0.97). This high correlation is also present in all seasons with boreal winter having the highest correlation of 0.96 and boreal summer having the lowest correlation of 0.92.

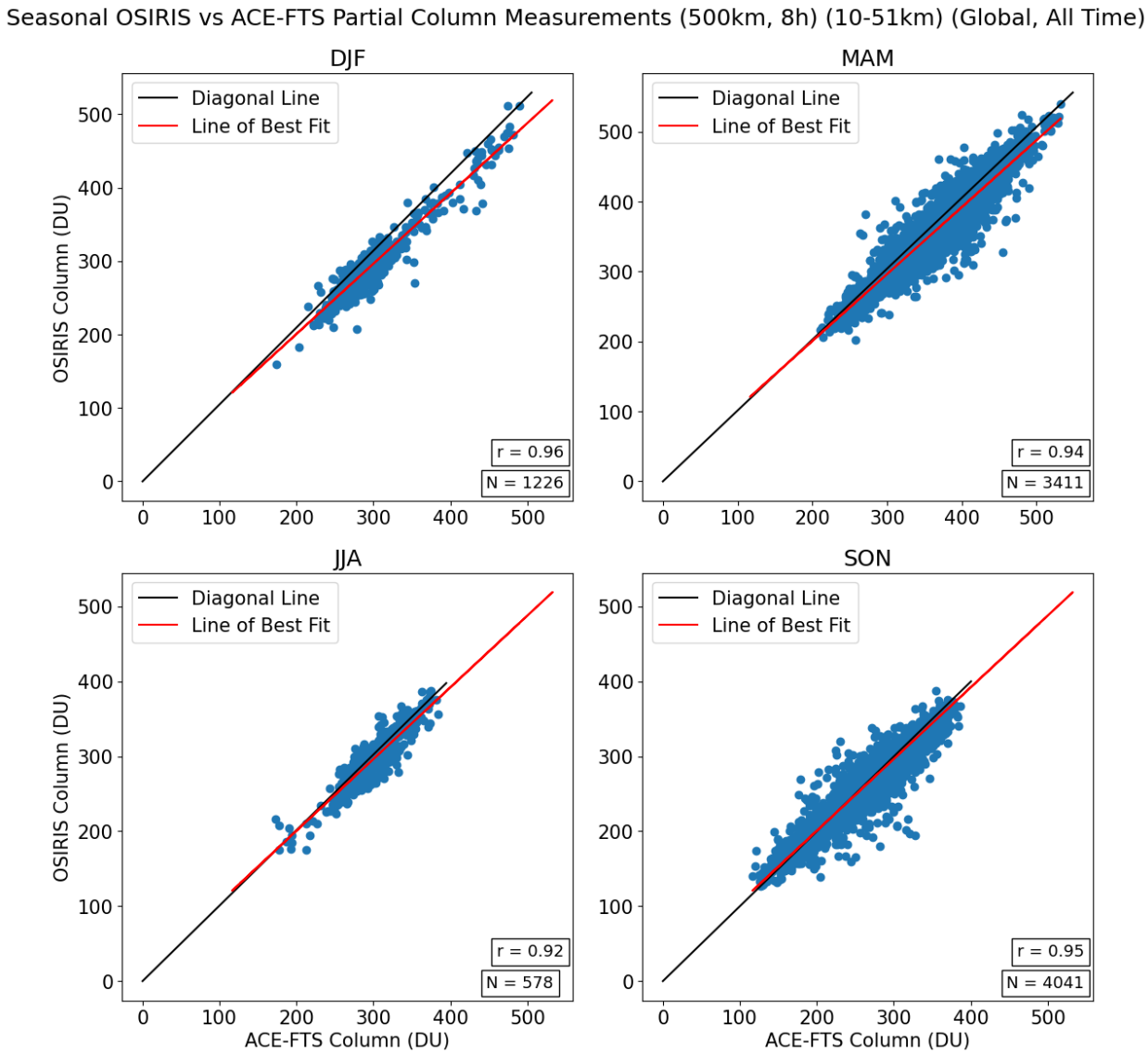

Figure 40. Seasonal plots of OSIRIS and ACE-FTS global coincident ozone column measurements. N and r represent number of coincidences and Pearson correlation coefficient, respectively.

Figures 41 and 42 further supports the conclusion that the instruments' column measurements are similar. Most of the absolute differences and relative differences in the plots are concentrated near 0 DU and 0 %, respectively, including the mean differences, indicating high consistency. This trend is consistent across all months, although, measurements made in March and November exhibit larger differences compared to other months.

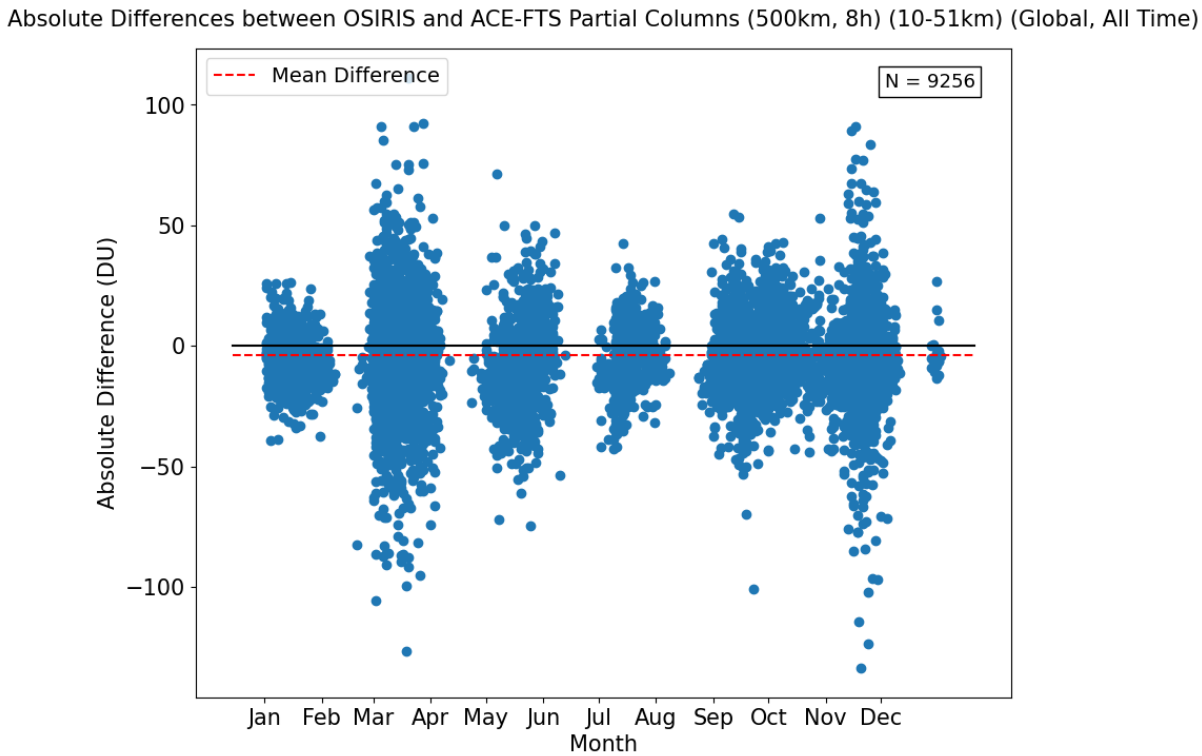

Figure 41. Plot of absolute differences between OSIRIS and ACE-FTS global coincident ozone column measurements. N is the number of coincidences.

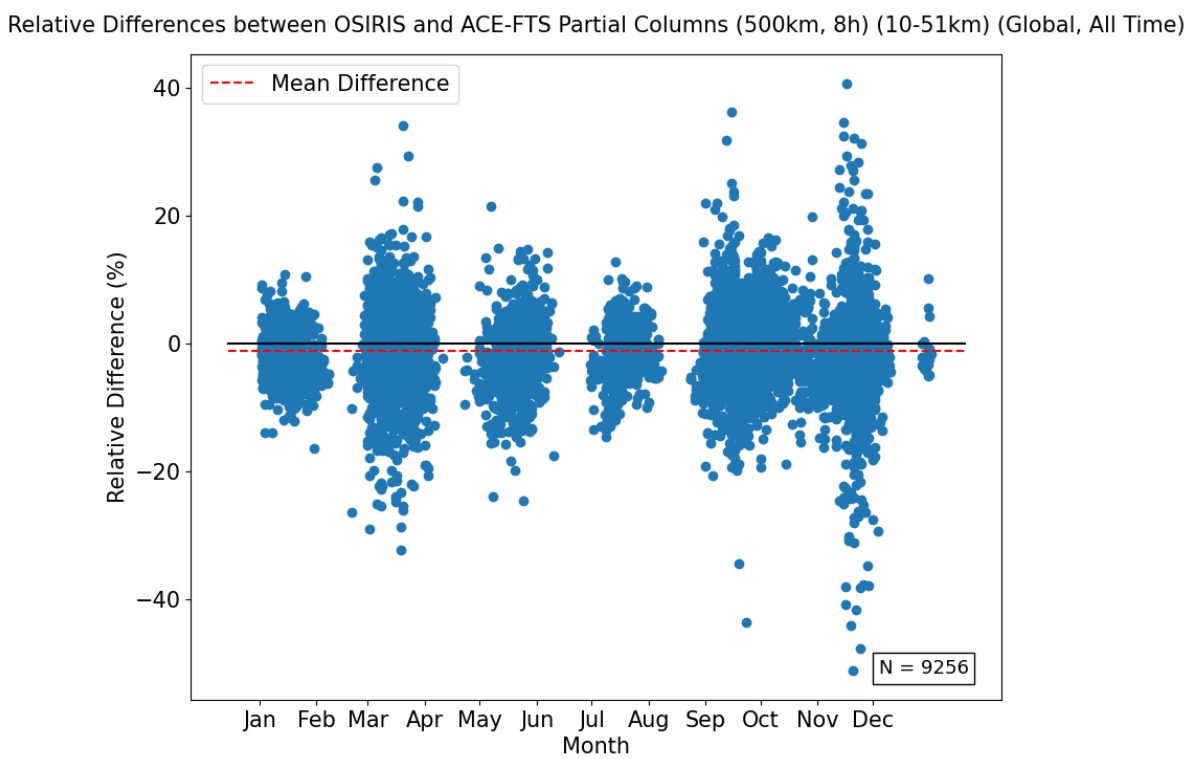

Figure 42. Plot of relative differences between OSIRIS and ACE-FTS global coincident ozone column measurements. N is the number of coincidences.

3.3.2.2 Above PEARL OSIRIS vs ACE-FTS Column Comparisons

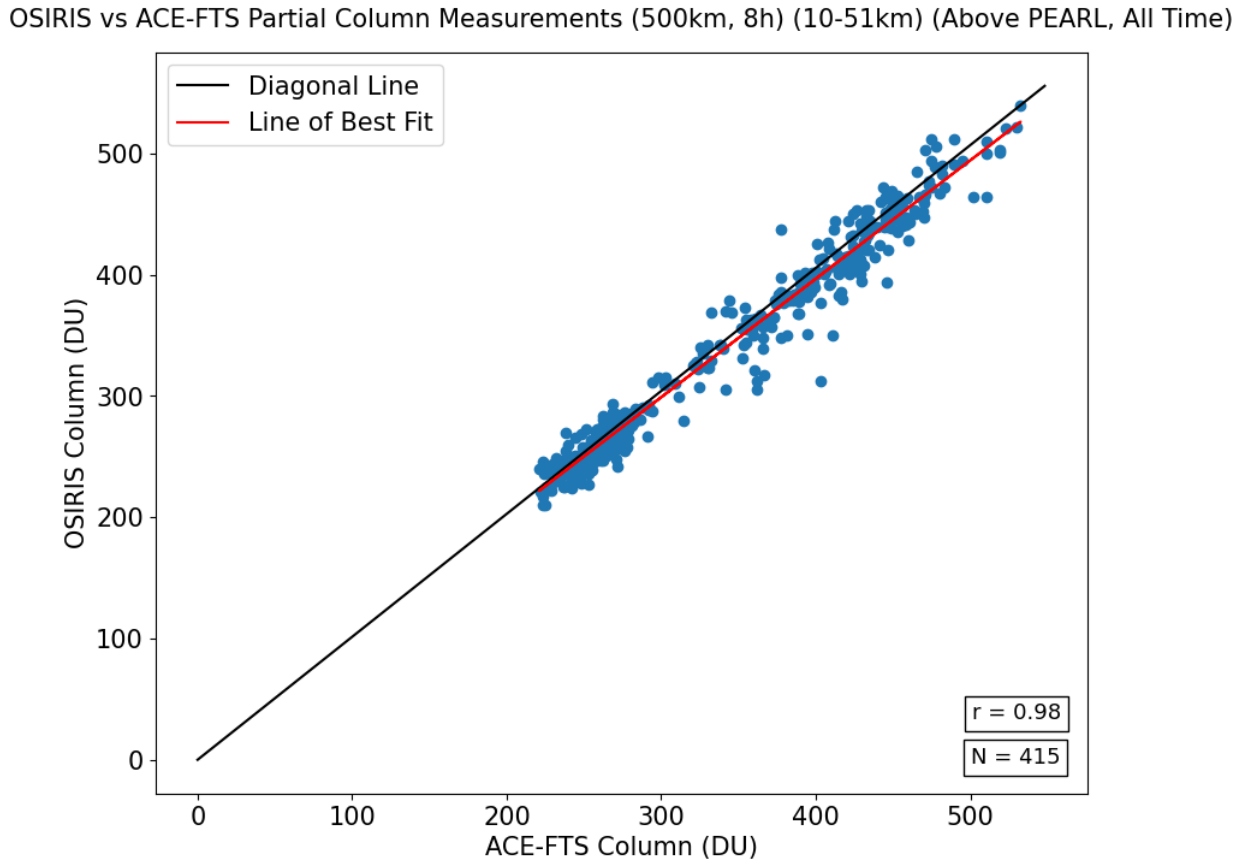

Figure 43. Plot of OSIRIS and ACE-FTS coincident ozone column measurements above PEARL. N and r represent number of coincidences and Pearson correlation coefficient, respectively.

Similar to Figures 39 and 40, Figures 43 and 44 show high correlation ($r > 0.8$) between column measurements across all seasons. However, there is a notable decrease in correlation in the boreal fall season compared to the other seasons. Overall, coincident measurements seem to have better agreement above PEARL than globally.

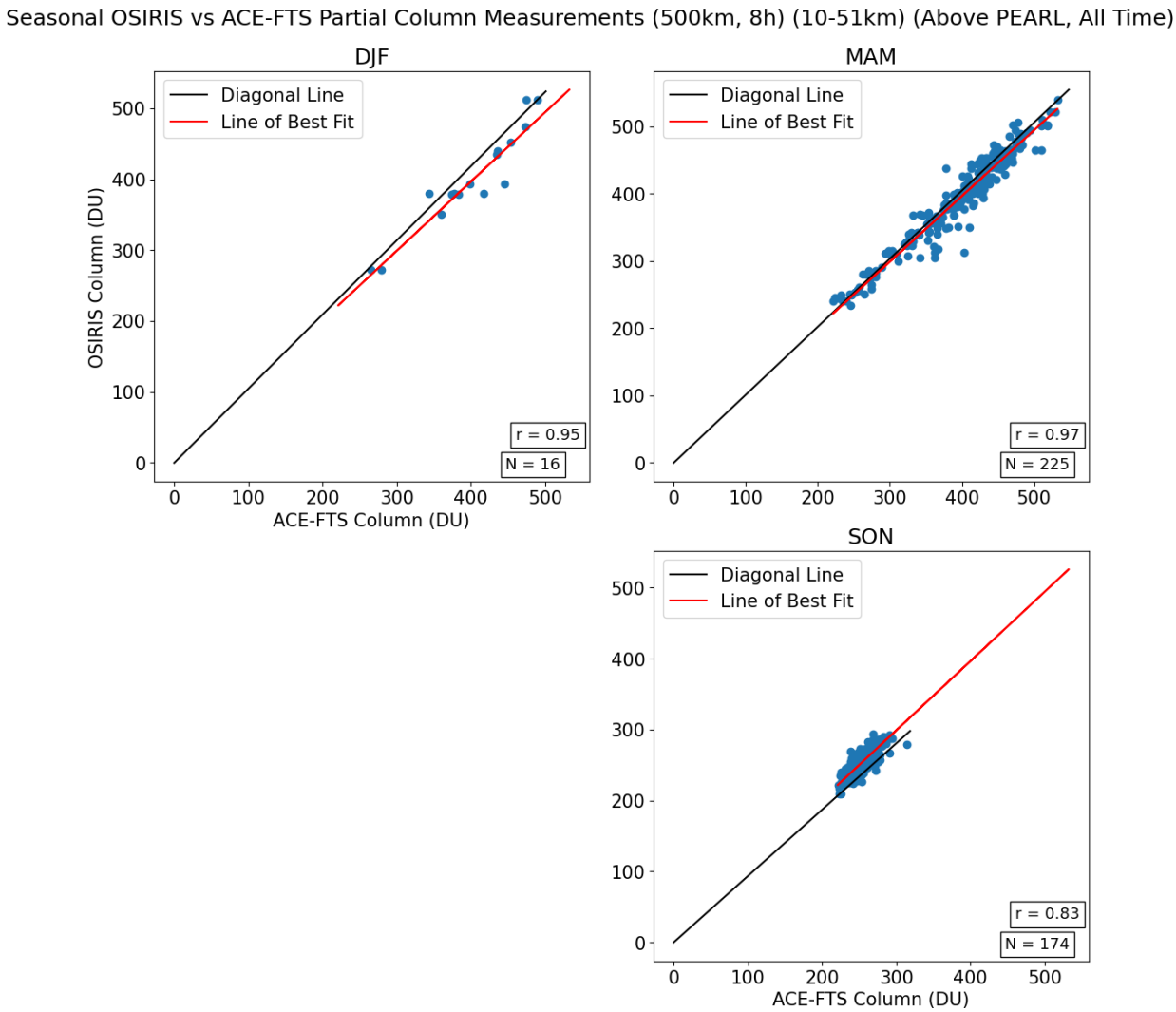

Figure 44. Seasonal plots of OSIRIS and ACE-FTS coincident ozone column measurements above PEARL. Plot of JJA season is missing due to lack of coincident measurements. N and r represent number of coincidences and Pearson correlation coefficient, respectively.

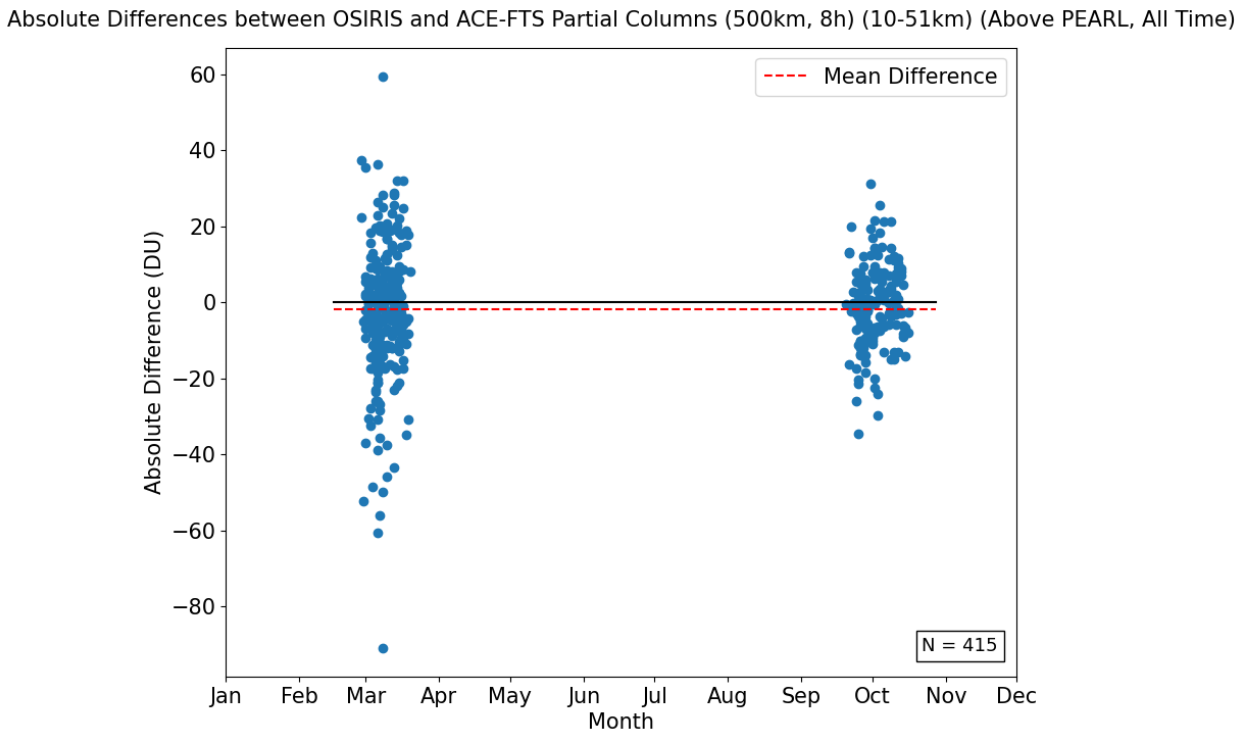

Figure 45. Plot of absolute differences between OSIRIS and ACE-FTS coincident ozone column measurements above PEARL. N is the number of coincidences.

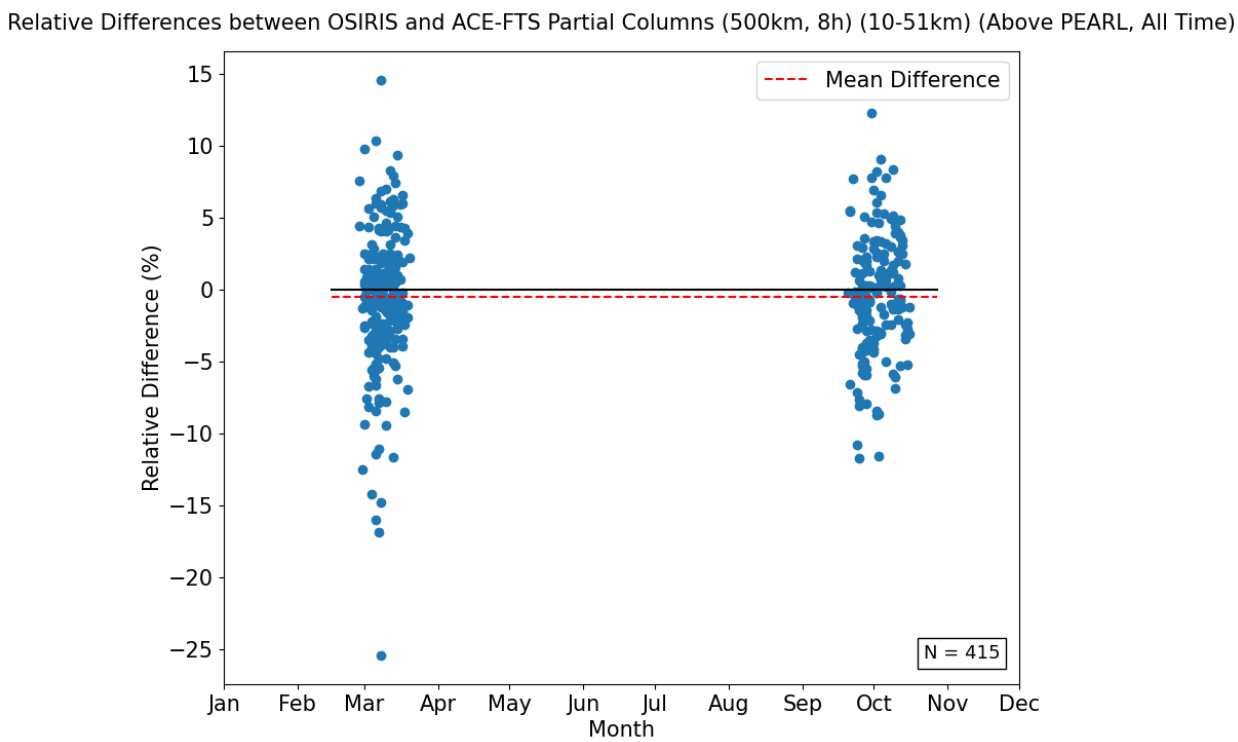

Figure 46. Plot of relative differences between OSIRIS and ACE-FTS coincident ozone column measurements above PEARL. N is the number of coincidences.

Due to the requirement that measurements are above PEARL, the coincident measurement differences in Figures 45 and 46 are sparser throughout the year. During the months where coincident measurements occur above PEARL, the differences are more concentrated and less scattered around zero compared to global coincident column differences. The differences plots demonstrate that the measurements are close in agreement due to most individual differences and the mean difference being close to 0 (DU or %).

3.3.3 Satellite-based vs PEARL FTIR Column Comparisons

3.3.3.1 ACE-FTS vs PEARL FTIR Column Comparisons

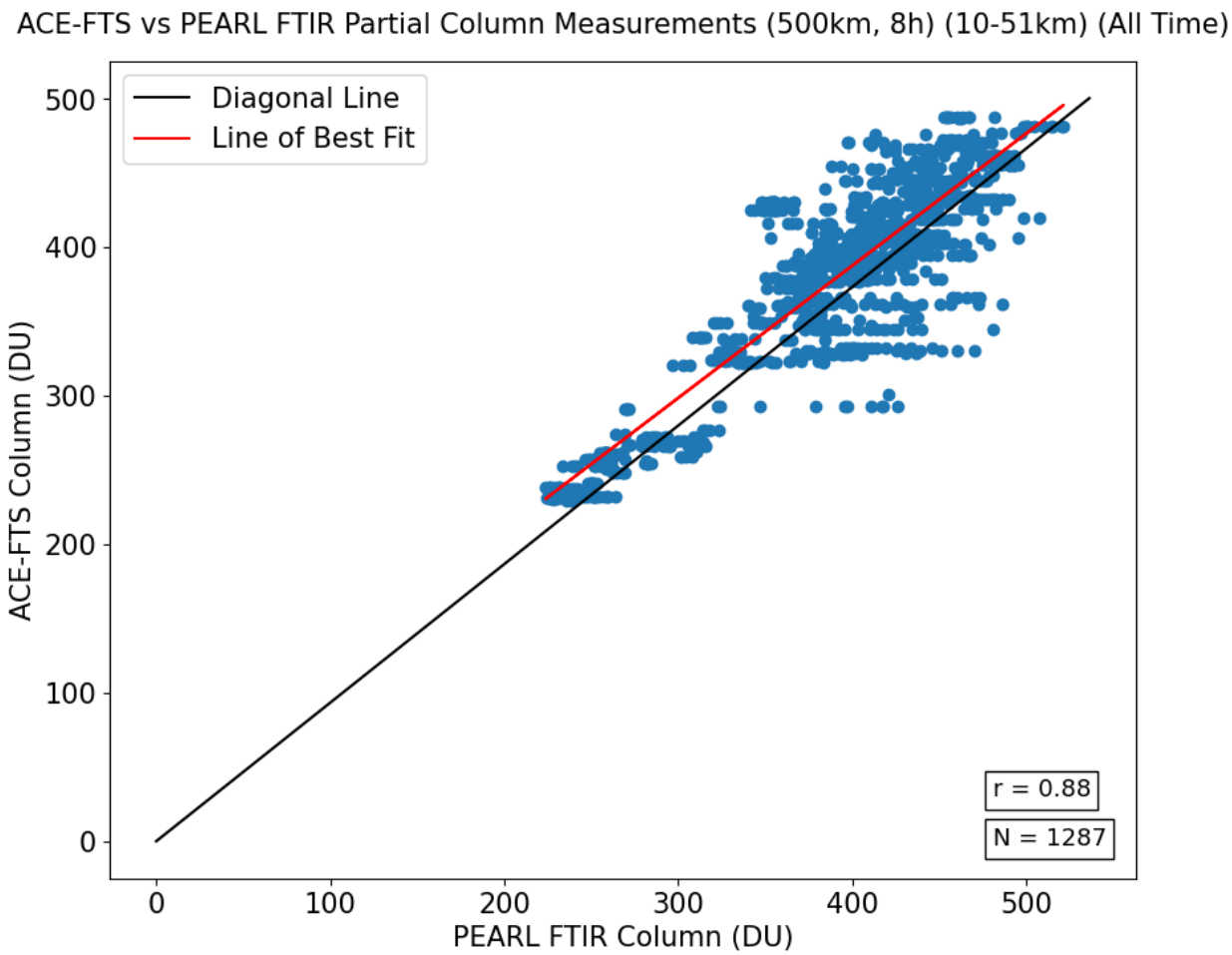

Figure 47. Plot of ACE-FTS and PEARL FTIR coincident ozone column measurements. N and r represent number of coincidences and Pearson correlation coefficient, respectively.

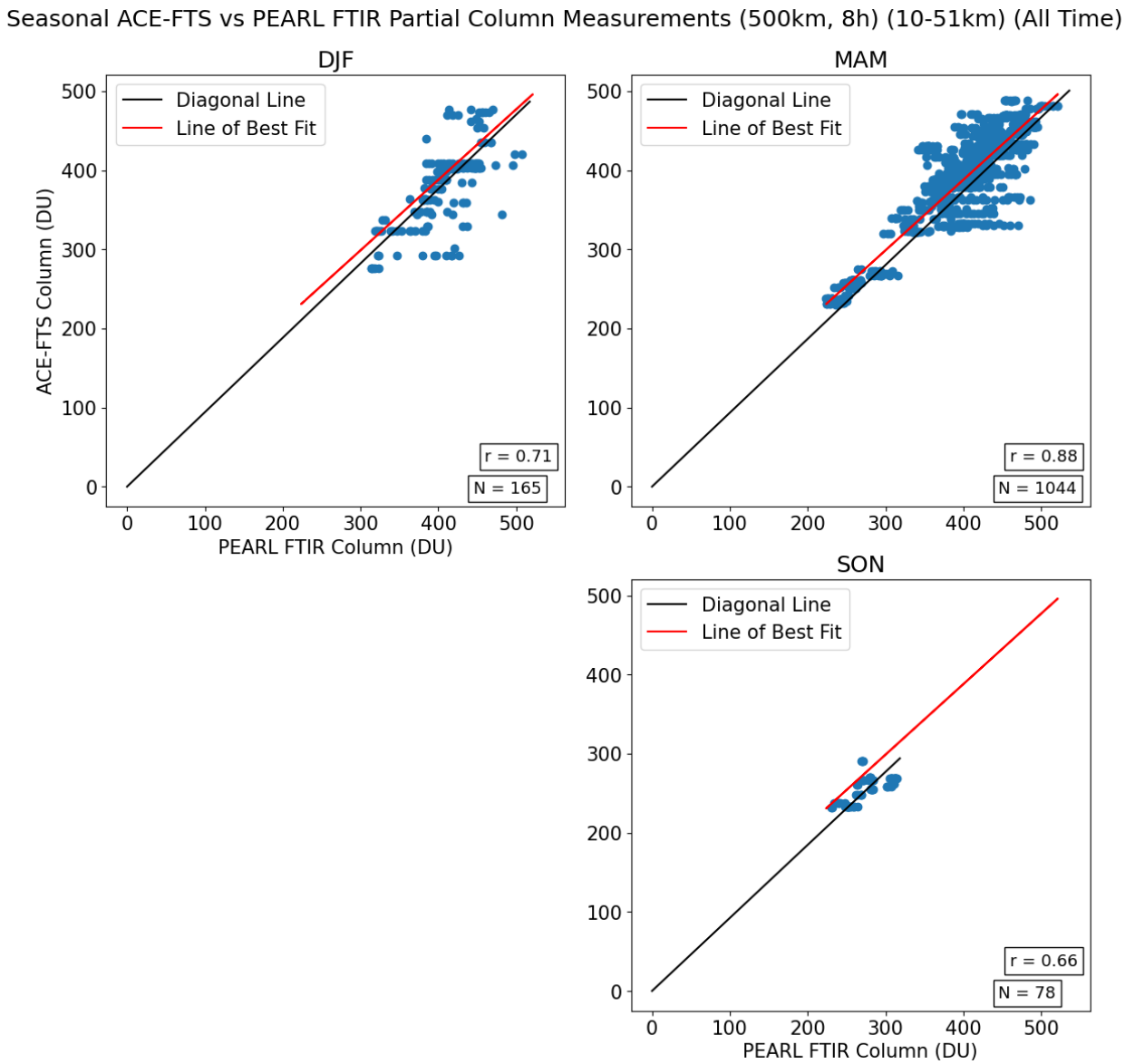

Figure 48. Seasonal plots of ACE-FTS and PEARL FTIR coincident ozone column measurements. Plot of JJA season is missing due to lack of coincident measurements. N and r represent number of coincidences and Pearson correlation coefficient, respectively.

Figure 47 show high correlation (r = 0.88) between ACE-FTS and PEAR FTIR measurements. Although, less correlated than OSIRIS and ACE-FTS column measurements and more variable between different seasons. Figure 48 shows that boreal fall measurements are the least correlated (r = 0.66), followed by boreal winter (r = 0.71). The reduced seasonal correlation might be due to lack of a representative sample size (N = 78 and N = 165 in boreal fall and winter, respectively).

Figures 49 and 50 depict high variability of the differences between coincident measurements, although, the measurements mostly agree since the differences are concentrated around 0 (DU or %) along with the mean differences. These plots affirm the trends observed in the previous plots.

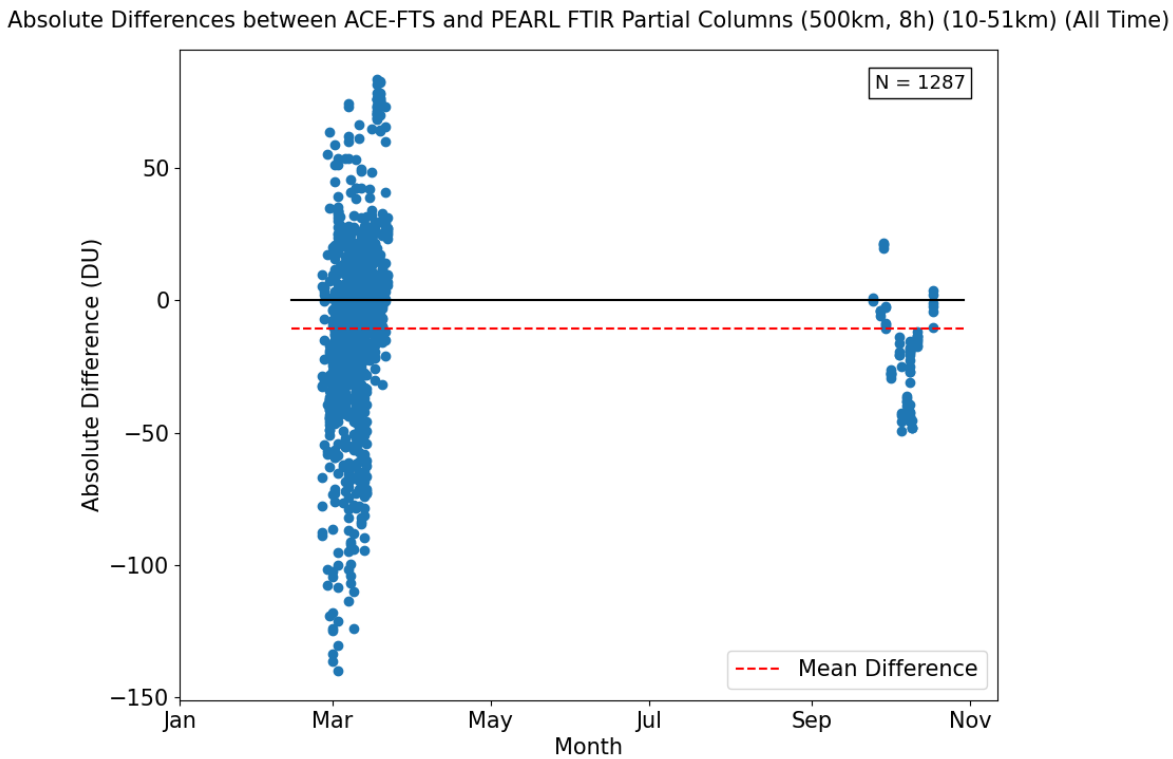

Figure 49. Plot of absolute differences between ACE-FTS and PEARL FTIR coincident ozone column measurements. N is the number of coincidences.

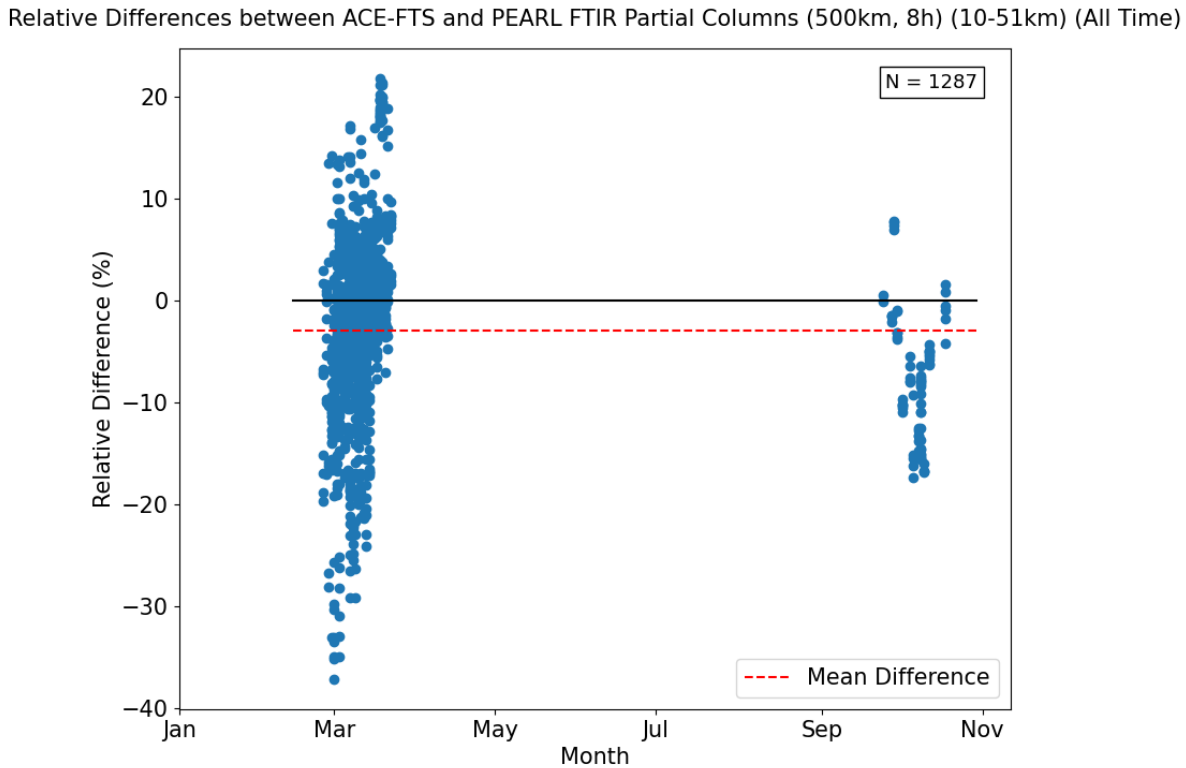

Figure 50. Plot of relative differences between ACE-FTS and PEARL FTIR coincident ozone column measurements. N is the number of coincidences.

3.3.3.2 OSIRIS vs PEARL FTIR Column Comparisons

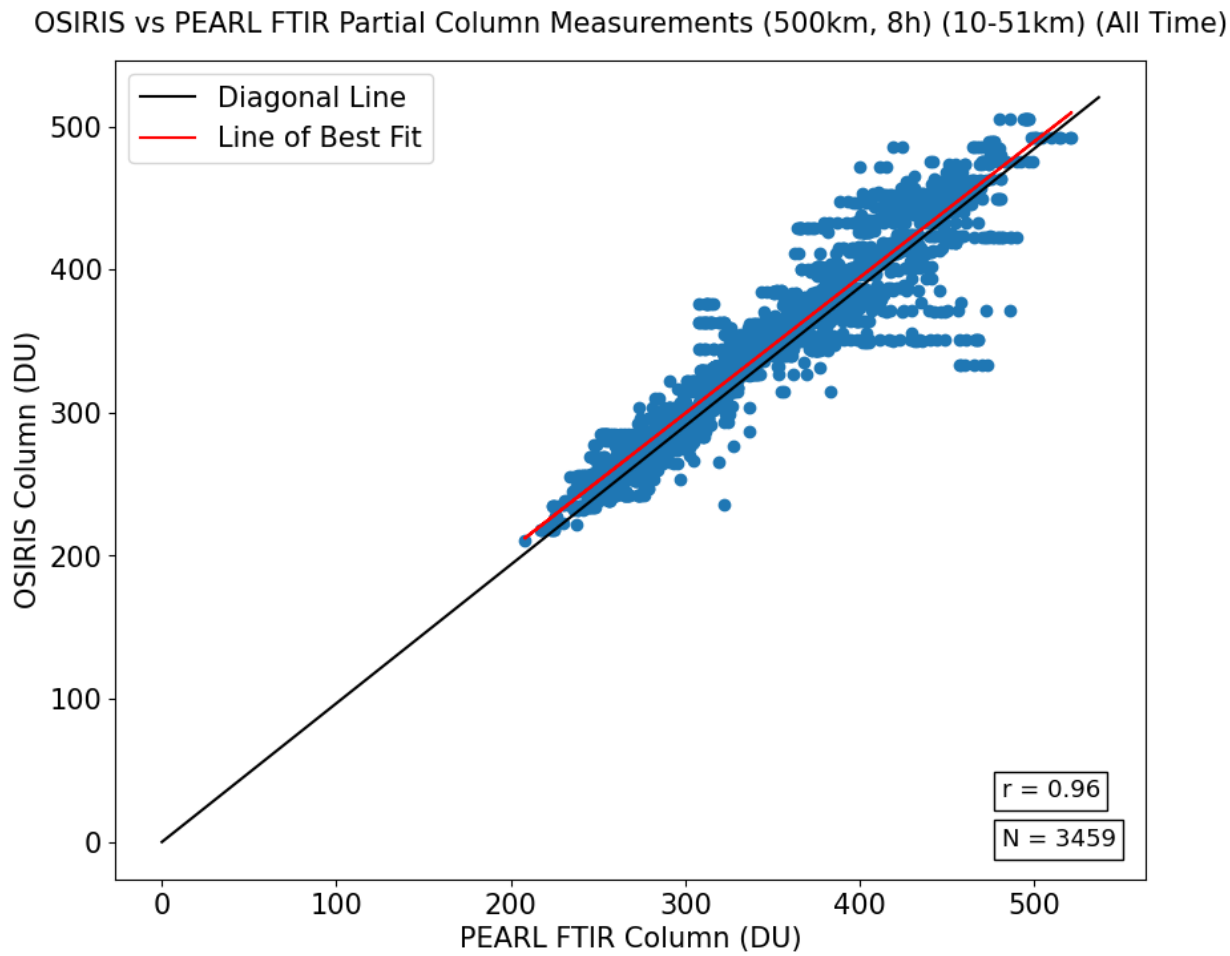

Figure 51. Plot of OSIRIS and PEARL FTIR coincident ozone column measurements. N and r represent number of coincidences and Pearson correlation coefficient, respectively.

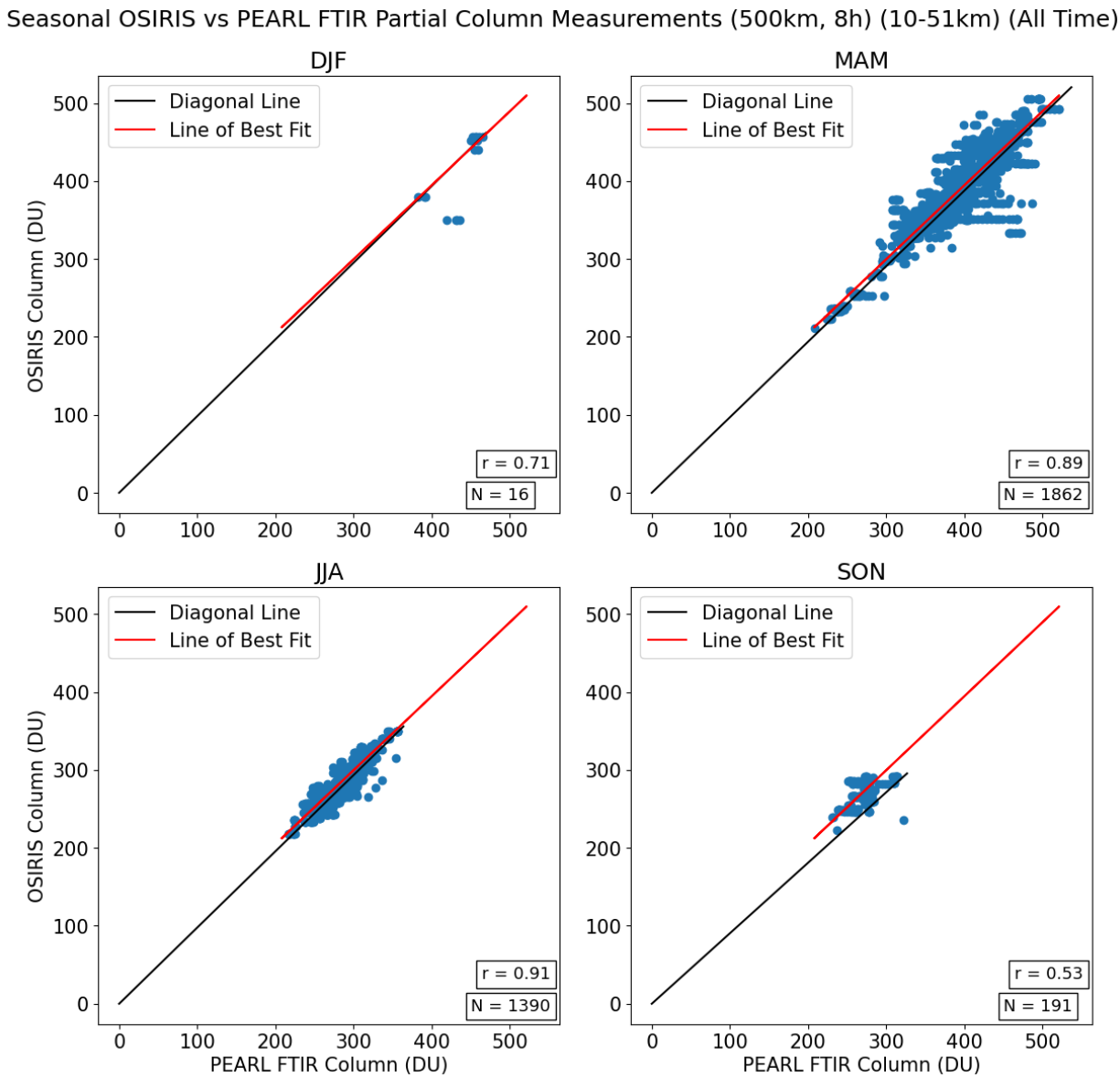

Figure 52. Seasonal plots of OSIRIS and PEARL FTIR coincident ozone column measurements. N and r represent number of coincidences and Pearson correlation coefficient, respectively.

Resembling previous column comparisons, OSIRIS and PEARL FTIR show good agreement with high correlation ($r = 0.96$) as seen in Figure 51. Figure 52 shows that the high correlation ($r > 0.80$) occurs only during boreal spring and summer. The boreal winter and fall seasons have lower correlation ($r = 0.71$ and $r = 0.53$ for winter and fall, respectively), potentially attributable to smaller sample sizes ($N = 16$ and $N = 191$, respectively) in these seasons.

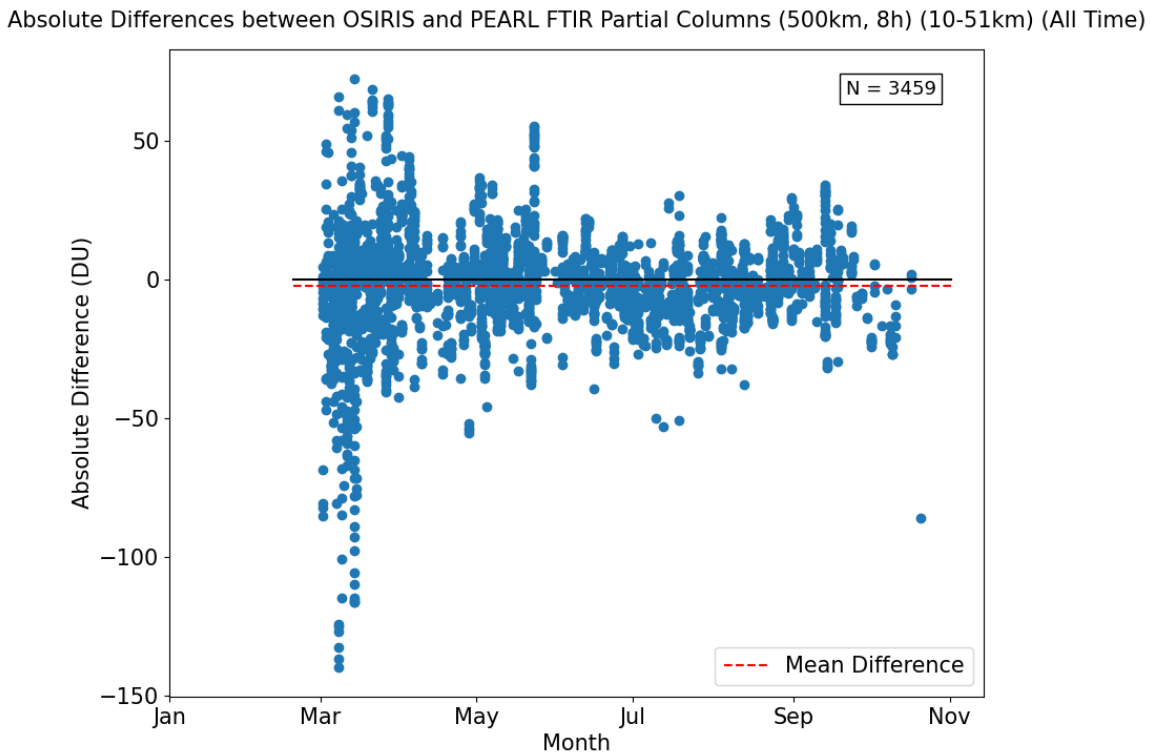

Figure 53. Plot of absolute differences between OSIRIS and PEARL FTIR coincident ozone column measurements. N is the number of coincidences.

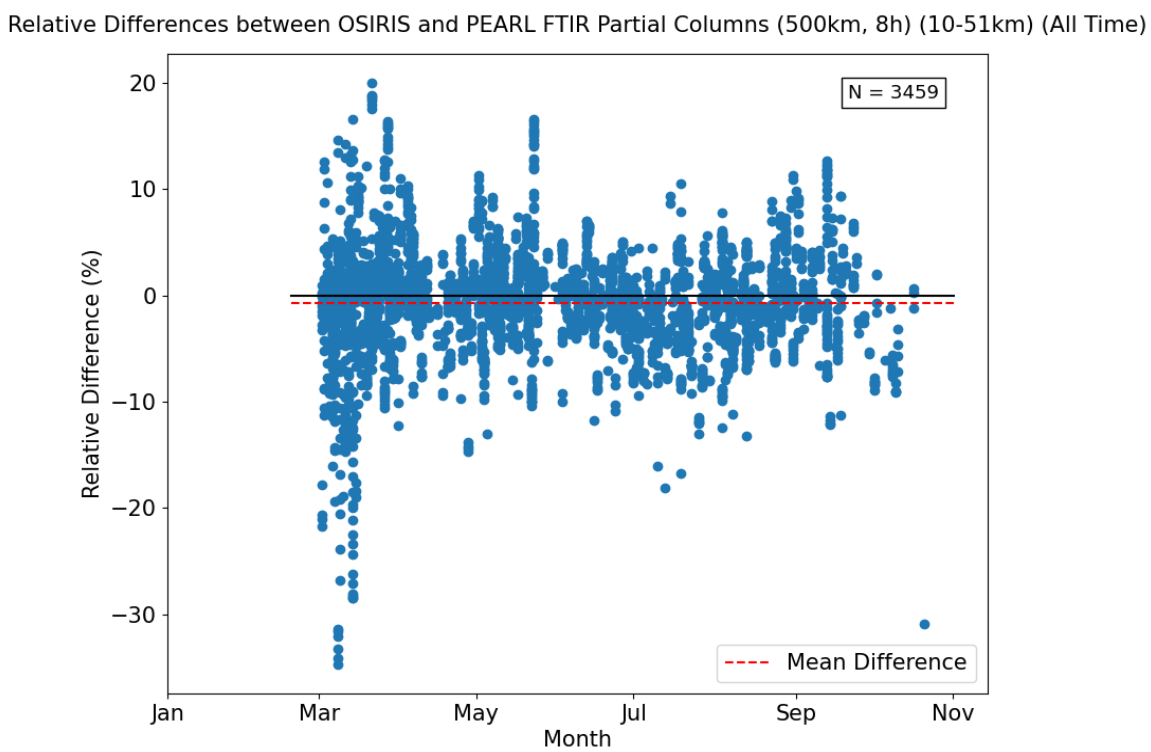

Figure 54. Plot of relative differences between OSIRIS and PEARL FTIR coincident ozone column measurements. N is the number of coincidences.

Figures 53 and 54 show that most differences are scattered and centered around 0 (DU or %), including the mean difference, confirming the result seen in previous plots showing high correlation. March shows more divergence between measurements, but majority of differences remain close to 0 (DU or %), so, the mean differences also remain close to 0 (DU or %).

3.3.4 Time Series Column Comparisons

A regression line was fit to time series plots of absolute and relative column differences for each pair of measurement. The slope of this fitted line along with its 95% confidence interval is used to infer the divergence of the instruments' measurements over time. The slopes and their confidence intervals are included in Table 2. The confidence intervals for the OSIRIS vs ACE-FTS (above PEARL) and ACE-FTS vs PEARL FTIR pairs include 0 (DU or %) per day, meaning, it cannot be concluded that the instruments' measurements are diverging. The other instrument pairs have confidence intervals not containing 0 (DU or %) per day but close to 0 (DU or %) per day. Nonetheless, the slopes do not indicate a significant divergence of measurement over time. For example, the maximum slope value computed is 0.00033 which indicates that it would take 10 years for the absolute difference to change by ~1 DU. Figures 58 to 65 in the appendix showcase the time series plots for visual observation.

Instrument Pair	Difference Type	Fitted Slope	Margin of Error	95% Confidence Interval	Units
OSIRIS vs ACE-FTS (Global)	Relative Difference	-0.90	0.7	(-1.5, -0.2)	10^{-4} %/day
OSIRIS vs ACE-FTS (Global)	Absolute Difference	-2.5	1.9	(-4.4, -0.6)	10^{-4} DU/day
OSIRIS vs ACE-FTS (above PEARL)	Relative Difference	1.0	2.3	(-1.3, 3.4)	10^{-4} %/day
OSIRIS vs ACE-FTS (above PEARL)	Absolute Difference	3.3	7.9	(-4.6, 11.2)	10^{-4} DU/day
ACE-FTS vs PEARL FTIR	Relative Difference	1.7	3.5	(-1.8, 5.2)	10^{-4} %/day
ACE-FTS vs PEARL FTIR	Absolute Difference	1.7	3.5	(-1.8, 5.2)	10^{-4} DU/day
OSIRIS vs PEARL FTIR	Relative Difference	2.0	1.2	(0.8, 3.2)	10^{-4} %/day
OSIRIS vs PEARL FTIR	Absolute Difference	2.0	1.2	(0.8, 3.2)	10^{-4} DU/day

Table 2. Relevant values corresponding to time series analysis of differences between coincident ozone column measurements of each instrument pair.

4 Conclusion

This project sought to assess the consistency of OSIRIS, ACE-FTS and PEARL FTIR ozone measurements. The assessment focused on comparing individual pairs of measurements within a great-circle distance of 500 km and temporal distance of 8 hours using various metrics. For each profile comparison, the relative and absolute differences plots suggest that the measurements between the pairs of instruments mostly agree with each other with most absolute and relative differences being between -20 % and 20 % and -0.5 ppmv and 0.5 ppmv, respectively, however, Pearson correlation coefficient plots do not always yield the same conclusions for the satellite vs PEARL FTIR comparisons. This discrepancy may be a result of general measurement variability or measurement variability intrinsic to the location of the measurements being above PEARL. Future work could focus on differentiating between measurements inside and outside the Northern Hemisphere polar vortex which may yield higher correlation for measurements above PEARL. Future work could also incorporate smoothing ozone profiles using averaging kernels and using linear interpolation of satellite data onto the PEARL FTIR altitude grid to compute ozone columns. Overall, there is good agreement between the profile measurements of all pairs of instruments on average. In aggregate (i.e. ignoring seasonal variability), column measurements for all pairs of instruments showed high correlation ($r > 0.8$), indicating consistency between the instruments' column measurements. Some inconsistencies arose when assessing seasonal correlation such as a difference of up to 0.38 in correlation between seasons, however, this could be attributed to those seasons having a non-representative sample size. Lastly, time series analysis of inter-instrument differences reveals no significant drift. Slopes are mostly negligible (max absolute slope = 3.3×10^{-4} DU/day, ~1 DU/decade) with confidence intervals either spanning zero or near zero.

5 Appendix

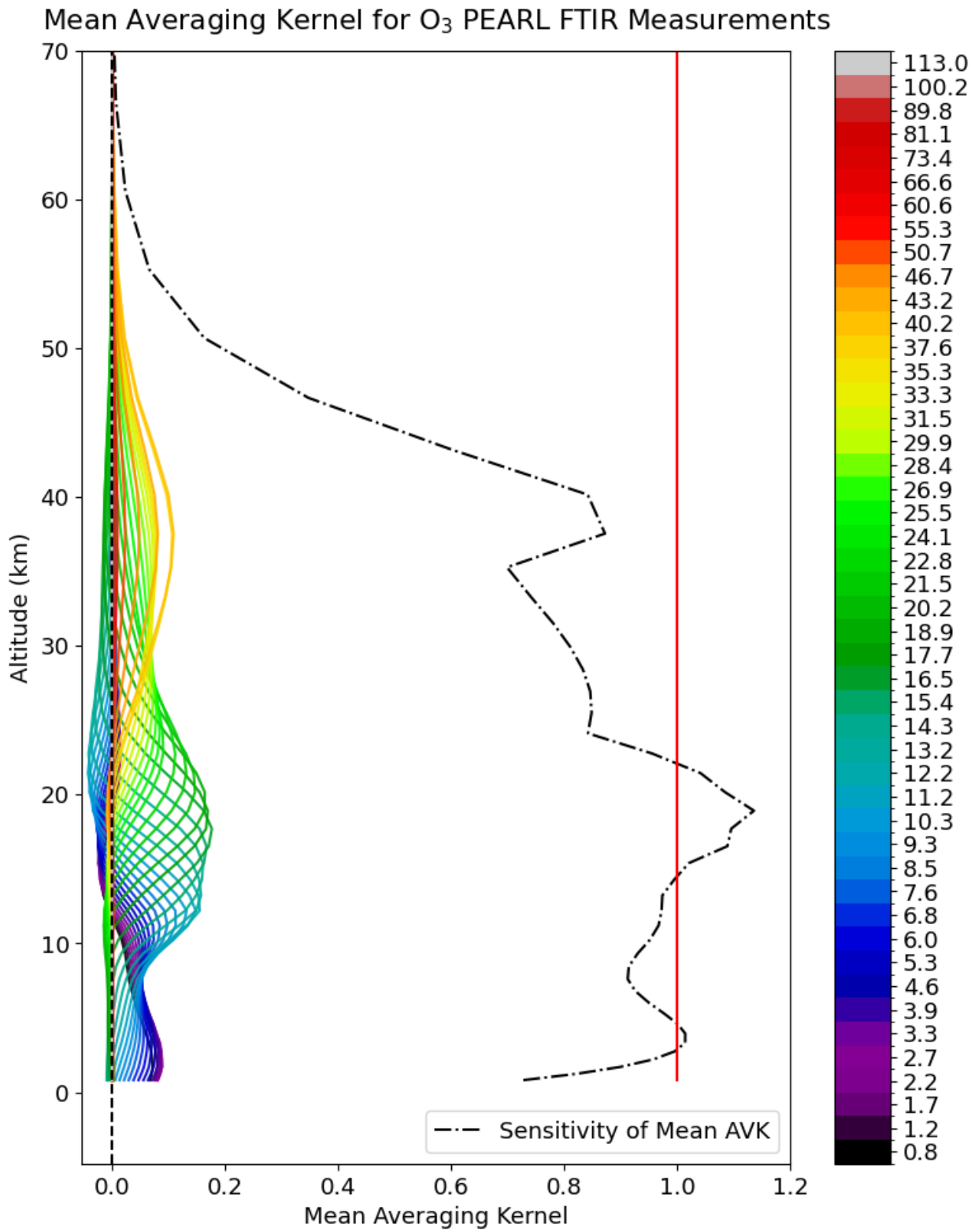

Figure 55. PEARL FTIR mean averaging kernel plot with mean sensitivity for each altitude.

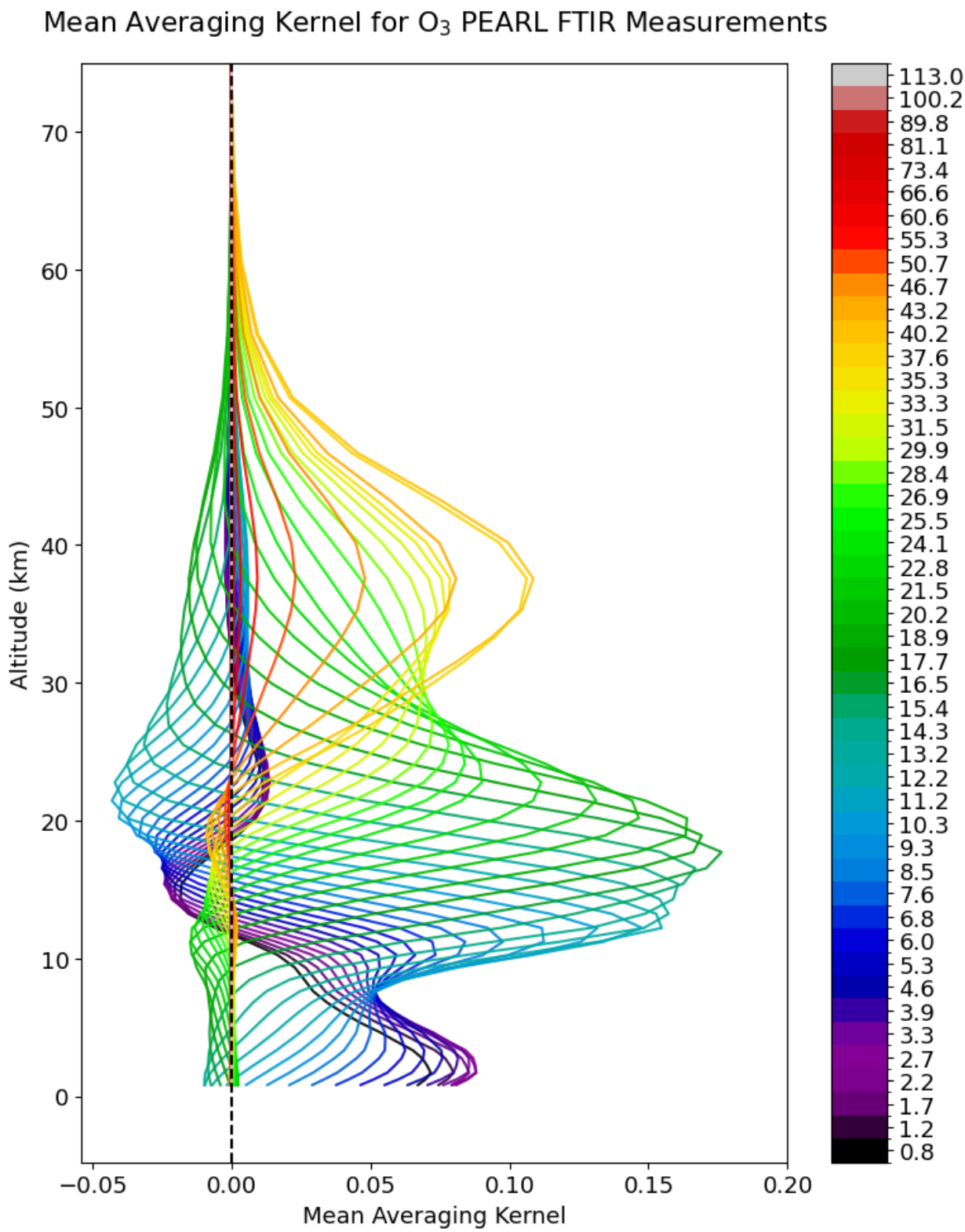

Figure 56. PEARL FTIR mean averaging kernel plot.

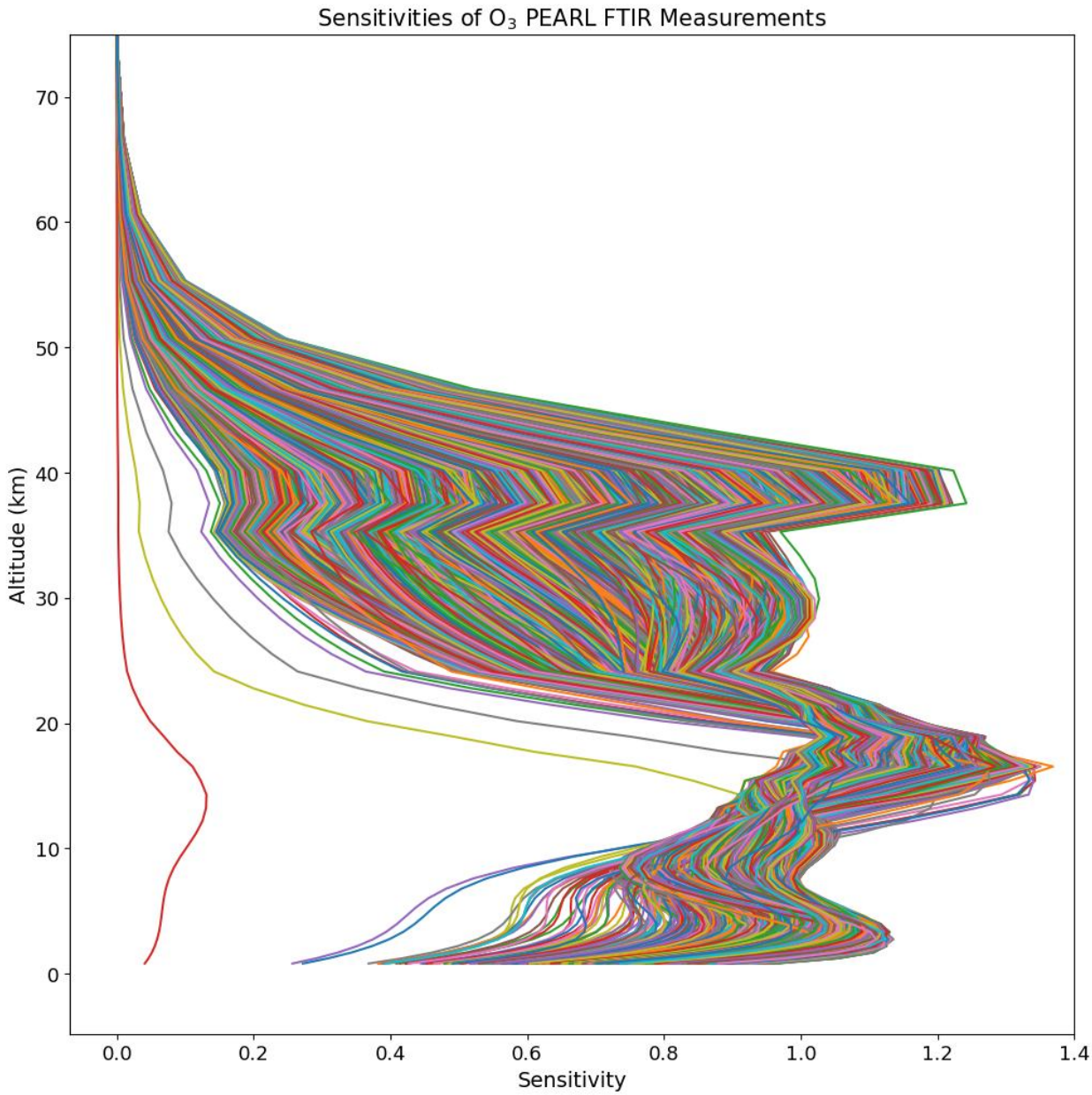

Figure 57. Plot of PEARL FTIR sensitivity at each altitude for all measurements.

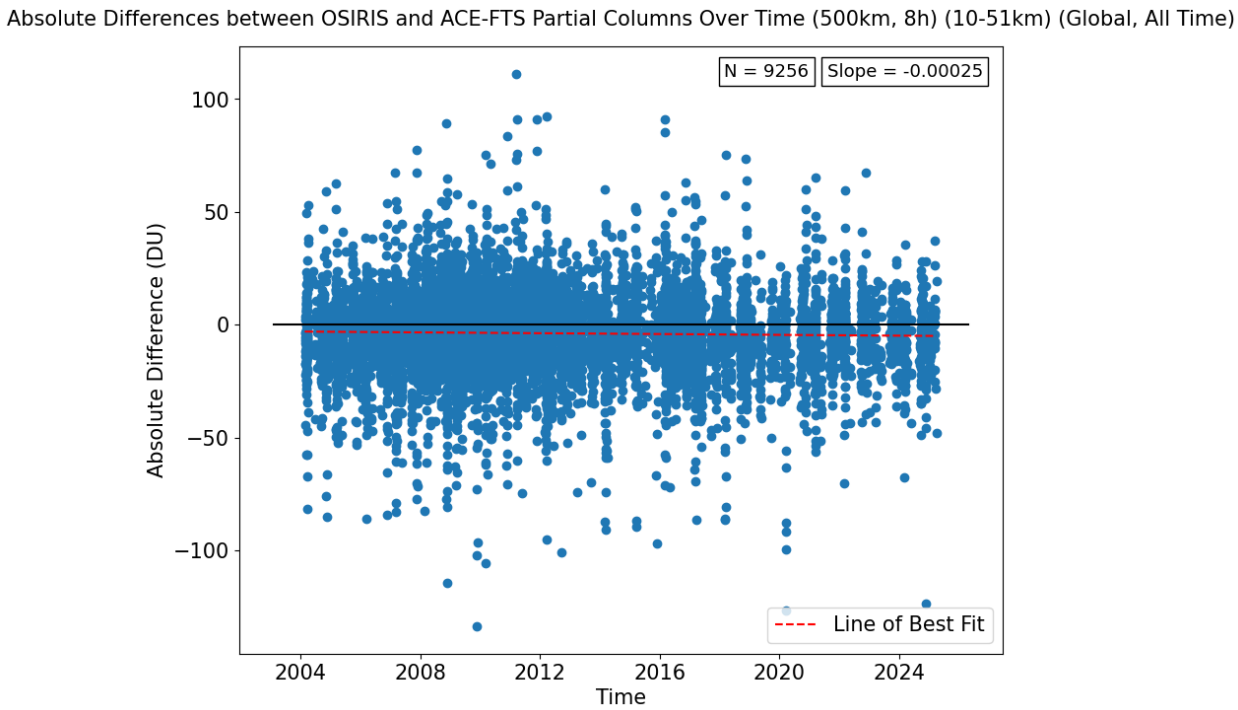

Figure 58. Time series plot of absolute differences between global coincident pairs of OSIRIS and ACE-FTS ozone column measurements.

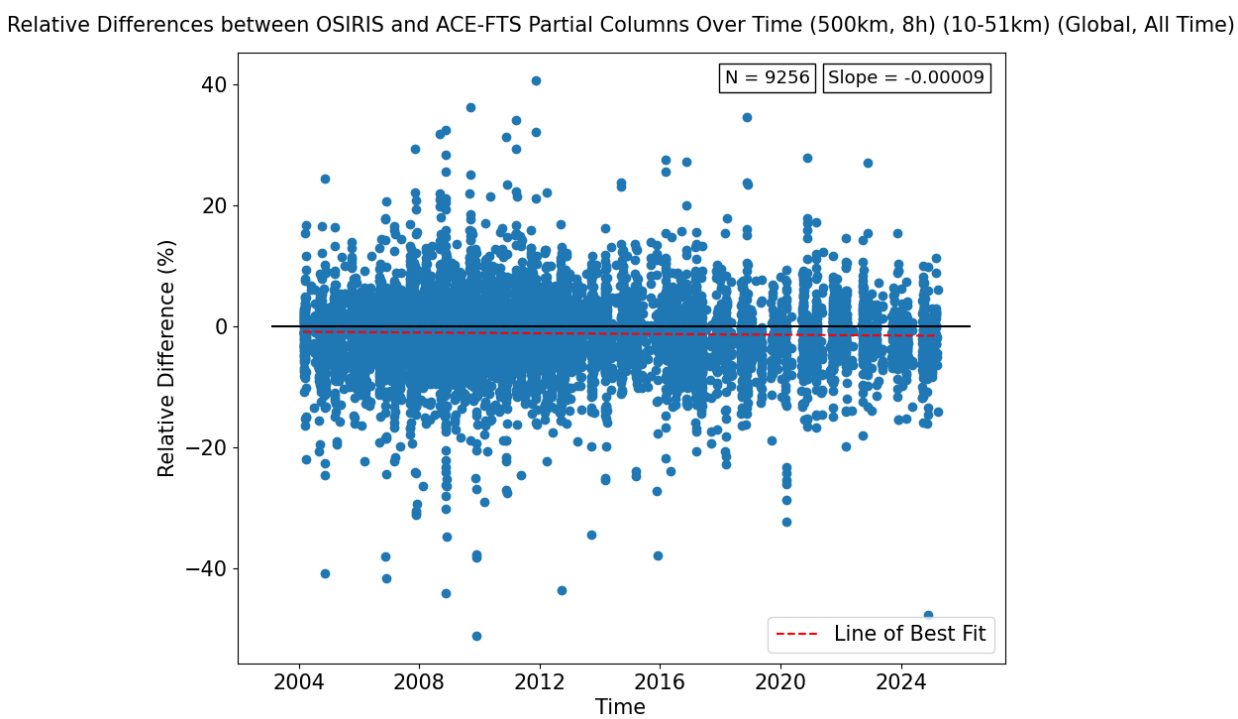

Figure 59. Time series plot of relative differences between global coincident pairs of OSIRIS and ACE-FTS ozone column measurements.

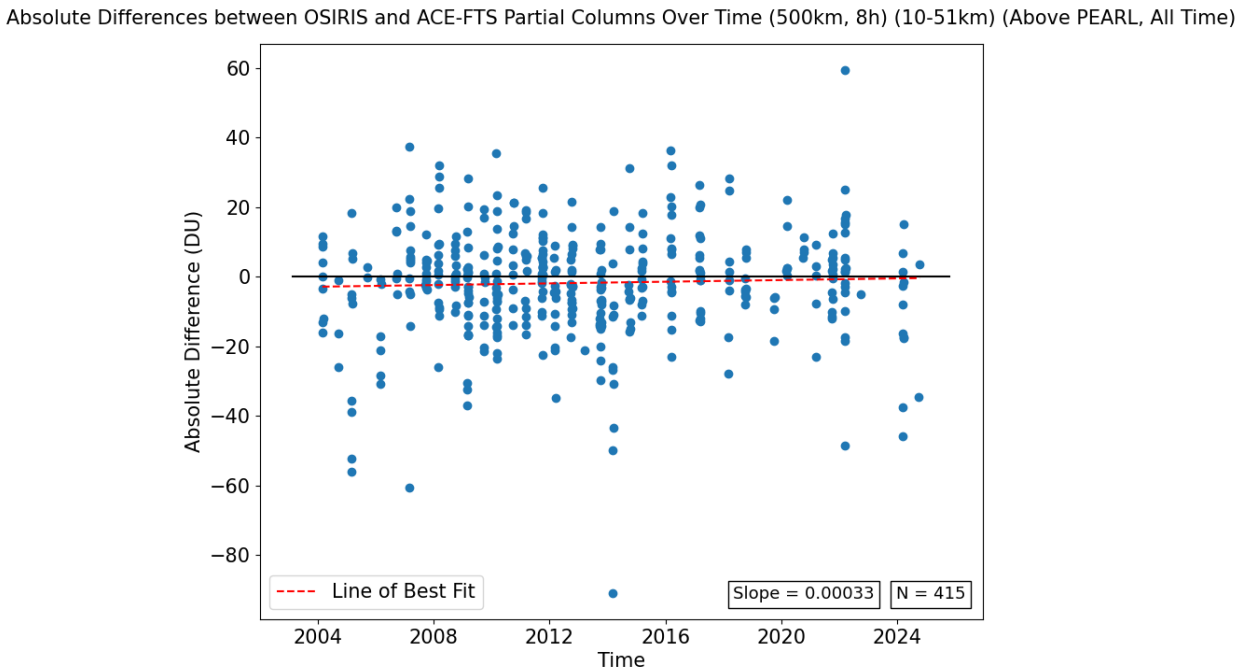

Figure 60. Time series plot of absolute differences between coincident pairs of OSIRIS and ACE-FTS ozone column measurements above PEARL.

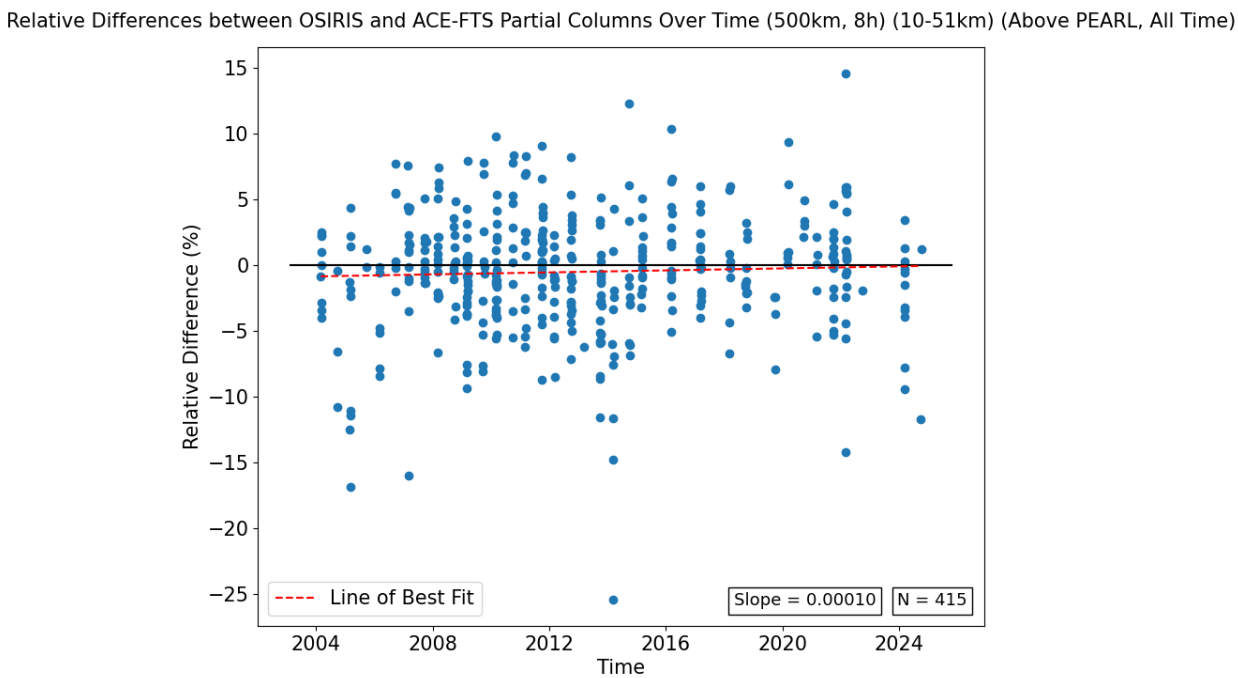

Figure 61. Time series plot of relative differences between coincident pairs of OSIRIS and ACE-FTS ozone column measurements above PEARL.

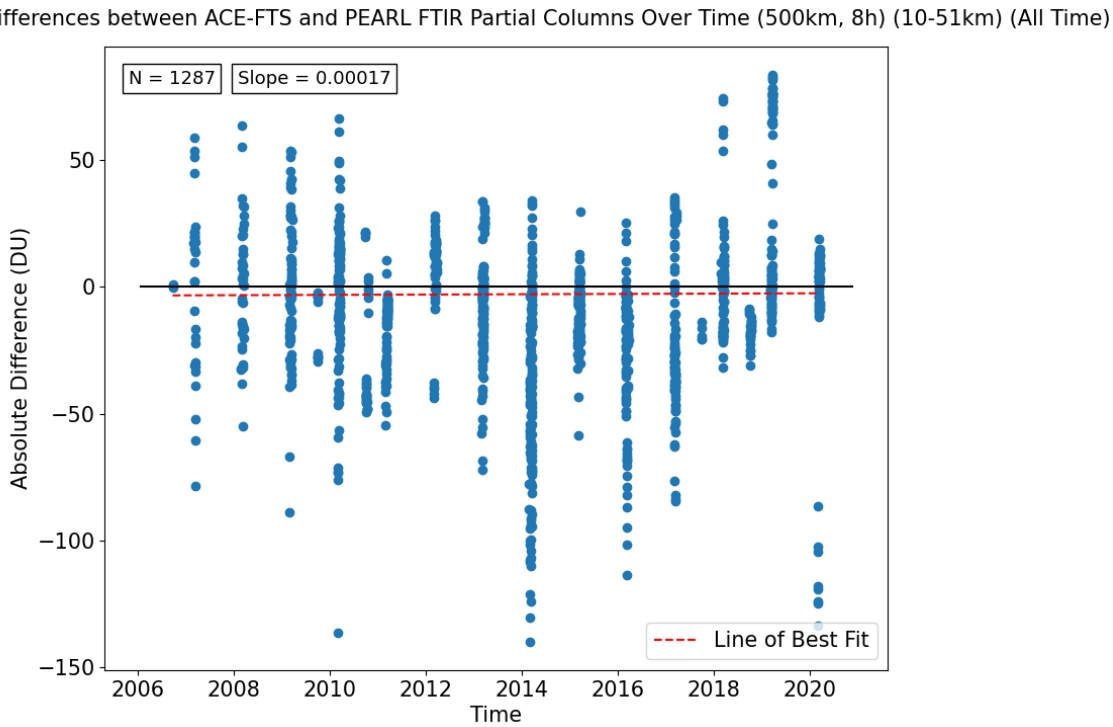

Figure 62. Time series plot of absolute differences between coincident pairs of ACE-FTS and PEARL FTIR ozone column measurements.

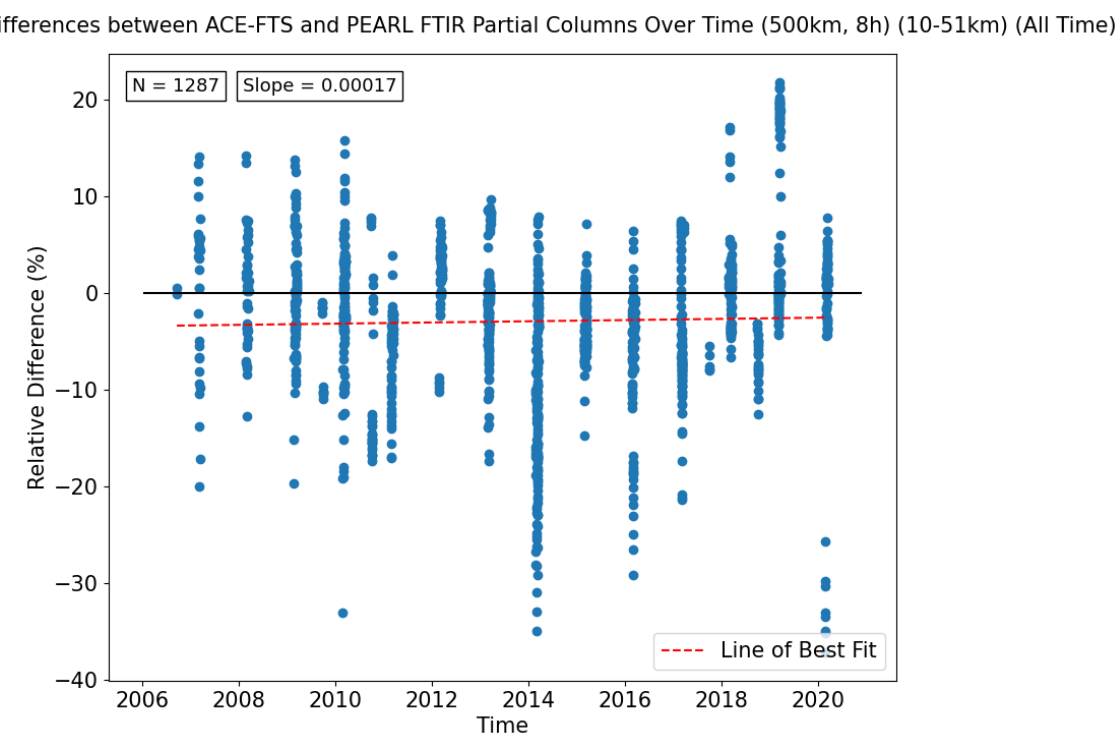

Figure 63. Time series plot of relative differences between coincident pairs of ACE-FTS and PEARL FTIR ozone column measurements.

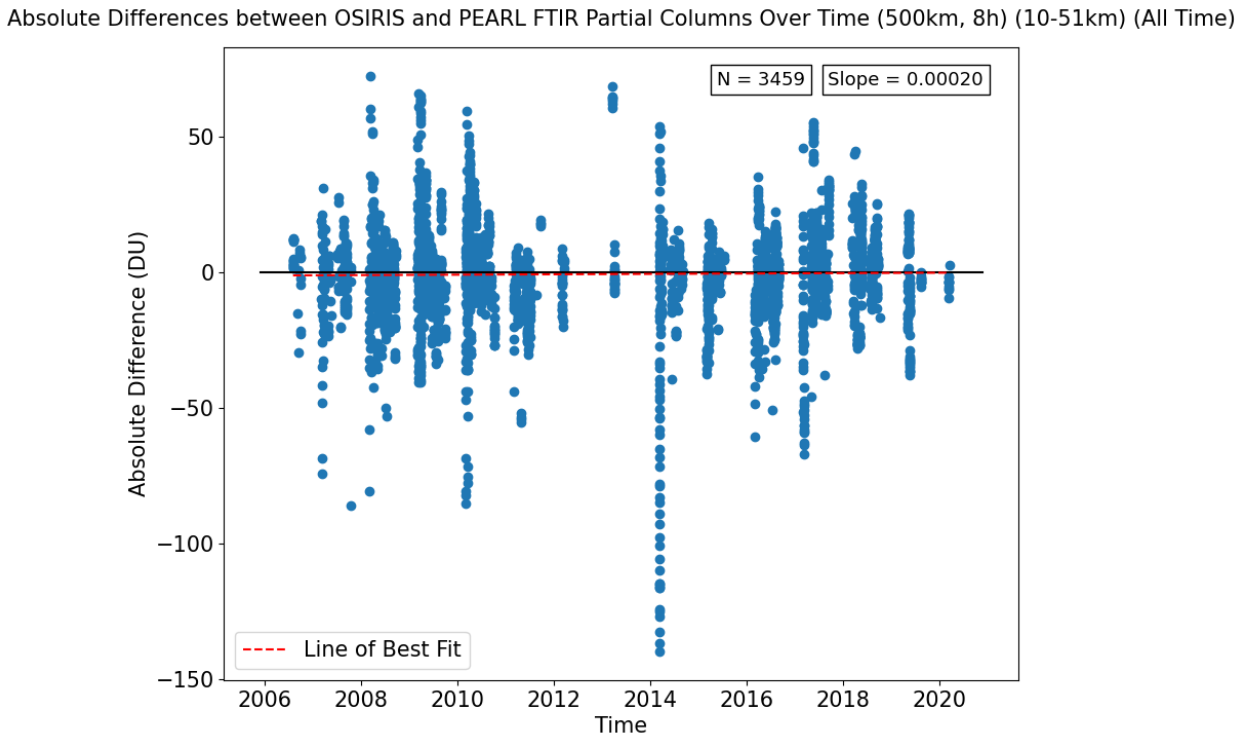

Figure 64. Time series plot of absolute differences between coincident pairs of OSIRIS and PEARL FTIR ozone column measurements.

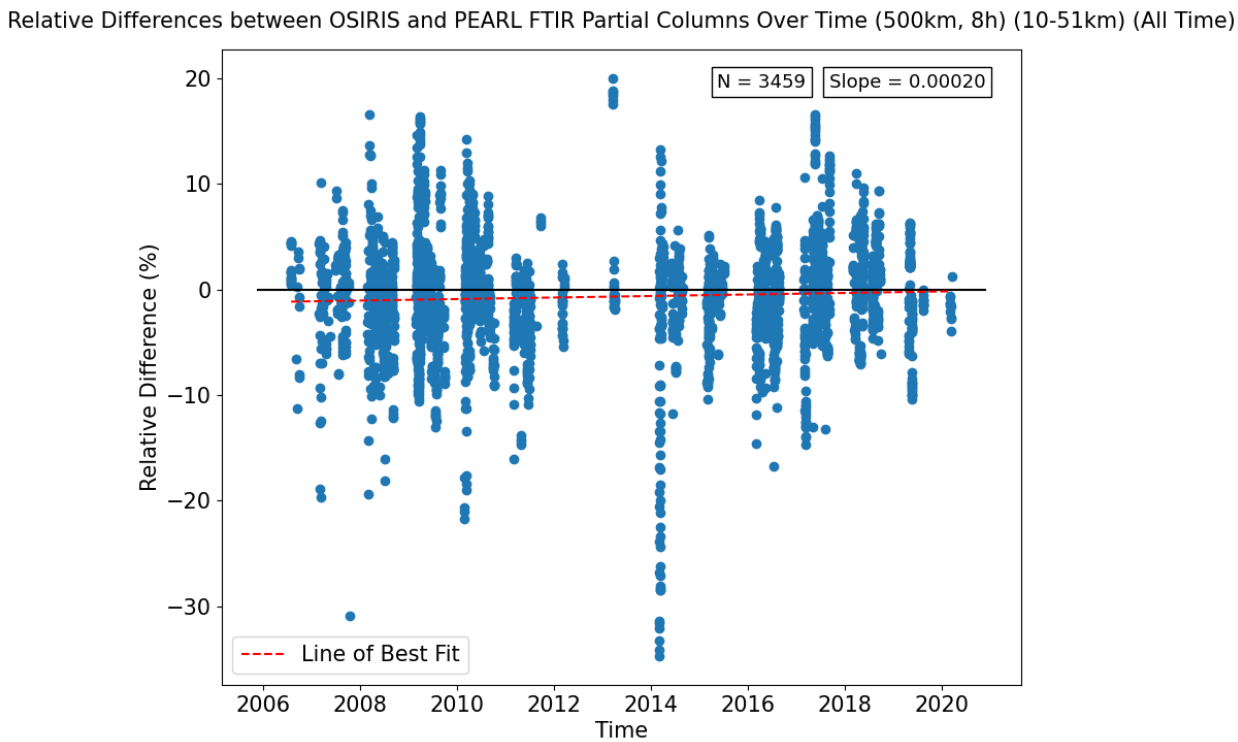

Figure 65. Time series plot of relative differences between coincident pairs of OSIRIS and PEARL FTIR ozone column measurements.

6 References

Adams, C., Strong, K., Batchelor, R. L., Bernath, P. F., Brohede, S., Boone, C., Degenstein, D., Daffer, W. H., Drummond, J. R., Fogal, P. F., Farahani, E., Fayt, C., Fraser, A., Goutail, F., Hendrick, F., Kolonjari, F., Lindenmaier, R., Manney, G., McElroy, C. T., … Zhao, X. (2012). Validation of ACE and OSIRIS ozone and NO_2 measurements using ground-based instruments at 80° N. *Atmospheric Measurement Techniques*, *5*(5), 927–953. https://doi.org/10.5194/amt-5-927-2012

Batchelor, R. L., Kolonjari, F., Lindenmaier, R., Mittermeier, R. L., Daffer, W., Fast, H., Manney, G., Strong, K., & Walker, K. A. (2010). Four Fourier transform spectrometers and the Arctic polar vortex: Instrument intercomparison and ACE-FTS validation at Eureka during the IPY springs of 2007 and 2008. *Atmospheric Measurement Techniques*, *3*(1), 51–66. https://doi.org/10.5194/amt-3-51-2010

Batchelor, R. L., Strong, K., Lindenmaier, R., Mittermeier, R. L., Fast, H., Drummond, J. R., & Fogal, P. F. (2009). *A New Bruker IFS 125HR FTIR Spectrometer for the Polar Environment Atmospheric Research Laboratory at Eureka, Nunavut, Canada: Measurements and Comparison with the Existing Bomem DA8 Spectrometer*. https://doi.org/10.1175/2009JTECHA1215.1

Bernath, P. F., McElroy, C. T., Abrams, M. C., Boone, C. D., Butler, M., Camy-Peyret, C., Carleer, M., Clerbaux, C., Coheur, P.-F., Colin, R., DeCola, P., DeMazière, M., Drummond, J. R., Dufour, D., Evans, W. F. J., Fast, H., Fussen, D., Gilbert, K., Jennings, D. E., … Zou, J. (2005). Atmospheric Chemistry Experiment (ACE): Mission overview. *Geophysical Research Letters*, *32*(15). https://doi.org/10.1029/2005GL022386

Department of Physics, University of Toronto. (n.d.). *Eureka Physics*. Retrieved July 31, 2025, from https://eureka.physics.utoronto.ca/

Griffin, D., Walker, K. A., Conway, S., Kolonjari, F., Strong, K., Batchelor, R., Boone, C. D., Dan, L., Drummond, J. R., Fogal, P. F., Fu, D., Lindenmaier, R., Manney, G. L., & Weaver, D. (2017). Multi-year comparisons of ground-based and space-borne Fourier transform spectrometers in the high Arctic between 2006 and 2013. *Atmospheric Measurement Techniques*, *10*(9), 3273–3294. https://doi.org/10.5194/amt-10-3273-2017

Jeffery, P. S. (2022). *Water Vapour and Ozone: Measuring Key Trace Gases in Challenging Regions*. http://hdl.handle.net/1807/123476

Kerzenmacher, T. E., Walker, K. A., Strong, K., Berman, R., Bernath, P. F., Boone, C. D., Drummond, J. R., Fast, H., Fraser, A., MacQuarrie, K., Midwinter, C., Sung, K., McElroy, C. T., Mittermeier, R. L., Walker, J., & Wu, H. (2005). Measurements of O3, NO2 and Temperature during the 2004 Canadian Arctic ACE Validation Campaign. *Geophysical Research Letters*, *32*(16). https://doi.org/10.1029/2005GL023032

Llewellyn, E. J., Lloyd, N. D., Degenstein, D. A., Gattinger, R. L., Petelina, S. V., Bourassa, A. E., Wiensz, J. T., Ivanov, E. V., McDade, I. C., Solheim, B. H., McConnell, J. C., Haley, C. S., von Savigny, C., Sioris, C. E., McLinden, C. A., Griffioen, E., Kaminski, J., Evans, W. F., Puckrin, E., … Nordh, L. (2004). The OSIRIS instrument on the Odin spacecraft. *Canadian Journal of Physics*, *82*(6), 411–422. https://doi.org/10.1139/p04-005

McElroy, C. T., Nowlan, C. R., Drummond, J. R., Bernath, P. F., Barton, D. V., Dufour, D. G., Midwinter, C., Hall, R. B., Ogyu, A., Ullberg, A., Wardle, D. I., Kar, J., Zou, J., Nichitiu, F., Boone, C. D., Walker, K. A., & Rowlands, N. (2007). The ACE-MAESTRO instrument on SCISAT: Description, performance, and preliminary results. *Applied Optics*, *46*(20), 4341–4356. https://doi.org/10.1364/ao.46.004341

Murtagh, D., Frisk, U., Merino, F., Ridal, M., Jonsson, A., Stegman, J., Witt, G., Eriksson, P., Jiménez, C., Megie, G., Noë, J. de la, Ricaud, P., Baron, P., Pardo, J. R., Hauchcorne, A., Llewellyn, E. J., Degenstein, D. A., Gattinger, R. L., Lloyd, N. D., … Oikarinen, L. (2002). An overview of the Odin atmospheric mission. *Canadian Journal of Physics*, *80*(4), 309–319. https://doi.org/10.1139/p01-157

National Oceanic and Atmospheric Administration. (2024a, August 20). *Layers of the Atmosphere*. https://www.noaa.gov/jetstream/atmosphere/layers-of-atmosphere

National Oceanic and Atmospheric Administration. (2024b, July 2). *The Atmosphere*. https://www.noaa.gov/jetstream/atmosphere

Salawitch, R. J., McBride, L. A., Thompson, C. R., Fleming, E. L., McKenzie, R. L., Rosenlof, K. H., Doherty, S. J., & Fahey, D. W. (2023). *Twenty questions and answers about the ozone layer: 2022 update* (Scientific Assessment of Ozone Depletion: 2022; 75 pp.). World Meteorological Organization.

Sheese, P. E., Boone, C. D., & Walker, K. A. (2015). Detecting physically unrealistic outliers in ACE-FTS atmospheric measurements. *Atmospheric Measurement Techniques*, *8*(2), 741–750. https://doi.org/10.5194/amt-8-741-2015